Title

An IL1RL1 genetic variant lowers soluble ST2 levels and the risk effects of APOE-ε4 in female patients with Alzheimer's disease.

Journal

Nature aging, 2(7)

ISSN

2662-8465

Authors

Jiang, Yuanbing
Zhou, Xiaopu
Wong, Hiu Yi
et al.

Publication Date

2022-07-01

DOI

10.1038/s43587-022-00241-9

ARTICLES
https://doi.org/10.1038/s43587-022-00241-9

nature aging

Check for updates

OPEN

An *IL1RL1* genetic variant lowers soluble ST2 levels and the risk effects of *APOE*-ε4 in female patients with Alzheimer's disease

Yuanbing Jiang[1,2] ✉, Xiaopu Zhou[1,2,3] ✉, Hiu Yi Wong[1,2] ✉, Li Ouyang[1,2] ✉, Fanny C. F. Ip[1,2,3] ✉, Vicky M. N. Chau[1,2] ✉, Shun-Fat Lau[1,2] ✉, Wei Wu[1,2] ✉, Daniel Y. K. Wong[1,2] ✉, Heukjin Seo[1] ✉, Wing-Yu Fu[1,2] ✉, Nicole C. H. Lai[1,2] ✉, Yuewen Chen[1,3,4] ✉, Yu Chen[1,3,4] ✉, Estella P. S. Tong[1,2] ✉, Alzheimer's Disease Neuroimaging Initiative*, Vincent C. T. Mok[5] ✉, Timothy C. Y. Kwok[6] ✉, Kin Y. Mok[1,2,7,8] ✉, Maryam Shoai[7,8] ✉, Benoit Lehallier[9,89] ✉, Patricia Morán Losada[9,10] ✉, Eleanor O'Brien[11,12] ✉, Tenielle Porter[11,12,13] ✉, Simon M. Laws[11,12,13] ✉, John Hardy[2,7,8,14] ✉, Tony Wyss-Coray[2,9,10,15] ✉, Colin L. Masters[16] ✉, Amy K. Y. Fu[1,2,3] ✉ and Nancy Y. Ip[1,2,3] ✉

Changes in the levels of circulating proteins are associated with Alzheimer's disease (AD), whereas their pathogenic roles in AD are unclear. Here, we identified soluble ST2 (sST2), a decoy receptor of interleukin-33–ST2 signaling, as a new disease-causing factor in AD. Increased circulating sST2 level is associated with more severe pathological changes in female individuals with AD. Genome-wide association analysis and CRISPR–Cas9 genome editing identified rs1921622, a genetic variant in an enhancer element of *IL1RL1*, which downregulates gene and protein levels of sST2. Mendelian randomization analysis using genetic variants, including rs1921622, demonstrated that decreased sST2 levels lower AD risk and related endophenotypes in females carrying the Apolipoprotein E (*APOE*)-ε4 genotype; the association is stronger in Chinese than in European-descent populations. Human and mouse transcriptome and immunohistochemical studies showed that rs1921622/sST2 regulates amyloid-beta (Aβ) pathology through the modulation of microglial activation and Aβ clearance. These findings demonstrate how sST2 level is modulated by a genetic variation and plays a disease-causing role in females with AD.

AD is the most common neurodegenerative disease and a leading cause of mortality in older people[1]. Its pathological hallmarks include the extracellular accumulation of Aβ peptides, which form Aβ plaques, and intracellular neurofibrillary tangles composed of hyperphosphorylated tau protein (P-tau)[2]. While the pathophysiological mechanisms underlying AD remain unclear, genome-wide association studies (GWASs) reveal more than 40 AD-associated genes linked with microglial functions (for example, *APOE*, *TREM2*, *BIN1* and *CD33*), suggesting that microglia play a key role in AD pathogenesis[3–5]. In particular, *APOE*-ε4, the strongest known risk factor for sporadic AD after chronological age[3], affects Aβ accumulation in AD[6,7] through regulating the clustering of microglia around Aβ and the subsequent degradation of Aβ plaques[4,8,9]. This suggests that microglial dysfunction plays an essential causative role in AD.

Recent studies show that, besides genetic factors, changes in secreted proteins in the brain milieu and/or circulatory system may also disrupt microglial activities and contribute to AD pathogenesis[10,11]. For example, soluble TREM2 protein (sTREM2) level is increased in the cerebrospinal fluid (CSF) of individuals with AD[12–14], and injection of sTREM2 in transgenic mouse models of

[1]Division of Life Science, State Key Laboratory of Molecular Neuroscience, Molecular Neuroscience Center, The Hong Kong University of Science and Technology, Clear Water Bay, Hong Kong, China. [2]Hong Kong Center for Neurodegenerative Diseases, Hong Kong Science Park, Hong Kong, China. [3]Guangdong Provincial Key Laboratory of Brain Science, Disease and Drug Development; Shenzhen–Hong Kong Institute of Brain Science, HKUST Shenzhen Research Institute, Shenzhen, China. [4]The Brain Cognition and Brain Disease Institute, Shenzhen Institutes of Advanced Technology, Chinese Academy of Sciences; Shenzhen–Hong Kong Institute of Brain Science–Shenzhen Fundamental Research Institutions, Shenzhen, China. [5]Gerald Choa Neuroscience Centre, Lui Che Woo Institute of Innovative Medicine, Therese Pei Fong Chow Research Centre for Prevention of Dementia, Division of Neurology, Department of Medicine and Therapeutics, The Chinese University of Hong Kong, Hong Kong, China. [6]Therese Pei Fong Chow Research Centre for Prevention of Dementia, Division of Geriatrics, Department of Medicine and Therapeutics, The Chinese University of Hong Kong, Hong Kong, China. [7]Department of Neurodegenerative Disease, UCL Queen Square Institute of Neurology, London, UK. [8]UK Dementia Research Institute, University College London, London, UK. [9]Department of Neurology and Neurological Sciences, Stanford University School of Medicine, Stanford, California, USA. [10]Wu Tsai Neurosciences Institute, Stanford University, Stanford, California, USA. [11]Centre for Precision Health, Edith Cowan University, Joondalup, Australia. [12]Collaborative Genomics and Translation Group, School of Medical and Health Sciences, Edith Cowan University, Joondalup, Australia. [13]School of Pharmacy and Biomedical Sciences, Faculty of Health Sciences, Curtin Health Innovation Research Institute, Curtin University, Bentley, Australia. [14]Institute for Advanced Study, The Hong Kong University of Science and Technology, Clear Water Bay, Hong Kong, China. [15]The Phil and Penny Knight Initiative for Brain Resilience, Stanford University, Stanford, California, USA. [16]The Florey Institute of Neuroscience and Mental Health, The University of Melbourne, Melbourne, Australia. [89]Present address: Alkahest Inc, San Carlos, California, USA. *A list of authors and their affiliations appears at the end of the paper. ✉e-mail: boip@ust.hk

amyloidosis alleviates Aβ accumulation by enhancing the interaction between microglia and Aβ and subsequent Aβ phagocytosis[15,16]. Moreover, the soluble form of a full-length VCAM1 protein in endothelial cells, sVCAM1, is increased in the plasma and CSF of individuals with AD[17,18]; this is suggested to mediate reduced hippocampal neurogenesis and a pro-inflammatory response by microglia during aging[19].

Other secreted proteins that contribute to AD pathogenesis include soluble cytokine receptors comprising the ectodomains of membrane-bound cytokine receptors, which function as decoy receptors to attenuate cytokine-mediated signaling[20,21]. In particular, sST2 is a secreted isoform of the interleukin-33 (IL-33) receptor ST2L (full-length ST2) that is produced by alternative promoter activation[22] (Extended Data Fig. 1). ST2L is expressed by microglia in the brain[23], and activation of IL-33–ST2 signaling decreases Aβ accumulation via enhanced microglial Aβ-clearance capacity in transgenic mouse models of amyloidosis[24,25]. Meanwhile, sST2 acts as a decoy receptor of IL-33 and inhibits IL-33–ST2 signaling[26,27]. Altered sST2 level in plasma is a biomarker of several inflammatory and cardiac diseases[28–31]. Notably, recent evidence shows that sST2 levels are also elevated in the blood of individuals with mild cognitive impairment (MCI) or AD[24,32]. Nonetheless, it is unclear what regulatory mechanisms underlie sST2 dysregulation and whether sST2 plays a pathological role in AD.

In the present study, we investigated sST2 regulation in AD and its roles in disease pathogenesis. We showed that sST2 level increases in the blood and brains of females with AD and is positively associated with disease progression. Moreover, we identified a single-nucleotide polymorphism (SNP), rs1921622, in *IL1RL1* (the gene encoding sST2 and ST2L) that is associated with decreased sST2 expression in human endothelial cells and decreased plasma and CSF sST2 levels. Mendelian randomization (MR) analysis showed that, in female *APOE*-ε4 carriers, decreased sST2 level results in reduced AD risk and less-severe AD-associated endophenotypes, suggesting a causal effect of sST2 in AD. Subsequent single-nucleus transcriptomic profiling revealed that the rs1921622 A allele is associated with enhanced microglial activation toward Aβ and lowered Aβ plaque load in female *APOE*-ε4 carriers with AD. Together, our findings suggest that a circulating protein, sST2, in the brain milieu plays a key role in *APOE*-ε4-dependent AD pathogenesis in females—by modulating the activation and Aβ-clearance capacity of microglia—and therefore might be a novel target for AD therapy.

Results

sST2 is associated with Alzheimer's disease and its pathological changes. To investigate how sST2 is involved in AD pathogenesis, we examined the associations between sST2 level and AD and its related endophenotypes. We measured the plasma sST2 level of Chinese individuals with AD (that is, those having Alzheimer's dementia with a Montreal Cognitive Assessment (MoCA) score < 21) and healthy controls (HCs) recruited in Hong Kong (the 'Chinese_cohort_1' hereafter; $n = 345$ HCs and $n = 345$ individuals with AD; Supplementary Table 1). We then performed a linear regression analysis between plasma sST2 level and AD and its related endophenotypes, adjusting for age, sex, status of cardiovascular diseases (CVDs; that is, heart disease, hypertension, diabetes mellitus and hyperlipidemia), body mass index (BMI) and education level, followed by multiple testing correction. The results show that plasma sST2 level was higher in individuals with AD when compared to HCs (β (effect size) = 2.072, false discovery rate (FDR) < 0.001; Fig. 1a). Moreover, plasma sST2 level was positively associated with the AD-related endophenotypes we examined—namely, the decreased volumes of gray matter ($\beta = -0.695$, FDR = 0.003; Fig. 1b) and increased levels of plasma biomarkers corresponding to AD (that is, P-tau181 (ref. [33]), $\beta = 0.413$, FDR = 0.005; Fig. 1c) and neurodegeneration (that is, neurofilament light polypeptide (NfL)[34], $\beta = 0.107$, FDR = 0.004; Fig. 1d). Notably, we found a differential regulation of plasma sST2 levels between sexes: while plasma sST2 level is lower in females than that in males, it exhibits a greater increase in AD in females (females, $\beta = 2.235$, FDR = 6.97×10^{-4}; males, $\beta = 1.926$, FDR = 0.148; Extended Data Fig. 2a). In particular, female *APOE*-ε4 carriers with AD had the greatest increase of plasma sST2 level compared to that in other subgroups ($\beta = 3.833$, FDR = 0.004; Extended Data Fig. 2b,c and Supplementary Table 2). Moreover, females showed stronger associations between plasma sST2 level and AD-related endophenotypes (including gray matter volumes, plasma P-tau181 levels and plasma NfL levels) than those in males (Supplementary Table 2). These results suggest that plasma sST2 level is associated with AD and its related endophenotypes in a female-specific manner.

We further showed that plasma and CSF sST2 levels are positively correlated within the same individual ($R^2 = 0.130$, $P < 0.0001$; $n = 107$ individuals from the Stanford Alzheimer's Disease Research Center (ADRC) cohort[35]; Fig. 1e). Accordingly, we performed a linear regression analysis between CSF sST2 level and AD and Aβ plaque load, adjusting for age, sex and postmortem duration (PMD), followed by multiple testing correction. Concordant with the regulation of plasma sST2 level in AD, in the UK Brain Banks Network (UKBBN) cohort ($n = 11$ HCs, $n = 75$ individuals with AD; Supplementary Data 1), the CSF sST2 level was higher in individuals with AD than in HCs ($\beta = 6.605$, FDR < 0.01; Fig. 1f), with a greater increase in females than that in males (females, $\beta = 7.766$, FDR = 0.034; males, $\beta = 4.019$, FDR = 0.241; Extended Data Fig. 3a). Moreover, CSF sST2 level was positively associated with Aβ plaque load in the frontal cortex in individuals with AD ($\beta = 0.191$, FDR = 0.031; Fig. 1g,h and Supplementary Fig. 1); this association was also stronger in females than in males (females, $\beta = 0.219$, FDR = 0.041; males, $\beta = 0.026$, FDR = 0.787; Extended Data Fig. 3b). Taken together, these findings suggest that sST2 levels in both the blood and CSF are increased in AD and associated with disease progression, specifically in female populations.

sST2 level is associated with a genetic variant of *IL1RL1*. To understand how sST2 is regulated in AD, we examined the contribution of various factors to the changes of sST2 levels. Specifically, we examined the associations between plasma/CSF sST2 levels and sex/age in three independent cohorts including Chinese_cohort_1, comprising HCs and individuals with AD, and a Japanese cohort[36] and a European-descent cohort (that is, INTERVAL and LonGenity cohorts[37]) comprising cognitively normal individuals. Our results show that plasma sST2 level was lower in females than in males ($\beta = -3.577$, $P < 0.001$) and, compared to males (Chinese, $R^2 = 0.001$, $P = 0.866$; European descent, $R^2 = 0.010$, $P = 0.009$), females show a greater association between plasma sST2 level and age (Chinese, $R^2 = 0.037$, $P = 0.002$; European descent, $R^2 = 0.020$, $P < 0.001$; Extended Data Fig. 4a–c). Furthermore, CSF sST2 level was associated with both age and sex in the Japanese cohort, and the association with age, specifically, was greater in females ($R^2 = 0.152$, $P = 0.001$) than in males ($R^2 = 0.044$, $P = 0.081$; Extended Data Fig. 4d). These data suggest that sST2 level is modulated by age and sex in both East Asian and European-descent populations. However, factors such as age and sex accounted for only 6.92% and 13.01% of the variance of plasma sST2 levels and CSF sST2 levels, respectively (Extended Data Fig. 4e,f), suggesting that other factors modulate such differences.

Pilot association studies have identified several genetic variants in the *IL1RL1* gene that are associated with plasma sST2 level[38,39], suggesting that genetic factors contribute to the regulation of sST2 level. Nonetheless, given that these identified SNPs form haplotype structures in this gene region[40], these SNPs might simply be inherited together with the causal variants. Therefore, to identify the key

genetic modulator(s) of sST2, we used our whole-genome sequencing (WGS) dataset[41] of Chinese_cohort_1 to perform a GWAS of plasma sST2 levels, adjusting for age, sex, AD diagnosis and population structure. Accordingly, we identified 575 genetic variants that were significantly associated with plasma sST2 level ($P < 1 \times 10^{-5}$) and found that these variants accounted for 54.86% of the variation thereof (Fig. 2a and Supplementary Fig. 2a). Among these 575 variants, 79 in or near *IL1RL1* that form a haplotype were most strongly associated with sST2 level (Fig. 2b, Supplementary Fig. 2b and Supplementary Data 2), and our fine-mapping analysis identified the sentinel variant rs1921622 (G/A) as the putative causal variant (with 99.9% probability; Supplementary Fig. 2c and Supplementary Table 3). In Chinese_cohort_1, the rs1921622 A allele was associated with a 20% decrease in plasma sST2 level in an allele dose-dependent manner ($\beta = -3.346$, $P < 0.001$; Fig. 2c). Moreover, CSF sST2 level was lower in rs1921622 A allele carriers than in non-carriers (UKBBN cohort; $\beta = -2.244$, $P < 0.05$; Fig. 2d). Notably, rs1921622 alone accounted for 18.04% and 18.29% of the variance in plasma and CSF sST2 levels, respectively, which is greater than the contributions of age and sex. Hence, our fine-mapping analysis using WGS data identified rs1921622 as a key genetic factor that modulates the plasma and CSF levels of sST2.

The rs1921622 locus regulates sST2 in brain endothelial cells. As rs1921622 is a noncoding variant located in the intronic region of ST2L, which is downstream of the region encoding sST2, we examined whether it modulates the expression of sST2 and ST2L. Association analysis using the Genotype-Tissue Expression (GTEx) dataset[42,43] showed that, compared to noncarriers, rs1921622 A allele carriers exhibited a lower transcript level of sST2, but not ST2L, in certain brain regions (for example, hippocampus and frontal cortex; $P < 0.05$; Fig. 3a and Supplementary Table 4). Furthermore, an analysis of our previously released human frontal cortex single-nucleus RNA-sequencing (snRNA-seq) dataset[44] revealed that sST2 is exclusively expressed by endothelial cells (that is, *CLDN5*-expressing cells; Fig. 3b,c). In addition, cell-type-specific association analysis showed that, compared to noncarriers, rs1921622 A allele carriers had a lower endothelial cell sST2 transcript level ($P < 0.01$) and fewer sST2-expressing endothelial cells ($P < 0.05$; Fig. 3d). These results collectively indicate that the rs1921622 variant is associated with decreased sST2 expression in human brain endothelial cells.

To investigate the specific role of rs1921622 in the decreased sST2 expression in endothelial cells, we examined whether rs1921622 and the surrounding genomic region (Fig. 3e) regulate sST2 transcription. Given that noncoding variants commonly modulate gene expression by functioning as enhancer elements[45], we examined enhancer activity at the rs1921622 locus in the human cerebral microvascular endothelial cell line (hCMEC/D3). Administration of the cytokine IL-33 increased the expression and secretion of sST2 in hCMEC/D3 cells (both $P < 0.001$; Supplementary Fig. 3a,b). Moreover, chromatin immunoprecipitation (ChIP) assay showed that these IL-33-treated hCMEC/D3 cells exhibit increased occupancy of an active enhancer histone mark (that is, acetylated

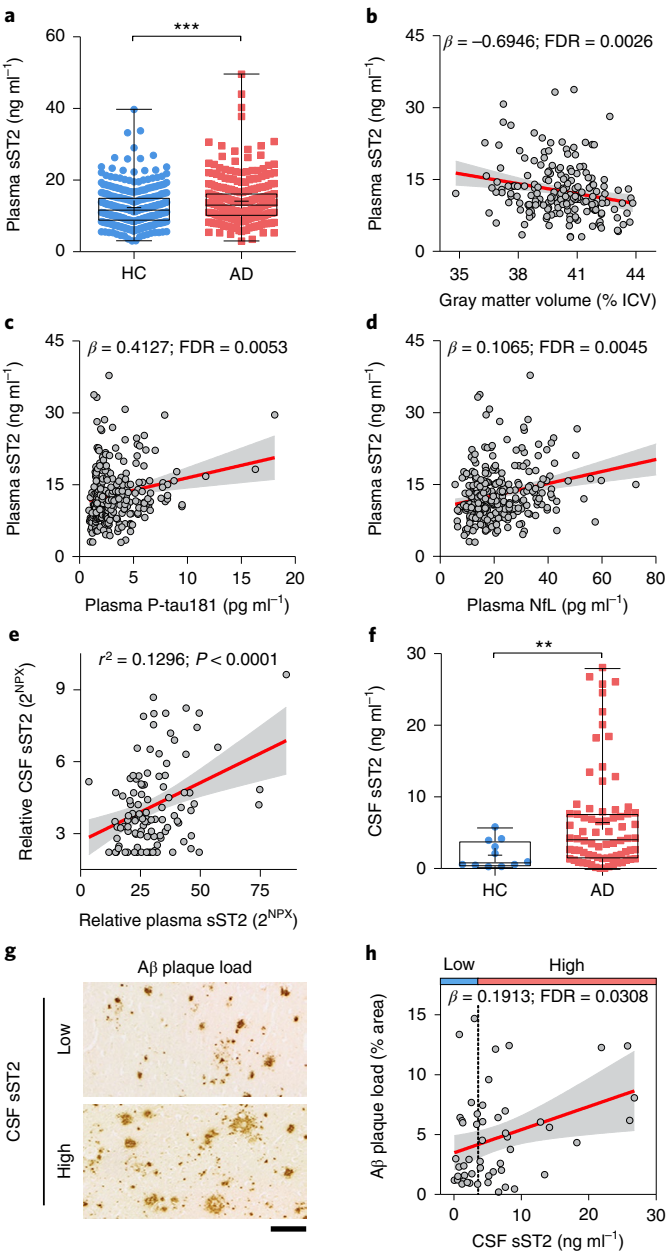

Fig. 1 | Soluble ST2 levels are associated with Alzheimer's disease and its pathological changes. a, Individual plasma sST2 levels stratified by disease phenotype ($n = 336$ HCs, $n = 277$ individuals with AD; Chinese_cohort_1). $\beta = 2.072$. **b**–**d**, Associations between plasma sST2 level and AD-associated endophenotypes in Chinese_cohort_1. **b**, The intracranial volume (ICV)-normalized gray matter volume ($n = 192$). **c**, plasma P-tau181 levels ($n = 290$). **d**, plasma NfL levels ($n = 289$). **e**, Correlation between CSF and plasma levels of sST2 ($n = 66$ HCs, $n = 23$ individuals with MCI, and $n = 18$ individuals with AD; ADRC cohort). Linear regression test, adjusted for age, sex and disease diagnosis. $\beta = 0.049$; r^2, Pearson's correlation coefficient. 2^{NPX}, linear form of normalized protein expression level. **f**, Individual CSF sST2 levels stratified by disease phenotype ($n = 11$ HCs, $n = 75$ individuals with AD; UKBBN cohort). $\beta = 6.605$. **g**,**h**, Associations between Aβ staining in the postmortem frontal cortex and CSF sST2 levels in individuals with AD ($n = 51$ individuals; UKBBN cohort). Individuals were stratified into two groups according to CSF sST2 levels: low, ≤3.6 ng ml^{-1}; high, >3.6 ng ml^{-1}. The vertical dashed line in **h** indicates the CSF sST2 level (3.6 ng ml^{-1}) with the largest Youden's index value for distinguishing HCs from individuals with AD. Representative images of Aβ staining in individuals with AD who had low and high CSF sST2 levels (**g**) and association analysis results (**h**). Scale bar, 100 µm. Data in box-and-whisker plots are presented with maximum, 75th percentile, median, 25th percentile and minimum values; plus signs denote mean values; data in regression lines are presented as the slope (red) and 95% confidence intervals (CIs; gray). Statistical tests for plasma sST2 were performed by linear regression analysis, adjusted for age, sex, CVD status, BMI and education level, with multiple testing correction. Statistical tests for CSF sST2 were performed by linear regression analysis, adjusted for age, sex and PMD, with multiple testing correction. *FDR < 0.05, **FDR < 0.01, ***FDR < 0.001.

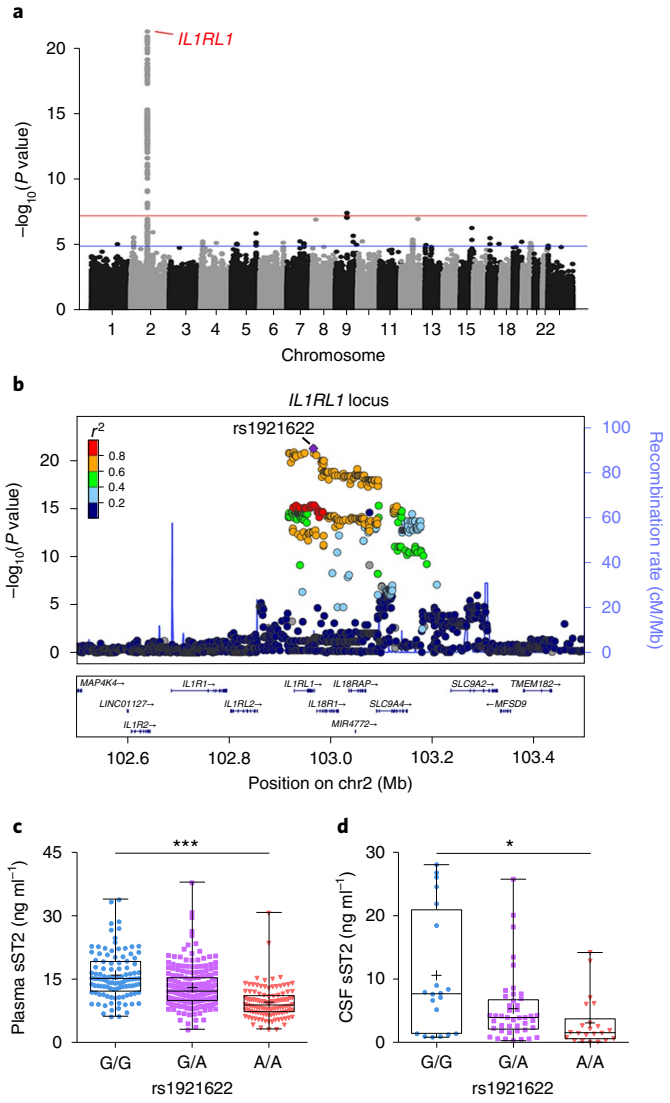

Fig. 2 | The rs1921622 A allele is associated with lower soluble ST2 level. **a**, Manhattan plot showing genetic variants at the *IL1RL1* locus that are associated with plasma sST2 level, as identified by a GWAS of plasma sST2 levels in Chinese_cohort_1. Horizontal lines indicate the suggestive threshold ($P=1\times10^{-5}$, blue) and genome-wide threshold ($P=5\times10^{-8}$, red). Linear regression test, adjusted for age, sex, AD diagnosis and population structure. **b**, Regional association plot of genetic variants at the *IL1RL1* locus and plasma sST2 level. The purple diamond indicates the sentinel variant rs1921622. The color scale indicates the linkage disequilibrium (LD; measured as r^2) between rs1921622 and its neighboring variants. **c**,**d**, Plasma (**c**) and CSF (**d**) sST2 levels in individuals stratified by rs1921622 genotype. Measurement of plasma sST2 level ($n=107$, 206 and 114 G/G, G/A and A/A carriers, respectively; Chinese_cohort_1). Linear regression test, adjusted for age, sex, AD diagnosis and population structure; $\beta=-3.346$, $P=5.35\times10^{-22}$. Measurement of CSF sST2 level ($n=20$, 44 and 22 G/G, G/A and A/A carriers, respectively; UKBBN cohort). Linear regression test, adjusted for age, sex, AD diagnosis and PMD; $\beta=-2.244$, $P=1.06\times10^{-2}$. Data in box-and-whisker plots include maximum, 75th percentile, median, 25th percentile and minimum values; plus signs denote corresponding mean values. $^*P<0.05$, $^{**}P<0.01$, $^{***}P<0.001$.

histone H3 Lys27 (H3K27ac)) at the rs1921622 locus, with a concomitant higher level of trimethylated histone H3 Lys4 (H3K4me3) histone modification (indicating active promoter regions) at the sST2 promoter region (both $P<0.05$; Fig. 3f and Supplementary Fig. 3c). These results suggest that rs1921622 is located at a potential enhancer element of the sST2 gene.

To demonstrate that the genomic region harboring the rs1921622 locus contributes to the regulation of sST2 expression, we deleted this region in hCMEC/D3 cells with a CRISPR–Cas9-based approach. We generated two different hCMEC/D3 cell lines with biallelic 38- or 67-base-pair (bp) deletions (Δ38 bp and Δ67 bp, respectively) encompassing the rs1921622 locus (Fig. 3e and Supplementary Fig. 4). Notably, loss of the 38 or 67 bp flanking the rs1921622 locus decreased the sST2 transcript level in hCMEC/D3 cells ($P<0.001$; Fig. 3g) and concomitantly abolished sST2 protein secretion ($P<0.001$; Fig. 3h). These results suggest that the rs1921622-containing region plays a putative regulatory role as an enhancer element that regulates sST2 expression in endothelial cells.

The rs1921622 A allele protects against Alzheimer's disease in female *APOE*-ε4 carriers. Dysregulation of a specific protein in a disease may indicate that the protein is a causative factor of the disease, or its altered level may simply be due to tissue damage/reaction. Notably, for a protein that is regulated by genetic variants, MR analysis examining the associations between the protein with its genetic modulators and a disease would help illustrate whether the protein has disease-causing effects[46]. Therefore, we investigated the causality between sST2 level and AD risk by examining the associations between the genetic modulators of sST2 (including rs1921622) and AD risk and its related endophenotypes. Specifically, we performed the two-sample MR analysis of sST2 on AD risk using eight AD datasets as the discovery cohorts: the Chinese_cohort_1 dataset, the WGS and array datasets of the Chinese_cohort_2 (ref. [47]) and five public datasets from populations of European descent (that is, the Late Onset Alzheimer's Disease (LOAD)[48], Alzheimer's Disease Center 1–3 (ADC1–3)[49,50] and Alzheimer's Disease Neuroimaging Initiative (ADNI) datasets; $n=5{,}477$ HCs, $n=5{,}910$ individuals with AD; Supplementary Tables 1 and 5). The results show that while sST2 level was not associated with AD risk in all individuals (Chinese, $\beta=-0.023$, FDR = 0.861; European descent, $\beta=0.077$, FDR = 0.131; Fig. 4a and Supplementary Table 6), increased sST2 level was associated with increased AD risk in female *APOE*-ε4 carriers in both Chinese and European-descent populations (Chinese, $\beta=0.772$, FDR $=1.70\times10^{-5}$; European-descent, $\beta=0.168$, FDR = 0.023; Fig. 4a,b and Supplementary Table 6). In particular, among the genetic modulators of sST2, the top variant, the rs1921622 A allele, exerted an AD-protective effect in female *APOE*-ε4 carriers (odds ratio (OR) = 0.757, meta-analysis *P* value using Han and Eskin's random-effects model (RE2 *P*)[51] $=7.78\times10^{-5}$, FDR $=5.44\times10^{-4}$; Fig. 4c), whereas this effect is absent in the overall population (OR = 0.942, RE2 $P=0.044$, FDR = 0.102) or other subgroups including male *APOE*-ε4 carriers (OR = 1.086, RE2 $P=0.412$, FDR = 0.577), male *APOE*-ε4 noncarriers (OR = 0.960, RE2 $P=0.586$, FDR = 0.684) and female *APOE*-ε4 noncarriers (OR = 0.961, RE2 $P=0.233$, FDR = 0.408; Supplementary Tables 7 and 8). Interestingly, both the MR analysis of sST2 and the meta-analysis of rs1921622 showed that the associations between AD risk and sST2/rs1921622 in female *APOE*-ε4 carriers are stronger in the Chinese population than those in the European-descent populations (Chinese versus European descent, $P=5.55\times10^{-4}$ and 0.017 for the MR analysis of sST2 and meta-analysis of rs1921622, respectively; Fig. 4a–c and Supplementary Tables 6–8), suggesting an ethnic-specific effect of sST2/rs1921622 in modulating AD risk.

Next, we examined the effects of the rs1921622 A allele on the AD-associated endophenotypes in the discovery cohorts. Consistent with its AD-protective effects (Supplementary Table 9), the rs1921622 A allele was associated with delayed onset age of dementia (hazard ratio (HR) = 0.874, FDR = 0.011; Fig. 5a), better cognitive scores ($\beta=1.622$, FDR = 0.001; Fig. 5b) and larger ento-

rhinal cortex volumes ($\beta = 0.214$, FDR = 0.027; Fig. 5c) in female *APOE*-ε4 carriers.

To further confirm the AD-protective effects of the rs1921622 A allele, we examined AD-related endophenotypes in an independent replication cohort: the Australian Imaging, Biomarkers and Lifestyle cohort (AIBL; $n = 190$), in which the Aβ deposition (that is, $A\beta^+$) in the brains of individuals was confirmed by positron emission tomography[52]. Concordant with our findings from the discovery cohorts, in female $A\beta^+$ *APOE*-ε4 carriers, the presence of the rs1921622 A allele was associated with improved cognitive performance as indicated by AIBL Preclinical Alzheimer Cognitive Composite (AIBLPACC) score and scores related to cognitive subprocesses including attention processing, episodic recall and recognition (all FDR < 0.05; Fig. 5d and Extended Data Fig. 5). Importantly, in a subgroup of female $A\beta^+$ *APOE*-ε4 carriers whose gray matter volume was traced for 7 years, rs1921622 A allele carriers showed a slower progression of gray matter atrophy ($\beta = -0.027$) than that in noncarriers ($\beta = -0.159$; FDR < 0.05; Fig. 5e and Extended Data Fig. 6). Thus, these results validate the protective effects of the rs1921622 A allele against cognitive decline and gray matter atrophy among female *APOE*-ε4 carriers in an independent $A\beta^+$ cohort.

The rs1921622 A allele is associated with microglial activation in female *APOE*-ε4 carriers with Alzheimer's disease. Given our findings that the rs1921622 A allele exerts AD-protective effects in female *APOE*-ε4 carriers, we subsequently examined whether this variant modulates Aβ deposition in postmortem human brains. Among individuals with AD, specifically in females, the *APOE*-ε4 carriers exhibited greater Aβ deposition in the frontal cortex than that in the *APOE*-ε4 noncarriers (females, $\beta = 1.967$, $P < 0.05$; males, $\beta = -0.621$, $P = 0.422$; Extended Data Fig. 7a,b). However, upon further stratification by rs1921622 genotype, female *APOE*-ε4 carriers harboring the rs1921622 A allele exhibited less Aβ deposition than those without the allele ($\beta = -2.262$, $P < 0.05$; Fig. 6a,b and Extended Data Fig. 7c), suggesting that this allele attenuates the effects of *APOE*-ε4 on Aβ-related pathological changes in females. Moreover, immunohistochemical analysis revealed that harboring *APOE*-ε4 in AD is associated with less microglial coverage of Aβ plaques (that is, decreased proportion of Aβ colocalized with Iba-1^+ microglia) in females (females, $\beta = -2.818$, $P < 0.01$; males, $\beta = -0.965$, $P = 0.327$; Extended Data Fig. 7d,e). In contrast, female *APOE*-ε4 carriers with AD who co-harbored the rs1921622 A allele showed increased colocalization between Iba-1^+ microglia and Aβ plaques ($\beta = 2.017$, $P < 0.05$; Fig. 6c,d and Extended Data Fig. 7f,g). Thus, these results suggest that in female *APOE*-ε4 carriers with AD, the rs1921622 A allele is associated with enhanced microglia–Aβ interaction and decreased Aβ pathological lesions.

Next, to investigate the regulatory effects of rs1921622 on microglial activities at the molecular level, we conducted an association analysis using the microglial snRNA-seq dataset in the frontal cortices[44]. We found a negative correlation between the effects of the rs1921622 A allele and the effects of CSF sST2 level on modulating microglial gene expression in female *APOE*-ε4 carriers with AD ($R^2 = 0.860$, $P < 0.0001$; Extended Data Fig. 8), supporting the notion that the variant exerts its modulatory effects on microglia through the regulation of CSF sST2 level. Specifically, we identified 1,639 microglial genes that were associated with rs1921622 genotype: 428 and 1,211 genes were upregulated and downregulated, respectively, in individuals carrying the rs1921622 A allele compared to noncarriers (FDR < 0.05; Fig. 6e). Gene Ontology (GO) analysis showed that those upregulated genes are associated with leukocyte migration ($FDR = 1.2 \times 10^{-4}$) and innate immune response ($FDR = 5.4 \times 10^{-3}$), whereas those with downregulated expression are mainly involved in protein refolding ($FDR = 8.1 \times 10^{-3}$) or mRNA splicing ($FDR = 7.7 \times 10^{-2}$; Fig. 6f).

Recent studies of microglia in mouse and human brains revealed a subset of 'microglial activation genes', including *CD74*, *APOE* and *TREM2*, whose expressions are upregulated in AD[53,54] and which are involved in microglial Aβ phagocytosis[4,55,56]. Therefore, we investigated whether these genes are associated with rs1921622. Interestingly, among female *APOE*-ε4 carriers with AD, the rs1921622 A allele was associated with increased expression of these microglial activation genes—specifically, increased transcript levels of *CD74*, *APOE* and *TREM2* in microglia as well as an increased proportion of *TMEM163*$^+$ microglia (Fig. 6g). In contrast, the rs1921622 A allele was associated with decreased expression of homeostatic genes including *SRGAP2*, *TMEM119* and *P2RY12*, whose expressions commonly indicate a less-reactive microglial state[4,55] (Fig. 6g). Therefore, these results suggest that the rs1921622 A allele promotes the transition of microglia to a more activated state in female *APOE*-ε4 carriers with AD.

sST2 treatment impairs microglial Aβ-clearance capacity in female mouse brains. Our genetic analyses showed that sST2 and its genetic modulators modulate AD risk and related pathologies possibly by regulating microglial activation and Aβ clearance. To verify the pathogenic roles of sST2 in AD, we examined the effect of sST2 injection on Aβ-associated pathological changes in an amyloidosis transgenic 5XFAD mouse model (Fig. 7a). Intracerebroventricular administration of mouse sST2 to 3-month-old 5XFAD mice for 28 d increased the Aβ plaque burden in the cortical regions of female ($P < 0.05$; Fig. 7b,c) but not male transgenic mice (Extended Data Fig. 9). In particular, the quantities of both the filamentous form (that is, X-34^+ diffuse fibrils without a dense core[57]) and the compact form (that is, X-34^+ dense cores with 4G8 halos) of Aβ plaques were increased in sST2-treated female 5XFAD mice ($P < 0.05$; Fig. 7d,e

Fig. 3 | Target deletion at rs1921622 decreases soluble ST2 expression and secretion in brain endothelial cells. a, Effects of rs1921622 on sST2 transcript levels in human tissues. Boxes and lines indicate the effect size and 95% CIs of the rs1921622 A allele for each tissue, respectively (Supplementary Table 4). Red and blue indicate significant ($P < 0.05$) and nonsignificant ($P \geq 0.05$) associations, respectively. Linear regression test, adjusted for age, sex, RNA integrity and population structure. **b**–**d**, snRNA-seq analysis revealed an association between rs1921622 and sST2 transcript level in brain endothelial cells. **b**, Uniform manifold approximation and projection (UMAP) plot showing cell types in the human frontal cortex ($n = 169{,}496$ cells from 21 individuals; UKBBN cohort). Excit, excitatory neurons; Inhibit, inhibitory neurons; Astro, astrocytes; Mic, microglia; Endo, endothelial cells; Oligo, oligodendrocytes; OPCs, oligodendrocyte progenitor cells. **c**,**d**, Expression profiles (**c**) and dot plots (**d**) of *sST2* and *CLDN5* transcripts in the endothelial cells, stratified by rs1921622 genotype. Norm. exp., normalized expression. **e**, CRISPR–Cas9 genome-editing strategy and locations of the two single-guide RNA (sgRNA) pairs for 67-bp deletion (Δ67 bp) and 38-bp deletion (Δ38 bp) targeting the rs1921622-harboring region (red). **f**, H3K27ac analysis of the rs1921622 locus in hCMEC/D3 cells after IL-33 administration for 24 h ($n = 3$ per group). $T = 4.593$, $P = 1.01 \times 10^{-2}$. **g**,**h**, Deletion of the rs1921622 locus decreases transcript level and protein secretion of sST2 in hCMEC/D3 cells. **g**, sST2 transcript levels ($n = 6$, 8 and 10 clones for isogenic control, Δ38 bp and Δ67 bp, respectively). For Δ38 bp versus control, $T = -5.444$, $P = 1.00 \times 10^{-4}$; Δ67 bp versus control, $T = -7.612$, $P < 1.00 \times 10^{-4}$. **h**, Levels of sST2 protein in conditioned medium (CM; $n = 3$, 3 and 4 clones for isogenic control, Δ38 bp and Δ67 bp, respectively). For Δ38 bp versus control: $T = -13.450$, $P = 2.00 \times 10^{-4}$; Δ67 bp versus control: $T = -16.030$, $P < 1.00 \times 10^{-4}$. Data in bar charts are the mean + s.e.m. Statistical tests for **f**–**h** were performed as two-sided unpaired Student's *t*-tests. $^*P < 0.05$, $^{**}P < 0.01$, $^{***}P < 0.001$.

and Supplementary Fig. 5). However, sST2 administration did not affect the burden of less-toxic inert Aβ plaques (that is, X-34$^+$ dense cores without 4G8 labeling) or the total number of Aβ plaques.

Next, we examined how sST2 regulates the interactions between microglia and Aβ plaques. In female 5XFAD mice, sST2 injection increased the total number of microglia, the clustering of microglia around Aβ plaques, and the number of proliferating (Ki67$^+$) microglia in the cortical regions (all $P < 0.05$; Supplementary Fig. 6), suggesting that sST2 treatment promotes the proliferation of microglia in the brain. However, compared to the vehicle-injected

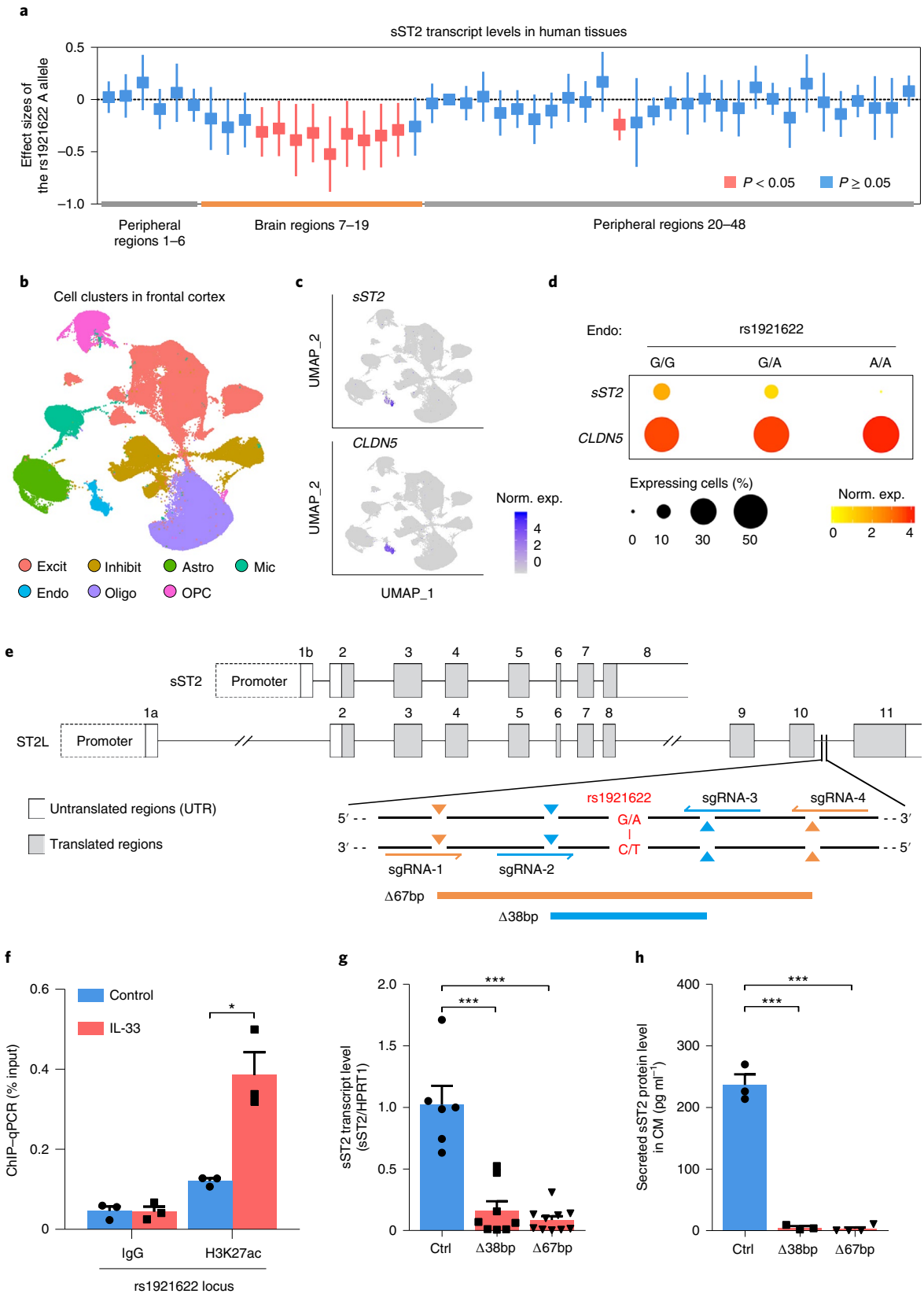

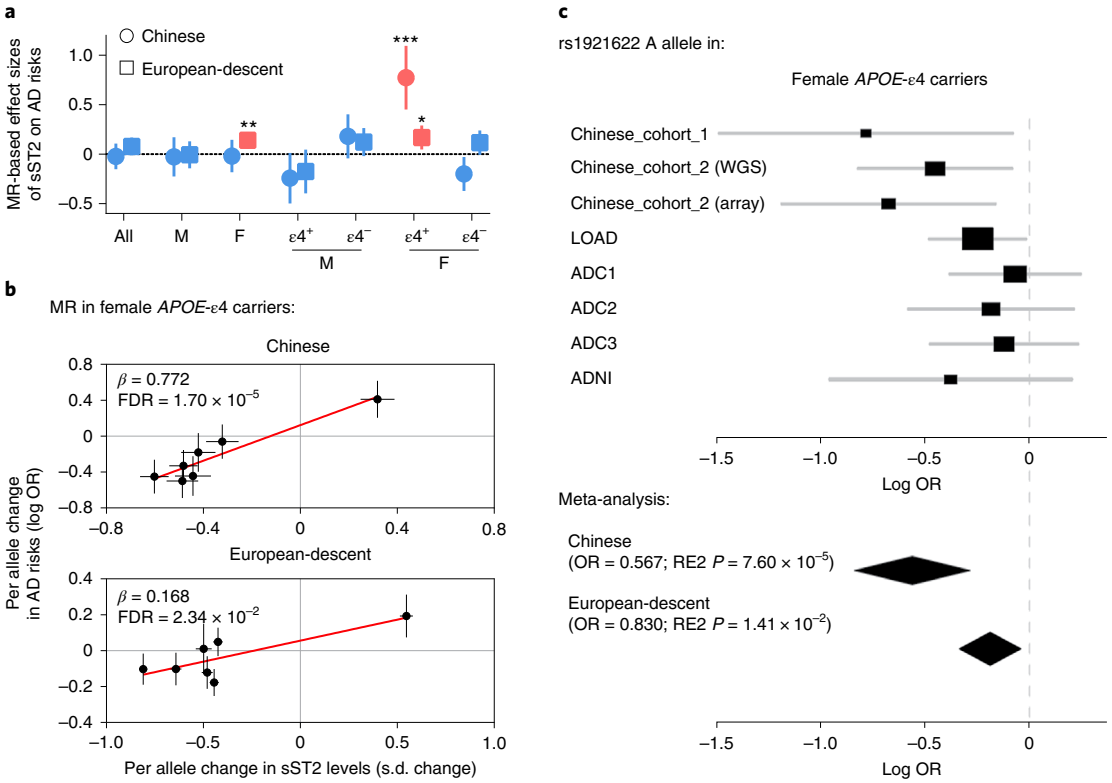

Fig. 4 | The rs1921622 A allele is associated with decreased Alzheimer's disease risk in female *APOE*-ε4 carriers. a, Two-sample MR analysis showing the effects of sST2 levels on AD risk in Chinese (circle) and European-descent (box) populations. Circles/boxes and lines indicate the effect sizes of sST2 and 95% CIs in each subgroup, respectively (Supplementary Table 6). Red and blue indicate significant (FDR < 0.05) and nonsignificant (FDR ≥ 0.05) associations, respectively. All, overall population; M, male; F, female; ε4+, *APOE*-ε4 carriers; ε4−, *APOE*-ε4 noncarriers. **b**, Two-sample MR analysis showing the associations between sST2 level and AD risk in female *APOE*-ε4 carriers in Chinese and European-descent populations. Circles and lines indicate the effect sizes and standard errors of each SNP, respectively. **c**, Forest plot showing the meta-analysis results of the rs1921622 A allele on AD risk in female *APOE*-ε4 carriers ($n = 912$ HCs, $n = 1{,}898$ individuals with AD). Rectangles and diamonds denote the effect sizes (log OR) obtained from independent datasets and meta-analysis, respectively. For the independent datasets, horizontal lines indicate 95% CIs, and rectangle size is proportional to the weight used in the meta-analysis. RE2 *P*, meta-analysis *P* value using Han and Eskin's random-effects model. *FDR < 0.05, **FDR < 0.01, ***FDR < 0.001.

condition, the cortical regions in sST2-injected female 5XFAD mice showed reduced microglial coverage of Aβ plaques (Fig. 7f,g, Supplementary Fig. 7 and Supplementary Video 1), suggesting that sST2 injection inhibits the microglial barrier formation around Aβ plaques. To verify the inhibitory effects of sST2 on microglial Aβ clearance, flow cytometry analysis showed that sST2 administration decreases the Aβ-phagocytic capacity of microglia as indicated by a decrease in the percentage of $Aβ^+$ microglia (that is, 23.57% methoxy-X04$^+$CD11b$^+$ microglia in the sST2-treated group versus 32.79% in the control group; $P < 0.01$; Fig. 7h,i and Supplementary Fig. 8) and an 11.3–17.0% decrease in Aβ uptake by microglia ($P < 0.05$; Extended Data Fig. 10). Together, these findings demonstrate that increased brain sST2 level impairs microglial Aβ-clearance capacity and exacerbates Aβ accumulation in female transgenic mice, suggesting its pathogenic roles in female AD.

Discussion

Here, we report that an endothelial cell-secreted protein, sST2, is upregulated in female individuals with AD. Meanwhile, endothelial expression of sST2 can be downregulated by the rs1921622 A allele, a genetic variant that exerts an AD-protective effect specifically in female *APOE*-ε4 carriers, a subgroup of people accounting for 24.3–33.6% and 32.5–50.4% of individuals with AD in Chinese and European-descent populations, respectively (Supplementary Tables 1 and 5). This variant is also associated with enhanced microglial activation, increased microglia–Aβ plaque interaction and decreased Aβ deposition. Taken together, we demonstrate that sST2 regulates microglial activities and that changes in sST2 levels in the brain milieu impair microglial Aβ-clearance capacity, thus modulating AD risk and its pathological changes.

As sST2 only comprises the extracellular domain of the functional receptor ST2L and is independently transcribed[22], it is a decoy receptor for IL-33–ST2 signaling. ST2L expression is mainly found in microglia in the brains of both humans and mice[58–60], and IL-33–ST2 signaling regulates microglial activities in tissue repair, Aβ clearance and synapse engulfment[24,25,61,62]. The expression profile of sST2 differs between humans and mice: in humans, sST2 is expressed by brain and peripheral endothelial cells[63–65] and monocytes/macrophages[60,66], mast cells[67] and T cells[68] in peripheral systems; while in mice, sST2 is expressed by microglia in the brain[59] and fibroblasts[69], mast cells[67] and T cells[68] in peripheral systems. However, given that sST2 is a secreted protein in the circulatory system[24,70], increased sST2 level likely impacts microglial functions and AD-related pathological changes in both humans and mice by blocking the binding of IL-33 to ST2L on microglia. In this study, sST2 treatment perturbed the interaction between microglia and Aβ as well as the subsequent Aβ phagocytosis in a mouse model of amyloidosis (Fig. 7). This finding is consistent with our previous observation that in these mice, IL-33 administration activates IL-33–ST2 signaling and initiates microglial chemotaxis toward Aβ plaques, subsequently enhancing Aβ phagocytosis[24,25]. Further corroborating the pathological role of sST2 in microglia in AD, among

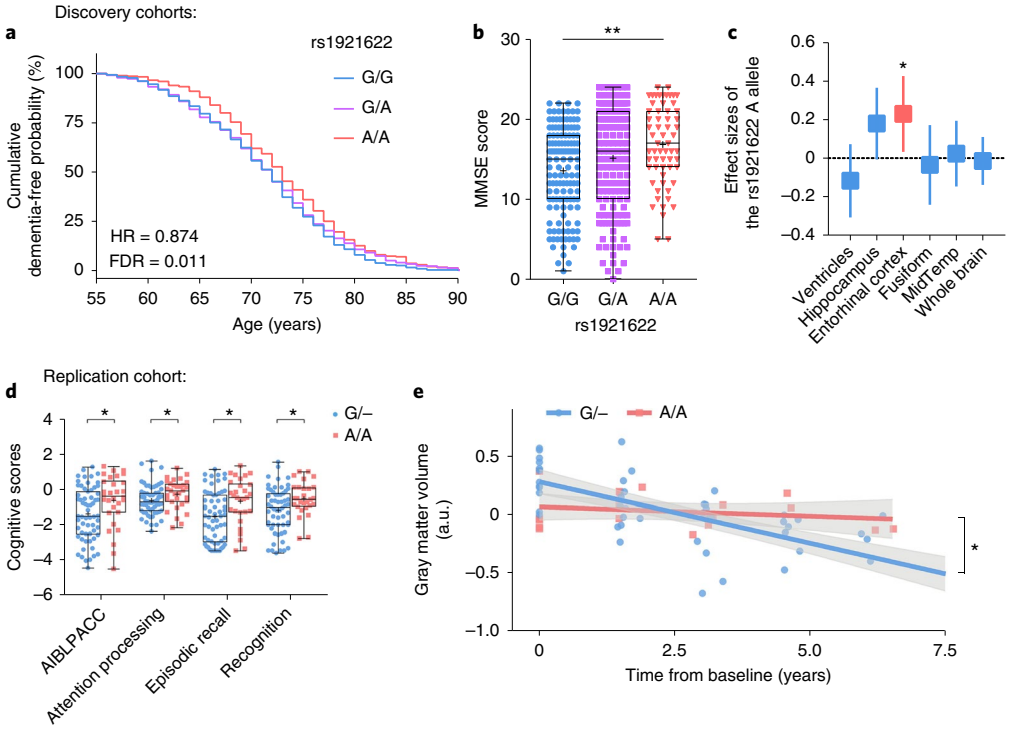

Fig. 5 | The rs1921622 A allele is associated with changes of Alzheimer's disease-related endophenotypes in female *APOE*-ε4 carriers. a, Cumulative dementia-free probability in female *APOE*-ε4 carriers with AD stratified by rs1921622 genotype ($n = 314$, 568 and 300 G/G, G/A and A/A carriers, respectively; LOAD and ADC1–3 cohorts). Cox regression test, adjusted for population structure, with multiple testing correction. **b**, Individual Mini-Mental State Exam (MMSE) scores of female *APOE*-ε4 carriers with AD stratified by rs1921622 genotype ($n = 131$, 158 and 61 G/G, G/A and A/A carriers, respectively; Chinese_cohort_2). Linear regression test, adjusted for age and population structure, with multiple testing correction. $\beta = 1.622$. **c**, Effect size of the rs1921622 A allele on brain region volume in female *APOE*-ε4 carriers with cognitive impairment ($n = 38$, 86 and 57 G/G, G/A and A/A carriers, respectively; ADNI cohort). Linear regression test, adjusted for age, ICV, magnetic resonance imaging (MRI) platforms, dementia stages and population structure, with multiple testing correction. Data are presented as effect sizes (boxes) and 95% CIs (lines). Red and blue indicate significant (FDR < 0.05) and nonsignificant (FDR ≥ 0.05) associations, respectively. Fusiform, fusiform gyrus; MidTemp, middle temporal gyrus. **d**, Individual cognitive scores in female Aβ+ *APOE*-ε4 carriers stratified by rs1921622 genotype ($n = 59$ G carriers (G/–), $n = 29$ A/A carriers; AIBL cohort). Wilcoxon rank-sum test, with multiple testing correction. $W = 1087.0$, 1115.5, 1083.0 and 916.5 for AIBLPACC, attention processing, episodic recall and recognition scores, respectively. **e**, Longitudinal gray matter volume in female Aβ+ *APOE*-ε4 carriers stratified by rs1921622 genotype ($n = 50$ and 19 data points from 12 G carriers (G/–) and 5 A/A carriers, respectively; AIBL cohort). Linear mixed model test; adjusted for baseline age and MRI scanners, with multiple testing correction. $\beta = -0.159$ (G/–) and −0.027 (A/A); $F = 8.804$. Data in box-and-whisker plots are presented with maximum, 75th percentile, median, 25th percentile and minimum values; plus signs denote mean values; data in regression lines are presented as the slope (red/blue) and 95% CIs (gray). *FDR < 0.05, **FDR < 0.01, ***FDR < 0.001. a.u., arbitrary units.

female *APOE*-ε4 carriers with AD, those carrying the rs1921622 A allele (who have lower sST2 levels) exhibit enhanced microglia–Aβ plaque interactions and a smaller Aβ plaque area than noncarriers. Thus, perturbation of endogenous IL-33–ST2 signaling by sST2 may lead to impaired microglial chemotaxis, Aβ uptake and barrier formation, which subsequently contribute to AD pathogenesis.

What are the regulatory mechanisms of sST2? In mice, sST2 expression is regulated by a proximal promoter located upstream of the 5′ untranslated region of sST2, which is increased by oncogenes, serum and other mitogenic stimuli[69]. While the regulatory mechanisms of sST2 expression might be different between humans and mice, sST2 regulation in humans remains largely unknown. Our analyses in Chinese and European-descent populations corroborate findings from previous studies that sST2 levels in humans are associated with age, sex and genetic variants[37,38], and reveal that genetic components play a dominant role in the regulation of sST2 levels, accounting for 54.86% of the variance of these levels. In particular, our GWAS and fine-mapping analyses identified rs1921622 as a putative causal variant associated with sST2 (causal probability of 99.99%), and our ChIP assay and CRISPR–Cas9 genome editing verified that the rs1921622-containing region is an enhancer element that regulates the sST2 gene in endothelial cells. Thus, as rs1921622 is a key genetic modulator of sST2, future investigations of the epigenetic events at the rs1921622 locus may help elucidate the regulatory mechanisms of sST2.

Single-nucleus transcriptomic profiling of postmortem human brains shows that sST2 is mainly expressed in brain endothelial cells (Fig. 3). Dysregulation of sST2 in the brain exacerbates AD-associated pathological changes, specifically by impairing the phagocytic capacity of microglia. Thus, we demonstrate a new pathogenic role of the brain vasculature in AD that regulates microglial activities via sST2. Indeed, apart from Aβ and tau-related pathological changes, neurovascular dysfunction occurs early in AD and is implicated in its pathogenesis[71]. While the exact pathological functions of this brain vasculature remain unclear, vasculature-secreted cytokines (for example, CXCL1) in the peripheral system regulate the activation and migration of immune cells, thereby mediating the immune response in tissues[72]. Similarly, emerging studies suggest that the brain vasculature serves as a critical source of soluble inflammatory proteins such as IL-1β, IL-6, IL-8, tumor necrosis factor, transforming growth factor and monocyte chemoattractant protein-1 (refs. [73,74]). Therefore, besides sST2, other soluble factor-based

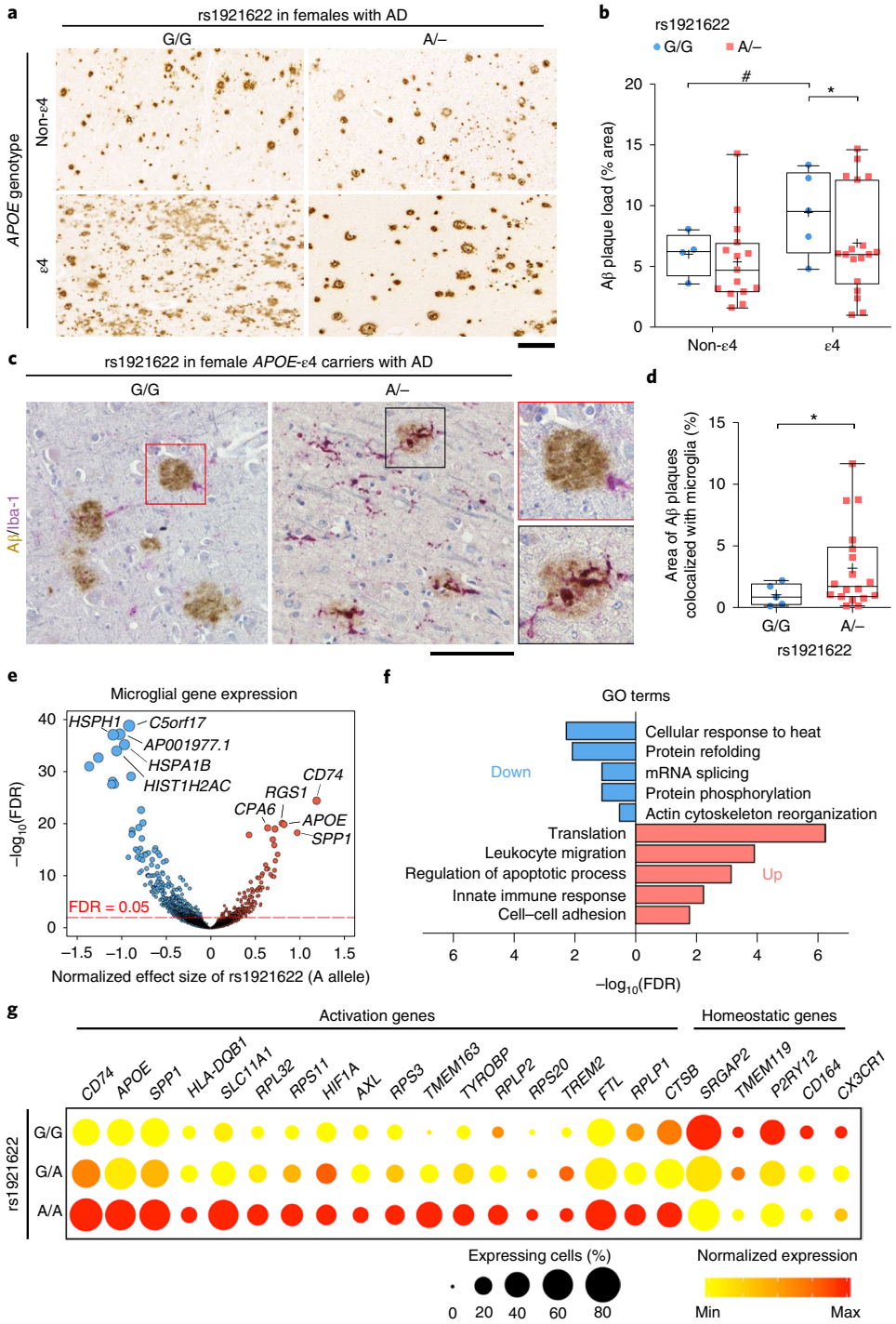

Fig. 6 | The rs1921622 A allele enhances microglial activities toward Aβ in female *APOE*-ε4 carriers with Alzheimer's disease. a,**b**, Representative images (**a**) and quantification (**b**) showing Aβ plaque area in the frontal cortices of females with AD stratified by *APOE*-ε4 and rs1921622 genotypes ($n = 4$ G/G carriers and 15 A carriers (A/−) among *APOE*-ε4 noncarriers (non-ε4); $n = 5$ G/G carriers and 18 A/− carriers among *APOE*-ε4 carriers (ε4); UKBBN cohort). Test for effects of *APOE*-ε4: $\beta = 3.448$ (G/G) and 1.549 (A/−), $P = 4.83 \times 10^{-2}$ (G/G) and 2.54×10^{-1} (A/−); test for effects of rs1921622, $\beta = 0.288$ (non-ε4) and −2.262 (ε4), $P = 7.02 \times 10^{-1}$ (non-ε4) and 3.71×10^{-2} (ε4). Scale bar, 200 μm. **c**,**d**, Representative images (**c**) and quantification (**d**) showing colocalization between Aβ plaques (brown) and Iba-1$^+$ microglia (purple) in the frontal cortices of female *APOE*-ε4 carriers with AD stratified by rs1921622 genotype ($n = 5$ G/G carriers, $n = 18$ A/− carriers; UKBBN cohort). $\beta = 2.017$, $P = 2.53 \times 10^{-2}$. Scale bar, 100 μm. **e**, Volcano plot showing the associations between rs1921622 and microglial genes in the frontal cortices of female *APOE*-ε4 carriers with AD ($n = 2{,}636$ microglia of eight individuals; UKBBN cohort). Blue and red dots indicate microglial genes that were negatively and positively associated with the rs1921622 A allele, respectively. Dot size is proportional to FDR ($\log_{10}$ scale). The top five negatively and positively associated genes are labeled. **f**, Representative GO terms enriched in the rs1921622-associated microglial genes. Blue and red indicate GO terms enriched for the downregulated and upregulated genes, respectively, in rs1921622 A allele carriers. **g**, Dot plot showing the expression levels of microglial activation genes and homeostatic genes stratified by rs1921622 genotype. Data in box-and-whisker plots are presented with maximum, 75th percentile, median, 25th percentile and minimum values; plus signs denote mean values. Statistical tests were performed by linear regression analysis, adjusted for age and PMD. $^*P < 0.05$, $^{**}P < 0.01$, $^{***}P < 0.001$; $^{\#}P < 0.05$, $^{\#\#}P < 0.01$, $^{\#\#\#}P < 0.001$.

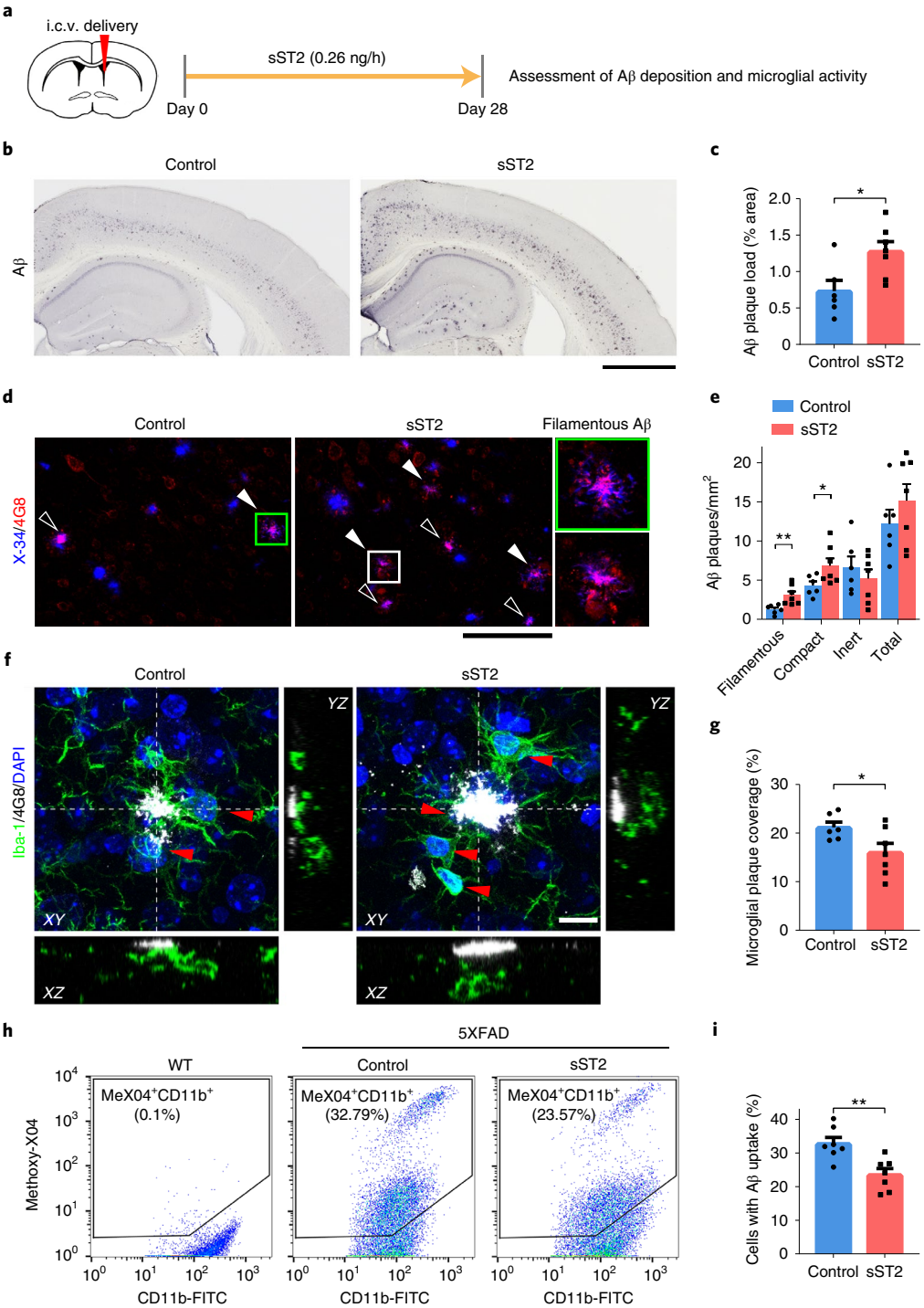

Fig. 7 | Increased brain soluble ST2 levels exacerbate Aβ accumulation and impair microglial Aβ clearance in female 5XFAD mice. **a**, Intracerebroventricular (i.c.v.) delivery of sST2 to 3-month-old 5XFAD mice. **b**–**e**, Aβ deposition in the cortices of 4-month-old female 5XFAD mice after i.c.v. delivery of sST2-Fc or Fc as a control. **b**,**c**, Representative images (**b**) and quantification (**c**) of Aβ plaques (percentage of total cortical area; control $n=6$ mice, sST2 $n=7$ mice). $T=2.758$, $P=1.86\times10^{-2}$. Scale bar, 1 mm. **d**, Confocal images of X-34-stained (blue) and 4G8-labeled (red) Aβ. Filamentous (filled arrowheads) and compact (hollow arrowheads) Aβ plaques. Scale bar, 100 µm. **e**, Quantification of filamentous, compact, inert and total Aβ plaques (control $n=6$ mice, sST2 $n=7$ mice). $T=3.235$, 2.274, −0.770 and 1.050, respectively; $P=7.95\times10^{-3}$, 4.40×10^{-2}, 4.57×10^{-1} and 3.16×10^{-1}, respectively. **f**, Merged confocal *z*-stack images with orthogonal *X*–*Z* and *Y*–*Z* views showing co-staining of 4G8-labeled Aβ plaques (white) and Iba-1$^+$ microglia (green; red arrowheads indicate microglial soma) in the cortices of 4-month-old female 5XFAD mice after i.c.v. delivery of sST2-Fc or Fc as a control (single-channel images in Supplementary Fig. 7). Scale bar, 10 µm. **g**, Quantification of microglial coverage of Aβ plaques (control $n=6$ mice, sST2 $n=7$ mice). $T=-2.298$, $P=4.22\times10^{-2}$. **h**,**i**, Microglial Aβ uptake activity in the cortices of 4-month-old female 5XFAD mice after i.c.v. delivery of sST2-Fc or Fc as a control. Representative scatterplots (**h**) and quantification (**i**) show the percentages of CD11b$^+$ cells containing methoxy-X04-labeled Aβ (control $n=7$ mice, sST2 $n=7$ mice; gating strategy in Supplementary Fig. 8). $T=-3.620$, $P=3.50\times10^{-3}$. The scatterplots of wild-type (WT) mice in **h** were used to gate methoxy-X04$^+$ microglia (that is, MeX04$^+$CD11b$^+$ cells). Data in bar charts are the mean + s.e.m. Statistical tests were performed as two-sided unpaired Student's *t*-tests. $^*P<0.05$, $^{**}P<0.01$, $^{***}P<0.001$.

cross-talk between the vasculature and other cell types likely occurs in the brain. Accordingly, identifying the proteins involved in this cross-talk may provide insights into novel pathological mechanisms of AD.

We show that sST2 plays a disease-causing role in AD in a female-specific manner. Indeed, emerging evidence suggests that sex is an important factor that underlies the heterogeneity of AD;[75] compared to males, females are more likely to develop AD[76] and experience faster cognitive decline after an MCI or AD diagnosis[76,77]. Given that sST2 inhibits IL-33–ST2 signaling and microglial activities, this sex-specific causal effect of sST2 in AD may be attributed to the differential regulation of IL-33–ST2 signaling and differential microglial activities between sexes. Concordant with previous studies[78], we show that microglia in female individuals with AD, particularly those who carry *APOE*-ε4, have significantly lower Aβ phagocytic capacity when compared to male individuals (Extended Data Fig. 7). Meanwhile, compared to males, females show a greater increase of sST2 upon AD development. Hence, it would be interesting to examine whether increased sST2 level in female brains exhibits a stronger inhibitory effect on microglial activities and impairs their Aβ-clearance capacity. Moreover, sex hormones (for example, testosterone) regulate IL-33 expression in mast cells, maintaining a higher activity of IL-33–ST2 signaling in men[79], which might protect men from being affected by increased sST2 levels. Together, increased sST2 levels, resulting from aging or the absence of the rs1921622 A allele, might have more detrimental impacts in microglial activities and functions in females, eventually leading to a greater risk of AD. Therefore, investigating the underlying mechanisms of this female-specific, disease-causing role of sST2 may be key to understanding the differential progression of AD between sexes.

In addition to its female-specific effects, our genetic analyses demonstrate that sST2/rs1921622 plays disease-causing effects in females with AD, specifically those carrying *APOE*-ε4, suggesting a potential interaction between IL-33–ST2 signaling and ApoE. In the brain, ApoE is mainly produced by astrocytes, and its expression is upregulated in microglia in AD[53,80]. Single-cell RNA-seq of amyloidosis mouse models revealed that a microglial subpopulation transitions from a homeostatic state to an activated state termed 'disease-associated microglia' or 'activated response microglia'[4,55], with increased expression of microglial activation genes (including *APOE*, *AXL*, *TREM2* and *CD74*)[53–56] that are crucial regulators of phagocytic processes[81–84]. In contrast, perturbation of ApoE functions in the brain abolishes the induction of this microglial activation state, resulting in reduced Aβ phagocytic capacity[4,55]. Thus, ApoE-mediated microglial activation may protect against AD and be required for Aβ clearance and brain homeostasis. Notably, the presence of the rs1921622 A allele modulates the transition of microglia from a homeostatic state to a more activated state in female *APOE*-ε4 carriers with AD, characterized by the increased expression of the aforementioned microglial activation genes (Fig. 6). Therefore, IL-33–ST2 signaling and ApoE might converge to regulate the expression of these specific genes in microglia, thereby modulating the activation state and Aβ-clearance capacity of microglia. Interestingly, in the periphery, IL-33 administration ameliorates the formation of macrophage foam cells (lipid-laden macrophages) and the development of atherosclerotic plaques in the ApoE$^{-/-}$ model of atherosclerosis[85]. Therefore, it would be of interest to determine whether the modulation of IL-33–ST2 signaling reduces the detrimental effects of *APOE*-ε4 on Aβ accumulation through the regulation of lipid metabolism in AD.

Our findings suggest that sST2 is a promising therapeutic target for AD. First, as sST2 is mainly expressed by endothelial cells, this enables cell-type-specific manipulation of sST2 expression, and that manipulation may not need to cross the blood–brain barrier. Second, sST2 levels are elevated in individuals with MCI or early-stage AD[24,32], suggesting the potential applicability of sST2 in early intervention strategies. Third, the deletion of the rs1921622 locus in a human brain endothelial cell line with high efficacy demonstrates the feasibility of this approach to silence sST2 expression and secretion without disrupting the activities of ST2L; this is because the epigenetic and transcriptional controls of sST2 are distinct from those of ST2L[86], and the rs1921622 A allele only modulates sST2 but not ST2L expression. Fourth, given our finding that the rs1921622 A allele is a common AD-associated variant, manipulations of sST2 by targeting this genetic variant could be developed for specific subgroups of individuals who have high sST2 levels (for example, female individuals who carry *APOE*-ε4 but not the rs1921622 A allele, accounting for 6.2–12.2% of individuals with AD), enabling patient stratification and precision medicine.

Nonetheless, there are some knowledge gaps regarding the functions and regulation of sST2 in AD. First, while MR analysis of cross-sectional studies shows that sST2 plays a causal role in AD, longitudinal studies investigating the associations between sST2 level and cognitive decline and/or AD risk in cognitively normal populations would help support the notion that sST2 has disease-causing effects in AD. Meanwhile, given that such effects are only observed in female *APOE*-ε4 carriers, they are likely masked in recent genetic studies of AD, in both the overall population ($P=0.881$)[87] and *APOE*-ε4 carriers ($P=0.798$)[88]. Therefore, stratification of AD datasets according to sex and *APOE*-ε4 genotypes may help to better investigate the disease effects of sST2 or other AD-associated factors. Moreover, as we observed that sST2/rs1921622 has stronger modulatory effects on AD risks in the Chinese population than in the European-descent populations, validation of this finding by future studies using larger datasets would help clarify this potential ethnic-specific effect of sST2. Lastly, while an increased brain level of sST2 contributes to AD pathogenesis, given the positive correlation between plasma and CSF sST2 levels, it would be interesting to examine whether peripheral sST2, produced by peripheral endothelial cells[65], monocytes/macrophages[60,66], T cells[68] and mast cells[67], is blood–brain barrier permeable and plays a pathogenic role in AD. Indeed, recent studies show that several drugs (for example, sacubitril/valsartan) can reduce peripheral sST2 levels in individuals with heart failure[89]. It is of interest to examine whether these drugs can also regulate peripheral sST2 levels in individuals with AD and ameliorate the disease-related pathological changes.

In summary, we uncovered an alternative pathogenic mechanism of AD that involves microglial dysfunctions mediated by sST2. Dysregulation of endothelial cell-secreted sST2 leads to increased plasma and CSF levels of sST2 and impairs Aβ clearance by microglia, resulting in increased Aβ accumulation in AD. Furthermore, we identified an AD-protective genetic variant, rs1921622, which downregulates sST2 expression and attenuates the *APOE*-ε4-related risk and pathological changes of AD through the regulation of microglial signaling. Thus, a better understanding of how sST2—a biomarker and potential drug target for AD—is genetically regulated can aid the design of AD intervention strategies and clinical trials.

Methods

Recruitment for Chinese_cohort_1. This study was approved by the Joint Chinese University of Hong Kong–New Territories East Cluster Clinical Research Ethics Committee at the Prince of Wales Hospital, the Chinese University of Hong Kong and the Hong Kong University of Science and Technology (HKUST). All individuals provided written informed consent for both study enrollment and sample collection. Specifically, we recruited a total of 690 Hong Kong Chinese individuals ≥ 60 years old, including 345 individuals with AD and 345 HCs, who visited the Specialist Outpatient Department of the Prince of Wales Hospital at the Chinese University of Hong Kong from April 2013 to February 2018. We established a clinical diagnosis of AD based on the American Psychiatric Association's Diagnostic and Statistical Manual of Mental Disorders, Fifth Edition[90]. All individuals underwent a medical history assessment, clinical assessment, cognitive and functional assessments using the MoCA test, and neuroimaging assessment by MRI[91,92], and only those with cognitive dysfunctions

(that is, those having Alzheimer's dementia with MoCA score < 21) were included in the AD group in this study. Individuals with any notable neurological disease besides AD or a psychiatric disorder were excluded. We recorded age, sex, years of education, medical history and history of CVDs. We prepared DNA and plasma samples from whole-blood samples and stored them at −80 °C until use. We used T1-weighted MRI to retrieve brain imaging data from 192 individuals (n = 77 individuals with AD, n = 115 HCs) from the Prince of Wales Hospital. Raw imaging files were deidentified and processed by AccuBrain IV1.2 (BrainNow Medical Technology) for the analysis of gray matter volumes.

UK Brain Banks Network dataset. We obtained the following samples of the Medical Research Council (MRC) UKBBN dataset (Bristol Brain Bank): CSF samples, frontal cortex sections, frozen frontal cortex tissues and genomic DNA samples (Supplementary Data 1), from South West Dementia Brain Bank (SWDBB), which receives approval from North Somerset and South Bristol Research Ethics Committee to operate as a research tissue bank. For our initial sample selection from the UKBBN dataset, we excluded individuals with other neurodegenerative diseases, severe vascular diseases (for example, stroke), an intoxicated state, infection, prions, severe inflammatory diseases (for example, autoimmune diseases), structural brain disorders, metabolic/nutritional diseases, trauma, delirium, genetic disorders (for example, Down syndrome) or other systemic diseases. For CSF samples, we further selected samples with a PMD ≤ 30 h, yielding a total of 86 individuals (n = 75 individuals with AD, n = 11 HCs). In addition, we obtained snRNA-seq data from frozen frontal cortical samples from the UKBBN (n = 12 individuals with AD, n = 9 HCs) from our previously published dataset[44].

Other cohorts and data for association studies. We obtained the following data for replication studies: (i) genomic, demographic and clinical data from Chinese_cohort_2 (ref. [47]); (ii) genomic, demographic and clinical data from the LOAD Family Study[48]; (iii) genomic, demographic and clinical data from the National Institute on Aging (NIA) ADC cohorts[49,50]; (iv) genomic, demographic, clinical and brain imaging data from the ADNI cohort; (v) genomic, demographic and transcriptomic data from the GTEx dataset;[42,43] (vi) plasma biomarker, CSF biomarker, demographic and clinical data from the Stanford ADRC cohort;[35] (vii) plasma biomarker and demographic data from the INTERVAL and LonGenity cohorts[37] retrieved from the online database (https://twc-stanford.shinyapps.io/aging_plasma_proteome/); (viii) CSF biomarker and demographic data from a Japanese cohort;[36] and (ix) genomic, demographic, clinical and brain imaging data from the AIBL cohort[52]. Details related to sample and data collection are presented in the Supplementary Notes.

DNA and plasma extraction from human blood samples. We collected whole-blood samples (3 ml) from individuals into K3EDTA tubes (VACUETTE). We centrifuged the samples at 2,000g for 15 min to separate the cell pellet and plasma. The plasma was collected, aliquoted and stored at −80 °C until use. We sent the cell pellets to the Centre for PanorOmic Sciences (Genomics and Bioinformatics Cores, University of Hong Kong) for genomic DNA extraction using the QIAsymphony DSP DNA Midi Kit (Qiagen) on a QIAsymphony SP platform (Qiagen). Genomic DNA was eluted with water or Elution Buffer ATE (Qiagen) and stored at 4 °C. We determined the DNA concentration by BioDrop µLITE+ (BioDrop).

Measurement of protein levels in human samples and cell lines. We measured the plasma level of sST2 in 613 individuals from Chinese_cohort_1 (n = 277 individuals with AD, n = 336 HCs); CSF level of sST2 in 86 individuals from the UKBBN cohort (n = 75 individuals with AD, n = 11 HCs); and the level of sST2 secreted by hCMEC/D3 cells using the Human ST2/IL-33 R Quantikine ELISA Kit (DST200; R&D Systems). The plasma levels of NfL (n = 154 individuals with AD, n = 135 HCs) and P-tau181 (n = 156 individuals with AD, n = 134 HCs) in individuals from Chinese_cohort_1 were measured by the Quanterix Accelerator Laboratory using the Quanterix NF-light SIMOA Assay Advantage Kit (103186) and P-Tau 181 Advantage V2 Kit (103714), respectively[93].

Whole-genome sequencing and single-nucleotide polymorphism array for genotyping. We submitted DNA samples from 427 individuals from Chinese_cohort_1 (n = 233 individuals with AD, n = 194 HCs) to Novogene for library construction and WGS. The samples were sequenced on the Illumina HiSeq X platform (average depth: 5×), and individual genotypes were analyzed using the GotCloud pipeline[41]. The genotype results, which were stored in VCF files, were used for principal-component analysis. The top five principal components were generated by PLINK software (v1.9)[94] with the following parameters: --pca header tabs, --maf 0.05, --hwe 0.00001 and --not-chr x y.

We subjected the rest of the genomic DNA samples, including 263 from Chinese_cohort_1 (n = 112 individuals with AD, n = 151 HCs) and 113 from the UKBBN cohort (n = 102 individuals with AD, n = 11 HCs), to SNP array for the genotyping of chr2: 102966067 (GRCh37/hg19), *APOE*-ε2 and *APOE*-ε4 using TaqMan Assays rs1921622, C___1226146_10, 4351376; rs7412, C___904973_10, 4351376; and rs429358, C___3084793_20, 4351376, respectively (Thermo Fisher Scientific). We performed real-time quantitative PCR (qPCR) using the 7500 Fast and QuantStudio 7 Flex Real-Time PCR System (Applied Biosystems). We stored the results in EDS files and input them into TaqMan Genotyper Software (Applied Biosystems) for the joint genotyping of SNPs.

Immunohistochemical staining of postmortem human brain sections. We obtained formalin-fixed, paraffin-embedded, postmortem, frontal cortex sections from 78 individuals with AD from the UKBBN cohort. We first deparaffinized and rehydrated the sections with xylene and graded ethanol solutions. To stain Aβ, we treated the sections with formic acid at room temperature (RT) for 5 min and quenched endogenous peroxidase activity with a 3% hydrogen peroxide solution. We then incubated the sections with a mouse anti-human Aβ antibody (1:500 dilution; clone NAB228, SC-32277, Santa Cruz Biotechnology) overnight at 4 °C. After washing, we incubated the sections with horseradish peroxidase (HRP)-labeled anti-mouse IgG (QD440-XAKE, RTU, BioGenex) and developed signals with 3,3′-diaminobenzidine (DAB) substrate (QD440-XAKE, BioGenex). To co-stain microglia and Aβ protein, we performed double immunohistochemical staining; after deparaffinization and rehydration, the sections were treated with sodium citrate buffer (10 mM sodium citrate, pH 6.0) for 25 min and blocked, then endogenous peroxidase activity was quenched by 3% hydrogen peroxide solution. We then incubated the sections with the mouse anti-human Aβ antibody (SC-32277) and rabbit anti-human Iba-1 (1:100 dilution; 019-19741, polyclonal, FUJIFILM Wako Pure Chemical) overnight at 4 °C. After washing, we incubated the sections with HRP-labeled anti-mouse and AP-labeled anti-rabbit (HK597-50K, Double Staining kit, BioGenex) followed by substrate development with DAB (QD440-XAKE, BioGenex) and Fast Red Substrate (HK182-5KE, BioGenex). We then counterstained the sections with Mayer's hematoxylin (HK100-9K, BioGenex) and mounted them with coverslips. We used Tris-buffered saline with 0.01% Triton X-100 as the buffer for washing and to dilute primary antibodies. We took images with a ZEISS Axio Scan.Z1 scanner and processed them with ZEN microscope software v3.2 (ZEISS).

To quantify Aβ plaques, we took ten random images of each section. After background subtraction and threshold adjustment, we analyzed the Aβ plaques using the Analyze Particles function in Fiji (ImageJ v1.53c). We determined the total Aβ area, number of Aβ plaques and median plaque size for each section. We calculated Aβ plaque load (percentage area) by dividing the total Aβ area by the total image area (10 mm^2). To quantify microglia–Aβ co-staining, we selected 20 random images of each section and processed them with the Colour Deconvolution function to separate the data into three color channels (that is, DAB, Fast Red and hematoxylin). After adjusting the threshold, we selected Aβ plaques and microglia using the Create Selection function, then analyzed them using the Analyze function. We determined the total Aβ area and Aβ area colocalized with Iba-1 staining. We calculated the Aβ plaque area colocalized with microglia (percentage total Aβ) by dividing the Aβ area colocalized with Iba-1 staining by the total Aβ area. Two independent researchers performed section staining, image acquisition and image quantification; they also randomly selected and quantified images in a blinded manner.

Association analysis and data visualization for the GWAS. We performed the association analysis between SNPs and plasma sST2 level at the genome-wide level in Chinese_cohort_1 with PLINK software (v1.9)[94], adjusting for age, sex, AD diagnosis and the top five principal components as covariates (given that they have relatively larger eigenvalues with higher power in explaining the population variation in the initially calculated 20 principal components; Supplementary Data 3), using the following parameters: --keep-allele-order, --linear, --ci 0.95, --hwe 0.00001 and --maf 0.05. To visualize the data, we generated a Manhattan plot and quantile–quantile plot using the manhattan() function and qq() function of the R qqman package (v0.1.4), respectively. We generated regional plots for the *IL1RL1* locus using LocusZoom. We performed fine-mapping analysis of the effects of the *IL1RL1* locus on plasma sST2 level using CAVIAR software (v2.2)[95] and generated association test results and pairwise LD information using PLINK software (v1.9) with the following parameters: --hwe 0.00001, --maf 0.05, --r, --matrix, --chr 2, --from-bp 102000000 and --to-bp 104000000. We generated the fine-mapped regional plot using the plot_ly() function of the R plotly package (v4.9.1) and plotted LD and haplotype structures using Haploview (v4.2). To identify all independent sST2-associated variants (r^2 < 0.2), we subjected variants with $P < 1 \times 10^{-5}$ according to the sST2 GWAS to analysis by PLINK software (v1.9; parameters: --hwe 0.00001, --maf 0.05, --clump-p1 0.00001, --clump-r2 0.2, --chr 2 and --clump-kb 2000), yielding 29 independent sST2-associated variants (Supplementary Data 2). We used the calc.relimp() function of the R relaimpo package (v2.2-3)[96,97] to quantify the contributions of genetic factors (that is, the 29 independent sST2-associated variants) and nongenetic factors (that is, age and sex) to sST2-level variance.

Association analysis of rs1921622 in transcriptome datasets. We used human tissue sST2 and ST2L transcript levels as well as rs1921622 genotype data from the GTEx dataset[42,43] for the genotype–expression association test, adjusting for age, sex, RNA integrity (that is, RNA integrity number) and population structure (that is, the top four principal components). We performed rank-based normalization of transcript levels using the rntransform() function of the R GenABEL package (v1.8).

We obtained the transcript levels of sST2 and ST2L in the human frontal cortex at the single-cell level by realigning the FASTQ files of our previously published snRNA-seq dataset[44] using a modified reference genome. Specifically, we separated the *IL1RL1* region (chr2: 102,311,563–102,352,037) in the GTF file of the original GRCh38/hg38 pre-mRNA reference genome into three parts: the sST2-specific region (chr2: 102,343,416–102,346,100), the ST2L-specific region (chr2: 102,311,563–102,337,147 and 102,346,101–102,352,037) and the overlapping region (chr2: 102,337,148–102,343,415). We generated a modified reference genome with Cell Ranger (v3.0.1) using the new GTF file and original FASTA file. In the subsequent quality-control step, we performed the quantification of gene levels and cell-type identification using Seurat (v3.0)[44]. For the association analysis between genotype and candidate gene expression in each cell cluster, we performed a linear regression analysis, adjusting for age, sex, AD diagnosis and PMD. The level of significance was set at an FDR < 0.05. We performed a GO analysis of associated genes using DAVID Bioinformatics Resources[98,99].

Analysis of the association between rs1921622 and Alzheimer's disease risk. We performed a meta-analysis to examine the effects of rs1921622 genotype on AD risk. Specifically, we determined the effect sizes (that is, log ORs) and standard errors from eight AD datasets (that is, the Chinese_cohort_1 dataset, the WGS and array datasets of Chinese_cohort_2 and the LOAD, ADC1, ADC2, ADC3 and ADNI datasets) using logistic regression with age, sex and the top five principal components as covariates. We summarized and processed the results by METASOFT (v2.0.0)[51] to estimate the joint risk effects and significance levels under Han and Eskin's random-effects model (RE2)[51]. We further performed multiple testing correction using the RE2 *P* values to generate the FDR values. We then input the results into ForestPMPlot (v1.0.2) to generate forest plots for data visualization.

Two-sample Mendelian randomization analysis. We performed the two-sample MR analyses of the associations between sST2 level and AD risk in the overall population and subgroups of individuals in the Chinese and European-descent populations using the mr() function and inverse-variance weighted method of the R TwoSampleMR package (v0.5.6), followed by multiple testing correction.

Accordingly, for the analysis in European-descent populations, we selected the *cis*-regulating (chr2: 102,820,000–103,100,000; GRCh37/hg19) protein quantitative trait loci (pQTL) for plasma sST2 levels[39] for downstream filtering. Specifically, we used the statistical results from an independent plasma sST2 *cis*-regulating pQTL dataset from European-descent populations[38] to filter out the loci that did not pass the genome-wide threshold ($P < 5 \times 10^{-8}$) or had the opposite direction of regulating effects in the two datasets. Moreover, we further used the statistical results from the GTEx dataset[42,43] to filter the loci, and only kept the loci associated with the altered sST2 expression in the expressing tissues (that is, meta $P < 1 \times 10^{-5}$ in the brain regions and lungs) but not the altered ST2L expression in the expressing tissues (that is, $P > 0.1$ in the lungs) for LD clumping by PLINK software (v1.9) with the following parameters: --maf 0.05, --hwe 0.00001, --clump-p1 0.00000005, --clump-r2 0.2 and --clump-kb 2000. We obtained a total of seven independent instrumental variables (rs1921622, rs13001325, rs4851575, rs10515922, rs11123935, rs10200945 and rs951774), then generated their effects on AD risk by the meta-analysis in European-descent populations using the LOAD, ADC1, ADC2, ADC3 and ADNI datasets.

For the analysis in Chinese populations, we subjected the *cis*-regulating (chr2: 102,820,000–103,100,000; GRCh37/hg19) pQTL for plasma sST2 levels in the Chinese_cohort_1 (WGS) dataset to LD clumping by PLINK software (v1.9) with the following parameters: --maf 0.05, --hwe 0.00001, --clump-p1 0.00001, --clump-r2 0.5 and --clump-kb 2000. We obtained a total of seven independent instrumental variables (rs1921622, rs55664618, rs62151861, rs2241116, rs1468790, rs1523199 and rs56238602), then generated their effects on AD risk by the association analysis in the Chinese_cohort_2 (WGS) dataset.

Mice. We housed all mice in the HKUST Animal and Plant Care Facility. All animal experiments were approved by the HKUST Animal Ethics Committee and conducted in accordance with the Guidelines of the Animal Care Facility of HKUST. We housed four mice of the same sex in each cage at 22 °C and at a relative humidity of 60%, with a 12-h light/dark cycle as well as food and water ad libitum. WT C57BL6J mice were obtained from the Jackson Laboratory. The 5XFAD mice were generated as previously described by overexpressing the p.Lys670Asn/p.Met671Leu (Swedish), p.Ile716Val (Florida) and p.Val717Ile (London) mutations in human *APP* as well as the p.Met146Leu and p.Leu286Val mutations in human *PSEN1* (ref. [100]). We confirmed genotypes by PCR analysis of tail or ear biopsy specimens. We performed all in vivo experiments on age-matched groups and randomly assigned the mice to the experimental conditions. We chose our sample sizes primarily based on our experience with similar types of experiments. We conducted all animal experiments during the light phase.

In vivo experiments in mice. We delivered murine recombinant sST2-Fc (1004-MR-050; R&D Systems) into 5XFAD mice (B6.Cg-Tg(APPSwFlLon,PSEN1*M146L*L286V)6799Vas/Mmjax) via mini-osmotic pumps (model 1004; Alzet) at 0.11 µl h^{-1}. Specifically, we implanted the pumps intracerebroventricularly above the right hemisphere and loaded them with murine recombinant sST2-Fc protein (240 ng per pump; 10 µg ml^{-1}) or human IgG (as a control; 009-000-008; Jackson ImmunoResearch) in artificial CSF (119 mM NaCl, 2.5 mM KCl, 2.5 mM $CaCl_2{\cdot}2H_2O$, 1 mM $NaH_2PO_4{\cdot}2H_2O$, 1.3 mM $MgCl_2{\cdot}6H_2O$, 26.2 mM $NaHCO_3$ and 11 mM D-glucose). After 28 d of administration, the mice were anesthetized with isoflurane and transcardially perfused with PBS, and their brains were collected.

Immunohistochemical and immunofluorescence staining of mouse brains. The left hemispheres of the mouse brains were fixed in 4% paraformaldehyde at 4 °C for 24 h, transferred to 30% sucrose and stored at 4 °C until sectioning. We cut the brains coronally into 50-µm sections with a vibrating blade microtome (VT1000S, Leica) and stored them in cryoprotectant solution (30% glycerol, 30% ethylene glycol and PBS) at −20 °C until use. For immunohistochemistry, we rinsed the sections with PBST (that is, 0.1% Triton X-100 in PBS), then treated them with formic acid at RT for 5 min for antigen retrieval, followed by 3% hydrogen peroxide solution for 30 min to quench endogenous peroxidase activity. We blocked the sections in 5% horse serum in PBST for 2 h, then labeled them with 4G8 antibody (1:1,000 dilution; 800703, BioLegend) or D54D2 antibody (1:1,000 dilution; 8243S, CST) in blocking buffer overnight at 4 °C. The next day, we incubated the sections with biotin-conjugated anti-mouse secondary antibodies (1:1,000 dilution; BA2000, Vector Laboratories) followed by an avidin–biotin–HRP complex (PK-6100, Vector Laboratories), and we developed signals with DAB kits (SK-4100, Vector Laboratories or QD430-XAKE, BioGenex). Imaging was performed using a Zeiss Axio Scan.Z1 Slide Scanner and processed in ZEN v3.3 (ZEISS). We analyzed the Aβ plaque areas in cortical sections using the Analyze Particles function in Fiji (ImageJ v1.53c). Specifically, we analyzed four brain sections from each mouse in cortical regions (~200–300 µm apart) and calculated the average percentage of the cortical area occupied by Aβ plaques.

For immunofluorescence analysis, we washed sections and incubated them in 1 µM X-34 for 10 min. We then washed them in X-34 buffer (40% ethanol in PBS), and then in PBS. We then blocked sections for 2 h in blocking buffer (4% horse serum, 1% BSA and 0.3% Triton X-100 in PBS). Primary antibodies used in experiments include mouse anti-Aβ (1:1,000 dilution; clone 4G8, 800703, BioLegend), rabbit anti-Iba-1 (1:1,000 dilution; 019-19741, Wako) and rat anti-Ki67 (1:200 dilution; clone SolA15, 14-5698-80, eBioscience); we diluted these in blocking buffer and incubated sections overnight at 4 °C. Sections were subsequently incubated with fluorophore-conjugated secondary antibodies against mouse, rabbit and rat Ig (Alexa Fluor 488, 568 and 647; 1:1,000 dilution; Life Technologies) in blocking buffer for 2 h at RT, extensively washed in PBST, stained with SYTOX Green (1:300,000 dilution; S7020, Life Technologies) or DAPI (1:5,000 dilution; D3571, Life Technologies) and mounted using FluorSave Reagent (345789, Millipore).

We performed imaging using a Leica TCS SP8 confocal microscope with a Leica ×40 oil immersion objective. We took five images from each mouse cortex with a step size of 1 µm for a total of 40 µm, then merged them into a single image with maximum intensity *z*-projection. We identified three different plaque morphologies using anti-Aβ immunolabeling (that is, 4G8) and X-34 staining: (i) filamentous plaques characterized by filamentous X-34 and 4G8 labeling with no plaque core, (ii) compact plaques characterized by 4G8 amyloid fibrils projecting radially outward with an X-34–labeled core and (iii) inert plaques characterized by an X-34-labeled core with no 4G8 labeling. We used a custom macro to segment individual Aβ plaques and identified the type of each plaque manually. For plaque-associated microglia, we counted the numbers of microglia surrounding small plaques (that is, radius ≤ 8 µm) and large plaques (that is, radius > 8 µm) manually, as defined by $DAPI^+$ nucleus staining within the barrier surrounding the plaques and processes in contact with the plaques. We defined the $Ki67^+$ microglia as microglia with Ki67 signals within the nucleus. To quantify microglial coverage of Aβ plaques, we selected only compact plaques. We used ten optical slices 0.5 µm apart through the center of the plaque for analysis. We processed all images with a customized macro in Fiji (ImageJ v1.53c). On each slice, after adjusting the threshold, we determined the perimeters of the plaque using the Analyse Particles and Area to Line functions. We also determined plaque perimeters and the arcs of plaque perimeters colocalized with microglial staining. We calculated the proportion of the plaque perimeter covered by microglia by summing the arcs of the plaque perimeter across three-dimensional (3D) stacks in close contact (within 1 µm) with Iba-1-immunolabeled cells (~25 plaques per group). We conducted the 3D reconstruction of microglia–plaque interaction using Imaris v9.7.2 (Oxford Instruments).

Assessment of microglial amyloid-beta phagocytic capacity. We examined microglial Aβ phagocytic capacity as previously described[25]. Briefly, we injected 4-month-old 5XFAD or WT mice intraperitoneally with methoxy-X04 (10 mg per kg body weight) to label the Aβ. We anesthetized the mice with isoflurane 3 h after methoxy-X04 injection and perfused the left ventricle with ice-cold PBS. We isolated, minced and incubated their forebrains at 37 °C for 30 min in 5 U ml^{-1} papain (LS003126) and 35 U ml^{-1} DNase I (LS002140; Worthington Biochemical) for enzymatic digestion. After incubation, we depleted myelin debris by 30% isotonic Percoll (P1644; Sigma-Aldrich) gradient centrifugation and obtained mononuclear cell suspensions in DMEM/F12 medium with ice-cold 10% heat-inactivated fetal bovine serum. We prepared unstained controls from mixtures

of different sample cell suspensions for cell population identification. To label microglia, we used an Alexa Fluor 488-conjugated mouse CD11b antibody (1:200 dilution; 53-0112-82; eBioscience) to stain the cell suspensions for 45 min at 4 °C. We analyzed the resultant labeled cell suspensions using a BD Influx cell sorter flow cytometer. We analyzed the recorded scatterplot data for the microglial cell population using FlowJo software v10.5.0 (TreeStar).

Cell culture. The hCMEC/D3 cell line was purchased from Cedarlane and cultured as previously described[101]. Briefly, we coated a tissue culture plate with 100 µg ml^{-1} type I collagen (Millipore) at 37 °C in 5% CO_2 for 1 h. We subsequently washed the plate with Dulbecco's phosphate-buffered saline (DPBS) and replaced it with a complete culture medium (endothelial cell growth medium-2 (Lonza) supplemented with 5% fetal bovine serum (HyClone), 1% chemically defined lipid concentrate (Gibco), 10 mM HEPES (Gibco), 5 µg ml^{-1} ascorbic acid (Sigma), 1.4 µM hydrocortisone (Sigma), 1 ng ml^{-1} basic fibroblast growth factor bFGF (PeproTech), 10 U ml^{-1} penicillin and 10 µg ml^{-1} streptomycin (Gibco)). Cultured cells were dissociated with 0.05% trypsin for 5 min, replated at 25,000 cells per cm^2 and returned to culture at 37 °C in a 5% CO_2 incubator. Three to four days after seeding, the cells reached confluence and could be passaged. We used cells at passages 27–35 for our experiments.

For the ChIP–qPCR experiment, we fully changed the medium of the hCMEC/D3 cells 2 h before treatment. We then treated cultured cells with recombinant human IL-33 (BioLegend) or DPBS as a vehicle control for 24 h.

To evaluate the efficiency of the sgRNA editing in endothelial cells, we transfected 5×10^5 hCMEC/D3 cells with a single CRISPR construct by nucleofection using the Human Umbilical Vein Endothelial Cell Nucleofector Kit (Lonza) with a Nucleofector 2b device (Lonza). One day after transfection, we changed the cultured medium to a complete culture medium with 1 µg ml^{-1} puromycin (Thermo Fisher Scientific). After 3 d of puromycin selection, we extracted genomic DNA using QuickExtract DNA Extraction Solution (Lucigen) followed by a T7EI (NEB) editing efficiency test. All four sgRNAs exhibited high editing efficiency (data not shown).

CRISPR/Cas9-mediated genome deletion of the rs1921622-harboring region. To delete the region harboring rs1921622 in hCMEC/D3 cells, we used a dual-guide, RNA-mediated knockout approach. The cells were genotyped from 300 bp upstream and downstream of rs1921622 by Sanger sequencing. We performed screening of potential *Streptococcus pyogenes* Cas9 (SpCas9)-guided RNAs using the CRISPR design tool (https://crispr.mit.edu/) 100 bp upstream and downstream of rs1921622. We used the following sgRNAs: sgRNA-1, 5′-TTATG GACAGAATTAAGAAG-3′; sgRNA-2, 5′-CTGTCCATAAGATTTGAAAG-3′; sgRNA-3, 5′-AATTTTGTTCTGGTAGCCAT-3′; and sgRNA-4, 5′-GGTAT TTCAGCTAGTGCCTA-3′. We subcloned the sgRNAs into PX459v2, which contains an sgRNA cassette, human codon-optimized SpCas9 and a puromycin resistance gene.

To generate a dual-gRNA-mediated deletion cell line, we transfected the hCMEC/D3 cells with plasmids containing sgRNA-1/sgRNA-4 (targeted 67-bp deletion), sgRNA-2/sgRNA-3 (targeted 38-bp deletion) or PX459v2 as a no-sgRNA control. After 3 d of puromycin selection (1 µg ml^{-1}) starting from the day after transfection, we seeded the puromycin-resistant cells in two 24-well plates. We changed the culture medium twice a week. After 3 weeks, when a single colony was observed, we passaged the wells containing only one colony into a 12-well plate. We genotyped each clone and subjected those in which the targeted deletion may have occurred to Sanger sequencing. This protocol generated six control lines, eight lines with a 38-bp deletion and ten lines with a 67-bp deletion.

RNA extraction and real-time PCR. We extracted RNA using a NucleoSpin RNA column (MACHEREY-NAGEL) according to the manufacturer's instructions. We first synthesized single-stranded cDNA using the PrimeScript RT Reagent Kit (Takara Bio). We performed quantitative real-time PCR with TaqMan probes (Thermo Fisher Scientific) and a Premix Ex Taq Kit (Takara Bio) using the 7500 Fast Real-Time PCR System (Applied Biosystems). The mRNA expression was normalized to that of *HPRT1*.

Chromatin immunoprecipitation coupled to quantitative PCR. We modified the ChIP–qPCR from the chromatin immunoprecipitation sequencing protocol as previously described[25]. In brief, we trypsinized cultured cells and washed them once with DPBS. Then, we immediately fixed 4×10^5 cells in suspension with 1.5% paraformaldehyde at RT for 10 min and quenched them with 0.125 M glycine for 5 min. We subsequently centrifuged the cells at 500*g* for 5 min. We resuspended the cell pellet in 0.25% SDS sonication buffer (10 mM Tris (pH 8.0), 0.25% SDS, 2 mM EDTA and protease inhibitors) and subjected it to sonication into 200–500-bp fragments using the S220 Focused-ultrasonicator system (Covaris). We diluted the DNA–protein mixture at a 1:1.5 ratio in equilibration buffer (10 mM Tris, 233 mM NaCl, 1.67% Triton X-100, 0.167% sodium-deoxycholate (Na-DOC), 1 mM EDTA and protease inhibitors). We spared 5% of the DNA–protein mixture as input, while we incubated the remainder with antibodies against H3K4me3 (3 µl; 39159; Active Motif), H3K27ac (5 µl; 39133; Active Motif) or normal IgG (6 µl; AB-105-C; R&D) overnight at 4 °C. Simultaneously, Protein A Dynabeads (Thermo Fisher Scientific) were washed twice and incubated with RIPA-LS buffer (10 mM Tris-HCl (pH 8.0), 140 mM NaCl, 1 mM EDTA (pH 8.0), 0.1% SDS, 0.1% Na-DOC, 1% Triton X-100 and protease inhibitors), then supplemented with 0.1% BSA overnight at 4 °C. The next day, we added 10 µl pre-blocked beads to each sample and incubated them for 2 h at 4 °C. We then washed protein-bound beads twice with ice-cold RIPA-LS buffer, twice with ice-cold RIPA-HS buffer (10 mM Tris-HCl (pH 8.0), 500 mM NaCl, 1 mM EDTA (pH 8.0), 0.1% SDS, 0.1% Na-DOC, 1% Triton X-100 and protease inhibitors), twice with ice-cold RIPA-LiCl buffer (10 mM Tris-HCl (pH 8.0), 250 mM LiCl, 1 mM EDTA (pH 8.0), 0.5% NP-40, 0.5% Na-DOC and protease inhibitors) and twice with ice-cold 10 mM Tris (pH 8.0) buffer on a precooled magnetic stand. We then reverse-crosslinked the protein-bound and chromatin-bound beads with protease K (NEB) in ChIP elution buffer (10 mM Tris-HCl (pH 8.0), 300 mM NaCl, 5 mM EDTA (pH 8.0) and 10% SDS) at 55 °C for 1 h, then at 65 °C for 6 h. We diluted the input to a final concentration of 0.4% SDS and 300 mM NaCl. Next, 2 µl protease K was added to the input and incubated at 55 °C for 1 h, then at 65 °C for 6 h. We purified both the eluted ChIP and input DNA with a MinElute column (Qiagen).

We performed real-time PCR for ChIP and input DNA using Power SYBR Green Master Mix (Applied Biosystems) with the following primer pairs: sST2_ promoter_F, 5′-GGGAAAAAAGCTTGACTTTG-3′; sST2_promoter_R, 5′-ATTTGACAAAGTTCACCCAG-3′; rs192_F, 5′-GCCACTTCTTAAT TCTGTCC-3′; and rs192_R, 5′-GGTATTTCAGCTAGTGCCTA-3′.

Statistics and reproducibility. No statistical methods were used to predetermine sample sizes, but our samples sizes are similar to those reported in previous publications[24,25,41,47]. No data were excluded from the analyses, and the data distribution was assumed to be normal, but this was not formally tested. We assigned random codes to human samples before experiments and analyses; and we randomly assigned nonhuman samples (for example, mice and cultured cells) into experimental groups before experiments and sample collection. The investigators were blinded to disease diagnosis and other demographic information (for humans) and experimental groups and conditions (for mice and cultured cells) during experiments.

For the remaining statistical analyses of human samples that are not mentioned in the above methods, we conducted a linear regression analysis to determine the significance of the associations between AD-associated endophenotypes (that is, cognitive performance, brain region volume and AD biomarkers) and sST2 level and/or rs1921622 genotype, adjusted for age, sex and other covariates as indicated in the main text and figure legends. We obtained the CSF sST2 level cutoff based on the CSF sST2 level with the maximum value of Youden's index using the optimal. cutpoints() function and the Youden method of the OptimalCutpoints package (v1.1-4) in R[102]. We performed Cox regression to examine the association between onset age of dementia and the rs1921622 A allele using the coxph() function of the R survival package (v1.3-24), with sex and the top five principal components as covariates. We tested the proportional hazard assumptions using the cox.zph() function of the R survival package (v1.3-24; Supplementary Data 4). The level of significance was set to $P < 0.05$ or FDR < 0.05. For data visualization, we used the plot() function of R to generate a volcano plot and the ggplot() function of the R ggplot2 package (v3.2.1) to generate dot plots. For the data obtained from mouse and cell culture system experiments, we assessed the significance of differences by unpaired Student's *t*-tests, or one-way or two-way analysis of variance followed by the Bonferroni post hoc test as indicated. The level of significance was set at $P < 0.05$. We generated all statistical plots using Prism v8.0 (GraphPad).

Reporting summary. Further information on research design is available in the Nature Research Reporting Summary linked to this article.

Data availability

Source data are available with this paper. All statistical data associated with this study are contained in the main text, Supplementary Information or Supplementary Data. All other data are available from the corresponding author upon reasonable request. The consent forms signed by individuals from Chinese_cohort_1 state that the research content will be kept private under the supervision of the hospital and research team. Therefore, the phenotypic, genomic and proteomic data of individuals will only be available and shared in formal collaborations. A review panel hosted at HKUST will process and review any applications for data sharing and project collaboration and promptly notify applicants with the decision. Researchers may contact HKUST (sklneurosci@ust.hk) for details about data sharing and project collaboration related to the present study. The GRCh38/hg38 reference genome is available at https://hgdownload.soe.ucsc.edu/downloads.html. The human frontal cortex snRNA-seq dataset of the UKBBN cohort has been deposited in the Gene Expression Omnibus (accession no. GSE157827). The genomic, demographic and clinical data of the LOAD cohort are available on the National Institutes of Health (NIH) database of Genotypes and Phenotypes (dbGaP) project (accession no. phs000168.v2.p2). The genomic, demographic and clinical data of the ADC1–3 cohorts are available on the NIH dbGaP project database (accession no. phs000372.v2.p1). The genomic, demographic, clinical and brain imaging data of the ADNI cohort are available at http://adni.loni.usc.edu/ upon request. The proteomic and demographic

data from the INTERVAL and LonGenity cohorts are available at https://twc-stanford.shinyapps.io/aging_plasma_proteome/. The genomic, demographic and transcriptomic data from the GTEx cohort are available on the NIH dbGaP project database (accession no. phs000424.v6.p1). The genomic, demographic, clinical and brain imaging data of the AIBL cohort are available at https://aibl.csiro.au/ upon request.

Code availability

The codes for our statistical analyses and data visualization are available at https://github.com/yjiangah/sST2-in-AD/.

Received: 16 June 2021; Accepted: 23 May 2022;
Published online: 15 July 2022

References

1. Alzheimer's Association. Alzheimer's disease facts and figures. *Alzheimers Dement.* **15**, 321–387 (2019).
2. Jack, C. R. Jr et al. NIA-AA research framework: toward a biological definition of Alzheimer's disease. *Alzheimers Dement.* **14**, 535–562 (2018).
3. Lambert, J.-C. et al. Meta-analysis of 74,046 individuals identifies 11 new susceptibility loci for Alzheimer's disease. *Nat. Genet.* **45**, 1452–1458 (2013).
4. Frigerio, C. S. et al. The major risk factors for Alzheimer's disease: age, sex and genes modulate the microglia response to Aβ plaques. *Cell Rep.* **27**, 1293–1306 (2019).
5. Yeh, F. L., Wang, Y., Tom, I., Gonzalez, L. C. & Sheng, M. TREM2 binds to apolipoproteins, including APOE and CLU/APOJ, and thereby facilitates uptake of amyloid-beta by microglia. *Neuron* **91**, 328–340 (2016).
6. Rebeck, G. W., Reiter, J. S., Strickland, D. K. & Hyman, B. T. Apolipoprotein E in sporadic Alzheimer's disease: allelic variation and receptor interactions. *Neuron* **11**, 575–580 (1993).
7. Kok, E. et al. Apolipoprotein E–dependent accumulation of Alzheimer disease–related lesions begins in middle age. *Ann. Neurol.* **65**, 650–657 (2009).
8. Castellano, J. M. et al. Human apoE isoforms differentially regulate brain amyloid-β peptide clearance. *Sci. Transl. Med.* **3**, 89ra57 (2011).
9. Stephen, T. L. et al. APOE genotype and sex affect microglial interactions with plaques in Alzheimer's disease mice. *Acta Neuropathol. Commun.* **7**, 82 (2019).
10. Hickman, S. E., Allison, E. K. & El Khoury, J. Microglial dysfunction and defective β-amyloid clearance pathways in aging Alzheimer's disease mice. *J. Neurosci.* **28**, 8354–8360 (2008).
11. Guillot-Sestier, M.-V. et al. Il10 deficiency rebalances innate immunity to mitigate Alzheimer-like pathology. *Neuron* **85**, 534–548 (2015).
12. Suárez-Calvet, M. et al. Early changes in CSF sTREM2 in dominantly inherited Alzheimer's disease occur after amyloid deposition and neuronal injury. *Sci. Transl. Med.* **8**, 369ra178 (2016).
13. Ewers, M. et al. Increased soluble TREM2 in cerebrospinal fluid is associated with reduced cognitive and clinical decline in Alzheimer's disease. *Sci. Transl. Med.* **11**, eaav6221 (2019).
14. Wood, H. Soluble TREM2 in CSF sheds light on microglial activation in AD. *Nat. Rev. Neurol.* **13**, 65–65 (2017).
15. Zhong, L. et al. Soluble TREM2 induces inflammatory responses and enhances microglial survival. *J. Exp. Med.* **214**, 597–607 (2017).
16. Zhong, L. et al. Soluble TREM2 ameliorates pathological phenotypes by modulating microglial functions in an Alzheimer's disease model. *Nat. Commun.* **10**, 1–16 (2019).
17. Janelidze, S. et al. CSF biomarkers of neuroinflammation and cerebrovascular dysfunction in early Alzheimer disease. *Neurology* **91**, e867–e877 (2018).
18. Huang, C.-W. et al. Clinical significance of circulating vascular cell adhesion molecule-1 to white matter disintegrity in Alzheimer's dementia. *Thromb. Haemost.* **114**, 1230–1240 (2015).
19. Yousef, H. et al. Aged blood impairs hippocampal neural precursor activity and activates microglia via brain endothelial cell VCAM1. *Nat. Med.* **25**, 988–1000 (2019).
20. Chakrabarty, P. et al. TLR5 decoy receptor as a novel anti-amyloid therapeutic for Alzheimer's disease. *J. Exp. Med.* **215**, 2247–2264 (2018).
21. Liu, Y. -L. et al. Amelioration of amyloid-β-induced deficits by DcR3 in an Alzheimer's disease model. *Mol. Neurodegener.* **12**, 30 (2017).
22. Griesenauer, B. & Paczesny, S. The ST2/IL-33 axis in immune cells during inflammatory diseases. *Front. Immunol.* **8**, 475 (2017).
23. Yasuoka, S. et al. Production and functions of IL-33 in the central nervous system. *Brain Res.* **1385**, 8–17 (2011).
24. Fu, A. K. et al. IL-33 ameliorates Alzheimer's disease-like pathology and cognitive decline. *Proc. Natl Acad. Sci. USA* **113**, E2705–E2713 (2016).
25. Lau, S.-F. et al. IL-33-PU.1 transcriptome reprogramming drives functional state transition and clearance activity of microglia in Alzheimer's disease. *Cell Rep.* **31**, 107530 (2020).
26. Trajkovic, V., Sweet, M. J. & Xu, D. T1/ST2—an IL-1 receptor-like modulator of immune responses. *Cytokine Growth Factor Rev.* **15**, 87–95 (2004).
27. Kakkar, R. & Lee, R. T. The IL-33/ST2 pathway: therapeutic target and novel biomarker. *Nat. Rev. Drug Discov.* **7**, 827–840 (2008).
28. Homsak, E. & Gruson, D. Soluble ST2: a complex and diverse role in several diseases. *Clin. Chim. Acta* **507**, 75–87 (2020).
29. Oshikawa, K. et al. Elevated soluble ST2 protein levels in sera of patients with asthma with an acute exacerbation. *Am. J. Respir. Crit. Care Med.* **164**, 277–281 (2001).
30. Bergis, D., Kassis, V. & Radeke, H. H. High plasma sST2 levels in gastric cancer and their association with metastatic disease. *Cancer Biomark.* **16**, 117–125 (2016).
31. Villacorta, H. & Maisel, A. S. Soluble ST2 testing: a promising biomarker in the management of heart failure. *Arq. Bras. Cardiol.* **106**, 145–152 (2016).
32. Saresella, M. et al. IL-33 and its decoy sST2 in patients with Alzheimer's disease and mild cognitive impairment. *J. Neuroinflammation* **17**, 174 (2020).
33. Karikari, T. K. et al. Blood phosphorylated tau 181 as a biomarker for Alzheimer's disease: a diagnostic performance and prediction modelling study using data from four prospective cohorts. *Lancet Neurol.* **19**, 422–433 (2020).
34. Preische, O. et al. Serum neurofilament dynamics predicts neurodegeneration and clinical progression in presymptomatic Alzheimer's disease. *Nat. Med.* **25**, 277–283 (2019).
35. Gate, D. et al. Clonally expanded CD8 T cells patrol the cerebrospinal fluid in Alzheimer's disease. *Nature* **577**, 399–404 (2020).
36. Sasayama, D. et al. Increased cerebrospinal fluid interleukin-6 levels in patients with schizophrenia and those with major depressive disorder. *J. Psychiatric Res.* **47**, 401–406 (2013).
37. Lehallier, B. et al. Undulating changes in human plasma proteome profiles across the lifespan. *Nat. Med.* **25**, 1843–1850 (2019).
38. Ho, J. E. et al. Common genetic variation at the IL1RL1 locus regulates IL-33/ST2 signaling. *J. Clin. Invest.* **123**, 4208–4218 (2013).
39. Sun, B. B. et al. Genomic atlas of the human plasma proteome. *Nature* **558**, 73–79 (2018).
40. Grotenboer, N. S., Ketelaar, M. E., Koppelman, G. H. & Nawijn, M. C. Decoding asthma: translating genetic variation in IL33 and IL1RL1 into disease pathophysiology. *J. Allergy Clin. Immunol.***131**, 856–865 (2013).
41. Zhou, X. et al. Non-coding variability at the APOE locus contributes to the Alzheimer's risk. *Nat. Commun.* **10**, 3310 (2019).
42. Lonsdale, J. et al. The Genotype-Tissue Expression project. *Nat. Genet.* **45**, 580–585 (2013).
43. Consortium, G. The Genotype-Tissue Expression pilot analysis: multitissue gene regulation in humans. *Science* **348**, 648–660 (2015).
44. Lau, S.-F., Cao, H., Fu, A. K. & Ip, N. Y. Single-nucleus transcriptome analysis reveals dysregulation of angiogenic endothelial cells and neuroprotective glia in Alzheimer's disease. *Proc. Natl Acad. Sci. USA* **117**, 25800–25809 (2020).
45. Li, W., Notani, D. & Rosenfeld, M. G. Enhancers as non-coding RNA transcription units: recent insights and future perspectives. *Nat. Rev. Genet.* **17**, 207–223 (2016).
46. Davies, N. M., Holmes, M. V. & Smith, G. D. Reading Mendelian randomisation studies: a guide, glossary and checklist for clinicians. *BMJ* **362**, k601 (2018).
47. Zhou, X. et al. Identification of genetic risk factors in the Chinese population implicates a role of immune system in Alzheimer's disease pathogenesis. *Proc. Natl Acad. Sci. USA* **115**, 1697–1706 (2018).
48. Lee, J. H., Cheng, R., Graff-Radford, N., Foroud, T. & Mayeux, R. Analyses of the National Institute on Aging late-onset alzheimer's disease family study: implication of additional loci. *Arch. Neurol.* **65**, 1518–1526 (2008).
49. Naj, A. C. et al. Common variants at MS4A4/MS4A6E, CD2AP, CD33 and EPHA1 are associated with late-onset Alzheimer's disease. *Nat. Genet.* **43**, 436–441 (2011).
50. Jun, G. et al. Meta-analysis confirms CR1, CLU and PICALM as alzheimer disease risk loci and reveals interactions with APOE genotypes. *Arch. Neurol.* **67**, 1473–1484 (2010).
51. Han, B. & Eskin, E. Random-effects model aimed at discovering associations in meta-analysis of genome-wide association studies. *Am. J. Hum. Genet.* **88**, 586–598 (2011).
52. Kathryn, A. E. et al. The Australian Imaging, Biomarkers and Lifestyle (AIBL) study of aging: methodology and baseline characteristics of 1,112 individuals recruited for a longitudinal study of Alzheimer's disease. *Int. Psychogeriatr.* **21**, 672–687 (2009).
53. Mathys, H. et al. Single-cell transcriptomic analysis of Alzheimer's disease. *Nature* **570**, 332–337 (2019).
54. Zhou, Y. et al. Human and mouse single-nucleus transcriptomics reveal TREM2-dependent and TREM2-independent cellular responses in Alzheimer's disease. *Nat. Med.* **26**, 131–142 (2020).

55. Keren-Shaul, H. et al. A unique microglia type associated with restricting development of Alzheimer's disease. *Cell* **169**, 1276–1290 (2017).
56. Thrupp, N. et al. Single-nucleus RNA-seq is not suitable for detection of microglial activation genes in humans. *Cell Rep.* **32**, 108189 (2020).
57. Yuan, P. et al. TREM2 haplodeficiency in mice and humans impairs the microglia barrier function leading to decreased amyloid compaction and severe axonal dystrophy. *Neuron* **90**, 724–739 (2016).
58. Wicher, G. et al. Interleukin-33 promotes recruitment of microglia/macrophages in response to traumatic brain injury. *J. Neurotrauma* **34**, 3173–3182 (2017).
59. Zhang, Y. et al. An RNA-sequencing transcriptome and splicing database of glia, neurons and vascular cells of the cerebral cortex. *J. Neurosci.* **34**, 11929–11947 (2014).
60. Gosselin, D. et al. An environment-dependent transcriptional network specifies human microglia identity. *Science* **356**, eaal3222 (2017).
61. Wang, Y. et al. Astrocyte-secreted IL-33 mediates homeostatic synaptic plasticity in the adult hippocampus. *Proc. Natl Acad. Sci. USA* **118**, e2020810118 (2021).
62. Nguyen, P. T. et al. Microglial remodeling of the extracellular matrix promotes synapse plasticity. *Cell* **182**, 388–403 (2020).
63. Zhang, Y. et al. Purification and characterization of progenitor and mature human astrocytes reveals transcriptional and functional differences with mouse. *Neuron* **89**, 37–53 (2016).
64. Kalari, K. R. et al. BBBomics—human blood–brain barrier transcriptomics hub. *Front. Neurosci.***10**, 71 (2016).
65. Demyanets, S. et al. Components of the interleukin-33/ST2 system are differentially expressed and regulated in human cardiac cells and in cells of the cardiac vasculature. *J. Mol. Cellular Cardiol.* **60**, 16–26 (2013).
66. Joshi, A. D. et al. Interleukin-33 contributes to both M1 and M2 chemokine marker expression in human macrophages. *BMC Immunol.* **11**, 52 (2010).
67. Bandara, G., Beaven, M. A., Olivera, A., Gilfillan, A. M. & Metcalfe, D. D. Activated mast cells synthesize and release soluble ST2-a decoy receptor for IL-33. *Eur. J. Immunol.* **45**, 3034–3044 (2015).
68. Zhang, J. et al. ST2 blockade reduces sST2-producing T cells while maintaining protective mST2-expressing T cells during graft-versus-host disease. *Sci. Transl. Med.* **7**, 308ra160 (2015).
69. Lipsky, B. P., Toy, D. Y., Swart, D. A., Smithgall, M. D. & Smith, D. Deletion of the ST2 proximal promoter disrupts fibroblast-specific expression but does not reduce the amount of soluble ST2 in circulation. *Eur. J. Immunol.* **42**, 1863–1869 (2012).
70. Kikuchi, M. et al. Altered behavior in mice overexpressing soluble ST2. *Mol. Brain* **13**, 74 (2020).
71. Zlokovic, B. V. Neurovascular pathways to neurodegeneration in Alzheimer's disease and other disorders. *Nat. Rev. Neurosci.* **12**, 723–738 (2011).
72. Hilscher, M. B. et al. Mechanical stretch increases expression of CXCL1 in liver sinusoidal endothelial cells to recruit neutrophils, generate sinusoidal microthombi and promote portal hypertension. *Gastroenterology* **157**, 193–209 (2019).
73. Grammas, P. & Ovase, R. Inflammatory factors are elevated in brain microvessels in Alzheimer's disease. *Neurobiol. Aging* **22**, 837–842 (2001).
74. Grammas, P. & Ovase, R. Cerebrovascular transforming growth factor-β contributes to inflammation in the Alzheimer's disease brain. *Am. J. Pathol.* **160**, 1583–1587 (2002).
75. Ferretti, M. T. et al. Sex differences in Alzheimer disease—the gateway to precision medicine. *Nat. Rev. Neurol.* **14**, 457–469 (2018).
76. Laws, K. R., Irvine, K. & Gale, T. M. Sex differences in Alzheimer's disease. *Curr. Opin. Psych.* **31**, 133–139 (2018).
77. Laws, K. R., Irvine, K. & Gale, T. M. Sex differences in cognitive impairment in Alzheimer's disease. *World J. Psychiatry* **6**, 54–65 (2016).
78. Guillot-Sestier, M. -V. et al. Microglial metabolism is a pivotal factor in sexual dimorphism in Alzheimer's disease. *Commun. Biol.* **4**, 711 (2021).
79. Russi, A. E., Ebel, M. E., Yang, Y. & Brown, M. A. Male-specific IL-33 expression regulates sex-dimorphic EAE susceptibility. *Proc. Natl Acad. Sci. USA* **115**, E1520–E1529 (2018).
80. Fernandez, C. G., Hamby, M. E., McReynolds, M. L. & Ray, W. J. The role of APOE4 in disrupting the homeostatic functions of astrocytes and microglia in aging and Alzheimer's disease. *Front. Aging Neurosci.* **11**, 14 (2019).
81. Fourgeaud, L. et al. TAM receptors regulate multiple features of microglial physiology. *Nature* **532**, 240–244 (2016).
82. Kim, J., Basak, J. M. & Holtzman, D. M. The role of apolipoprotein E in Alzheimer's disease. *Neuron* **63**, 287–303 (2009).
83. Wang, Y. et al. TREM2 lipid sensing sustains the microglial response in an Alzheimer's disease model. *Cell* **160**, 1061–1071 (2015).
84. Mittal, K. et al. CD4 T cells induce a subset of MHCII-expressing microglia that attenuates Alzheimer pathology. *iScience* **16**, 298–311 (2019).
85. Miller, A. M. et al. IL-33 reduces the development of atherosclerosis. *J. Exp. Med.* **205**, 339–346 (2008).
86. Baba, Y. et al. Involvement of PU.1 in mast cell/basophil-specific function of the human IL1RL1/ST2 promoter. *Allergol. Int.* **61**, 461–467 (2012).
87. Kunkle, B. W. et al. Genetic meta-analysis of diagnosed Alzheimer's disease identifies new risk loci and implicates Aβ, tau, immunity and lipid processing. *Nat. Genet.* **51**, 414–430 (2019).
88. Jun, G. et al. A novel Alzheimer disease locus located near the gene encoding tau protein. *Mol. Psychiatry* **21**, 108–117 (2016).
89. O'Meara, E. et al. Independent prognostic value of serum soluble ST2 measurements in patients with heart failure and a reduced ejection fraction in the PARADIGM-HF trial (prospective comparison of ARNI with ACEI to determine impact on global mortality and morbidity in heart failure). *Circ. Heart Fail.* **11**, e004446 (2018).
90. American Psychiatric Association. *Diagnostic and Statistical Manual of Mental Disorders* 5th edn. (American Psychiatric Association, 2013).
91. Pangman, V. C., Sloan, J. & Guse, L. An examination of psychometric properties of the Mini-Mental State Examination and the standardized mini-mental state examination: implications for clinical practice. *Appl. Nurs. Res.* **13**, 209–213 (2000).
92. Nasreddine, Z. S. et al. The Montreal Cognitive Assessment, MoCA: a brief screening tool for mild cognitive impairment. *J. Am. Geriatr. Soc.* **53**, 695–699 (2005).
93. Jiang, Y. et al. Large-scale plasma proteomic profiling identifies a high-performance biomarker panel for Alzheimer's disease screening and staging. *Alzheimers Dement.* **18**, 88–102 (2021).
94. Purcell, S. et al. PLINK: a tool set for whole-genome association and population-based linkage analyses. *Am. J. Hum. Genet.* **81**, 559–575 (2007).
95. Hormozdiari, F., Kostem, E., Kang, E. Y., Pasaniuc, B. & Eskin, E. Identifying causal variants at loci with multiple signals of association. *Genetics* **198**, 497–508 (2014).
96. Grömping, U. Relative importance for linear regression in R: the package relaimpo. *J. Stat. Softw.* **17**, 1–27 (2006).
97. Patin, E. et al. Natural variation in the parameters of innate immune cells is preferentially driven by genetic factors. *Nat. Immunol.* **19**, 302–314 (2018).
98. Huang, D. W., Sherman, B. T. & Lempicki, R. A. Bioinformatics enrichment tools: paths toward the comprehensive functional analysis of large gene lists. *Nucleic Acids Res.* **37**, 1–13 (2009).
99. Sherman, B. T. & Lempicki, R. A. Systematic and integrative analysis of large gene lists using DAVID bioinformatics resources. *Nat. Protoc.* **4**, 44–57 (2009).
100. Oakley, H. et al. Intraneuronal β-amyloid aggregates, neurodegeneration, and neuron loss in transgenic mice with five familial Alzheimer's disease mutations: potential factors in amyloid plaque formation. *J. Neurosci.* **26**, 10129–10140 (2006).
101. Weksler, B. et al. Blood–brain barrier-specific properties of a human adult brain endothelial cell line. *FASEB J.* **19**, 1872–1874 (2005).
102. Youden, W. J. Index for rating diagnostic tests. *Cancer* **3**, 32–35 (1950).

Acknowledgements

We thank P. Kwan, H. Mok, C. Y. Ling and R. M. N. Lo for coordinating the collection of clinical data. We also thank P. -O. Couraud (Institut national de la santé et de la recherche médicale) for providing advice on the cell line culturing. We thank J. K. Y. Lau, E. K. F. Tam, Y. Duan, A. Miranda, C. W. S. Kwong, X. Yang, H. Cao, J. Xu, A. S. L. Yuen and G. P. O. Chiu for their excellent technical assistance as well as other members of the Ip Laboratory for their many helpful discussions. We thank the SWDBB for providing brain tissue for this study. The SWDBB is part of the Brains for Dementia Research program, jointly funded by Alzheimer's Research UK and Alzheimer's Society and supported by BRACE (Bristol Research into Alzheimer's and Care of the Elderly) and the MRC. We thank the AIBL study (https://aibl.csiro.au/). The AIBL study is a consortium between the Commonwealth Scientific and Industrial Research Organisation (CSIRO), Edith Cowan University, The Florey Institute and Austin Health. Partial financial support was provided by the US Alzheimer's Association, the Alzheimer's Drug Discovery Foundation, an anonymous foundation, the Cooperative Research Centre for Mental Health, the CSIRO Science and Industry Endowment Fund, the Dementia Collaborative Research Centres, the Victorian Government Operational Infrastructure Support program, the Australian Alzheimer's Research Foundation, the National Health and MRC and the Yulgilbar Foundation. We also thank M. Vacher for providing advice on the data analysis. Please refer to the Supplementary Notes for corresponding acknowledgments for the ADNI dataset, Alzheimer's Disease Genetics Consortium GWAS–NIA Alzheimer's Disease Centers Cohort (ADC dataset), the NIA–LOAD dataset and the GTEx Project. Part of the data used in the preparation of this article was obtained from the ADNI database. As such, the investigators within ADNI contributed to the design and implementation of ADNI and/or provided data but did not participate in the analysis or writing of this report. A complete listing of ADNI investigators can be found in the Supplementary Notes and at http://adni.loni.usc.edu/wp-content/uploads/how_to_apply/ADNI_Acknowledgement_List.pdf.

This study was supported in part by the National Key R&D Program of China (2018YFE0203600 and 2017YFE0190000); the Hong Kong Research Grants Council Theme-based Research Scheme (T13-605/18-W); the Area of Excellence Scheme of the University Grants Committee (AoE/M-604/16); the Innovation and Technology Commission (ITCPD/17-9, MRP/042/18X and INNOHK18SC01); the National

Natural Science Foundation of China (31671047); the Guangdong Provincial Key S&T Program (2018B030336001); the Guangdong Provincial Fund for Basic and Applied Basic Research (2019B1515130004); the Shenzhen Knowledge Innovation Program (JCYJ20180507183642005 and JCYJ20170413173717055); and the Chow Tai Fook Charity Foundation (CTFCF18SC01). Analyses in AIBL were supported through NHMRC (Australia) funding awarded to S.M.L. (APP1161706). The funders had no role in the study design, data collection and analysis, decision to publish or preparation of the manuscript.

Author contributions

Y.J., X.Z., A.K.F. and N.Y.I. conceived the study; F.C.I., Y.C., E.P.T., V.C.M. and T.C.K. organized recruitment and sample collection; Y.J., H.Y.W., L.O., V.M.C., W.W., D.Y.W., H.S. and N.C.L. performed the experiments; Y.J. and X.Z. set up the data-processing pipelines; Y.J., X.Z., H.Y.W., L.O., V.M.C., S.L., W.W., D.Y.W., H.S., W.F., N.C.L., K.Y.M., M.S., B.L., P.M.L., E.O., T.P., S.M.L., J.H., T.W., C.L.M., A.K.F. and N.Y.I. analyzed the data; and Y.J., A.K.F. and N.Y.I. wrote the manuscript with input from all authors; the ADNI contributed part of the study data.

Competing interests

All authors declare no competing interests.

Additional information

Extended data is available for this paper at https://doi.org/10.1038/s43587-022-00241-9.

Supplementary information is available for this paper at https://doi.org/10.1038/s43587-022-00241-9.

Correspondence and requests for materials should be addressed to Yuanbing Jiang, Xiaopu Zhou, Hiu Yi Wong, Li Ouyang, Fanny C. F. Ip, Vicky M. N. Chau, Shun-Fat Lau, Wei Wu, Daniel Y. K. Wong, Heukjin Seo, Wing-Yu Fu, Nicole C. H. Lai, Yuewen Chen, Yu Chen, Estella P. S. Tong, Vincent C. T. Mok, Timothy C. Y. Kwok, Kin Y. Mok, Maryam Shoai, Benoit Lehallier, Patricia Morán Losada, Eleanor O'Brien, Tenielle Porter, Simon M. Laws, John Hardy, Tony Wyss-Coray, Colin L. Masters, Amy K. Y. Fu or Nancy Y. Ip.

Peer review information *Nature Aging* thanks Keenan Walker, Sven van der Lee, Alberto Pascual and the other, anonymous, reviewer(s) for their contribution to the peer review of this work.

Alzheimer's Disease Neuroimaging Initiative

Michael W. Weiner[17], Paul Aisen[18], Ronald Petersen[19], Clifford R. Jack[19], William Jagust[20], John Q. Trojanowski[21], Arthur W. Toga[22], Laurel Beckett[23], Robert C. Green[24], Andrew J. Saykin[25], John Morris[26], Leslie M. Shaw[21], Zaven Khachaturian[23,27], Greg Sorensen[28], Lew Kuller[29], Marcus Raichle[26], Steven Paul[30], Peter Davies[31], Howard Fillit[32], Franz Hefti[33], David Holtzman[26], Marek M. Mesulam[34], William Potter[35], Peter Snyder[36], Adam Schwartz[37], Tom Montine[38], Ronald G. Thomas[38], Michael Donohue[38], Sarah Walter[38], Devon Gessert[38], Tamie Sather[38], Gus Jiminez[38], Danielle Harvey[23], Matthew Bernstein[19], Paul Thompson[39], Norbert Schuff[17,23], Bret Borowski[19], Jeff Gunter[19], Matt Senjem[19], Prashanthi Vemuri[19], David Jones[19], Kejal Kantarci[19], Chad Ward[19], Robert A. Koeppe[40], Norm Foster[41], Eric M. Reiman[42], Kewei Chen[42], Chet Mathis[32], Susan Landau[20], Nigel J. Cairns[26], Erin Householder[26], Lisa Taylor-Reinwald[26], Virginia Lee[21], Magdalena Korecka[21], Michal Figurski[21], Karen Crawford[22], Scott Neu[22], Tatiana M. Foroud[25], Steven G. Potkin[43], Li Shen[25], Kelley Faber[25], Sungeun Kim[25], Kwangsik Nho[25], Leon Thal[18], Neil Buckholtz[44], Marylyn Albert[45], Richard Frank[46], John Hsiao[44], Jeffrey Kaye[47], Joseph Quinn[47], Betty Lind[47], Raina Carter[47], Sara Dolen[47], Lon S. Schneider[22], Sonia Pawluczyk[22], Mauricio Beccera[22], Liberty Teodoro[22], Bryan M. Spann[22], James Brewer[18], Helen Vanderswag[18], Adam Fleisher[18,42], Judith L. Heidebrink[40], Joanne L. Lord[40], Sara S. Mason[19], Colleen S. Albers[19], David Knopman[19], Kris Johnson[19], Rachelle S. Doody[48], Javier Villanueva-Meyer[48], Munir Chowdhury[48], Susan Rountree[48], Mimi Dang[48], Yaakov Stern[48], Lawrence S. Honig[48], Karen L. Bell[48], Beau Ances[26], Maria Carroll[26], Sue Leon[26], Mark A. Mintun[26], Stacy Schneider[26], Angela Oliver[26], Daniel Marson[49], Randall Griffith[49], David Clark[49], David Geldmacher[49], John Brockington[49], Erik Roberson[49], Hillel Grossman[50], Effie Mitsis[50], Leyla de Toledo-Morrell[51], Raj C. Shah[51], Ranjan Duara[52], Daniel Varon[52], Maria T. Greig[52], Peggy Roberts[52], Chiadi Onyike[45], Daniel D'Agostino[45], Stephanie Kielb[45], James E. Galvin[53], Brittany Cerbone[53], Christina A. Michel[53], Henry Rusinek[53], Mony J. de Leon[53], Lidia Glodzik[53], Susan De Santi[53], P. Murali Doraiswamy[54], Jeffrey R. Petrella[54], Terence Z. Wong[54], Steven E. Arnold[21], Jason H. Karlawish[21], David Wolk[21], Charles D. Smith[55],

Greg Jicha[55], Peter Hardy[55], Partha Sinha[55], Elizabeth Oates[55], Gary Conrad[55], Oscar L. Lopez[29], MaryAnn Oakley[29], Donna M. Simpson[45], Anton P. Porsteinsson[56], Bonnie S. Goldstein[57], Kim Martin[57], Kelly M. Makino[57], M. Saleem Ismail[57], Connie Brand[57], Ruth A. Mulnard[43], Gaby Thai[43], Catherine McAdams-Ortiz[43], Kyle Womack[57], Dana Mathews[57], Mary Quiceno[57], Ramon Diaz-Arrastia[57], Richard King[57], Myron Weiner[57], Kristen Martin-Cook[57], Michael DeVous[57], Allan I. Levey[58], James J. Lah[58], Janet S. Cellar[58], Jeffrey M. Burns[59], Heather S. Anderson[59], Russell H. Swerdlow[59], Liana Apostolova[39], Kathleen Tingus[39], Ellen Woo[39], Daniel H. S. Silverman[39], Po H. Lu[39], George Bartzokis[39], Neill R. Graff-Radford[60], Francine Parfitt[60], Tracy Kendall[60], Heather Johnson[60], Martin R. Farlow[25], Ann Marie Hake[25], Brandy R. Matthews[25], Scott Herring[25], Cynthia Hunt[25], Christopher H. van Dyck[61], Richard E. Carson[61], Martha G. MacAvoy[61], Howard Chertkow[62], Howard Bergman[62], Chris Hosein[62], Ging-Yuek Robin Hsiung[63], Howard Feldman[63], Benita Mudge[63], Michele Assaly[63], Charles Bernick[64], Donna Munic[64], Andrew Kertesz[65], John Rogers[65], Dick Trost[65], Diana Kerwin[34], Kristine Lipowski[34], Chuang-Kuo Wu[34], Nancy Johnson[34], Carl Sadowsky[66], Walter Martinez[66], Teresa Villena[66], Raymond Scott Turner[67], Kathleen Johnson[67], Brigid Reynolds[67], Reisa A. Sperling[24], Keith A. Johnson[24], Gad Marshall[24], Meghan Frey[24], Barton Lane[24], Allyson Rosen[24], Jared Tinklenberg[24], Marwan N. Sabbagh[68], Christine M. Belden[68], Sandra A. Jacobson[68], Sherye A. Sirrel[68], Neil Kowall[68], Ronald Killiany[69], Andrew E. Budson[69], Alexander Norbash[69], Patricia Lynn Johnson[69], Joanne Allard[70], Alan Lerner[71], Paula Ogrocki[71], Leon Hudson[71], Evan Fletcher[23], Owen Carmichael[23], John Olichney[23], Charles DeCarli[23], Smita Kittur[72], Michael Borrie[73], T-Y. Lee[73], Rob Bartha[73], Sterling Johnson[74], Sanjay Asthana[74], Cynthia M. Carlsson[74], Adrian Preda[39], Dana Nguyen[39], Pierre Tariot[41], Stephanie Reeder[41], Vernice Bates[75], Horacio Capote[75], Michelle Rainka[75], Douglas W. Scharre[76], Maria Kataki[76], Anahita Adeli[76], Earl A. Zimmerman[77], Dzintra Celmins[77], Alice D. Brown[77], Godfrey D. Pearlson[78], Karen Blank[78], Karen Anderson[78], Robert B. Santulli[79], Tamar J. Kitzmiller[79], Eben S. Schwartz[79], Kaycee M. Sink[80], Jeff D. Williamson[80], Pradeep Garg[80], Franklin Watkins[80], Brian R. Ott[81], Henry Querfurth[81], Geoffrey Tremont[81], Stephen Salloway[82], Paul Malloy[82], Stephen Correia[82], Howard J. Rosen[17], Bruce L. Miller[17], Jacobo Mintzer[83], Kenneth Spicer[83], David Bachman[83], Stephen Pasternak[65], Irina Rachinsky[65], Dick Drost[65], Nunzio Pomara[84], Raymundo Hernando[84], Antero Sarrael[84], Susan K. Schultz[85], Laura L. Boles Ponto[85], Hyungsub Shim[85], Karen Elizabeth Smith[85], Norman Relkin[30], Gloria Chaing[30], Lisa Raudin[27,30], Amanda Smith[86], Kristin Fargher[86], Balebail Ashok Raj[86], Thomas Neylan[17], Jordan Grafman[34], Melissa Davis[18], Rosemary Morrison[18], Jacqueline Hayes[17], Shannon Finley[17], Karl Friedl[87], Debra Fleischman[51], Konstantinos Arfanakis[51], Olga James[54], Dino Massoglia[83], J. Jay Fruehling[74], Sandra Harding[74], Elaine R. Peskind[38], Eric C. Petrie[76], Gail Li[76], Jerome A. Yesavage[88], Joy L. Taylor[88] and Ansgar J. Furst[88]

[17]UC San Francisco, San Francisco, California, USA. [18]UC San Diego, San Diego, California, USA. [19]Mayo Clinic, Rochester, New York, USA. [20]UC Berkeley, Berkeley, California, USA. [21]University of Pennsylvania, Philadelphia, Pennsylvania, USA. [22]University of Southern California, Los Angeles, California, USA. [23]UC Davis, Davis, California, USA. [24]Brigham and Women's Hospital/Harvard Medical School, Boston, Massachusetts, USA. [25]Indiana University, Bloomington, Indiana, USA. [26]Washington University in St. Louis, St. Louis, Missouri, USA. [27]Prevent Alzheimer's Disease 2020, Rockville, Maryland, USA. [28]Siemens, Munich, Germany. [29]University of Pittsburgh, Pittsburgh, Pennsylvania, USA. [30]Weill Cornell Medical College, Cornell University, New York City, New York, USA. [31]Albert Einstein College of Medicine, Yeshiva University, Bronx, New York, USA. [32]Alzheimer's Drug Discovery Foundation, New York City, New York, USA. [33]Acumen Pharmaceuticals, Livermore, California, USA. [34]Northwestern University, Evanston and Chicago, Evanston, Illinois, USA. [35]National Institute of Mental Health, Rockville, Maryland, USA. [36]Brown University, Providence, Rhode Island, USA. [37]Eli Lilly, Indianapolis, Indiana, USA. [38]University of Washington, Seattle, Washington, USA. [39]UCLA, Los Angeles, California, USA. [40]University of Michigan, Ann Arbor, Michigan, USA. [41]University of Utah, Salt Lake City, Utah, USA. [42]Banner Alzheimer's Institute, Phoenix, Arizona, USA. [43]UC Irvine, Irvine, California, USA. [44]National Institute on Aging, Bethesda, Maryland, USA. [45]Johns Hopkins University, Baltimore, Maryland, USA. [46]Richard Frank Consulting, Washington,

USA. [47]Oregon Health and Science University, Portland, Oregon, USA. [48]Baylor College of Medicine, Houston, Texas, USA. [49]University of Alabama, Birmingham, Alabama, USA. [50]Mount Sinai School of Medicine, New York City, New York, USA. [51]Rush University Medical Center, Chicago, Illinois, USA. [52]Wien Center, Miami, Florida, USA. [53]New York University, New York City, New York, USA. [54]Duke University Medical Center, Durham, North Carolina, USA. [55]University of Kentucky, Lexington, Kentucky, USA. [56]University of Rochester Medical Center, Rochester, New York, USA. [57]University of Texas Southwestern Medical School, Dallas, Texas, USA. [58]Emory University, Atlanta, Georgia, USA. [59]Medical Center, University of Kansas, Kansas City, Kansas, USA. [60]Mayo Clinic, Jacksonville, Florida, USA. [61]Yale University School of Medicine, New Haven, Connecticut, USA. [62]McGill University/Montreal-Jewish General Hospital, Montreal, Quebec, Canada. [63]University of British Columbia Clinic for Alzheimer's Disease and Related Disorders, Vancouver, British Columbia, Canada. [64]Cleveland Clinic Lou Ruvo Center for Brain Health, Las Vegas, Nevada, USA. [65]St Joseph's Health Care, London, Ontario, Canada. [66]Premiere Research Institute, Palm Beach Neurology, Miami, Florida, USA. [67]Georgetown University Medical Center, Washington, D.C., USA. [68]Banner Sun Health Research Institute, Sun City, Arizona, USA. [69]Boston University, Boston, Massachusetts, USA. [70]Howard University, Washington, D.C., USA. [71]Case Western Reserve University, Cleveland, Ohio, USA. [72]Neurological Care of CNY, Liverpool, New York, USA. [73]Parkwood Hospital, London, Ontario, Canada. [74]University of Wisconsin, Madison, Wisconsin, USA. [75]Dent Neurologic Institute, Amherst, New York, USA. [76]Ohio State University, Columbus, Ohio, USA. [77]Albany Medical College, Albany, New York, USA. [78]Olin Neuropsychiatry Research Center, Hartford Hospital, Hartford, Connecticut, USA. [79]Dartmouth-Hitchcock Medical Center, Lebanon, New Hampshire, USA. [80]Wake Forest University Health Sciences, Winston-Salem, North Carolina, USA. [81]Rhode Island Hospital, Providence, Rhode Island, USA. [82]Butler Hospital, Providence, Rhode Island, USA. [83]Medical University South Carolina, Charleston, South Carolina, USA. [84]Nathan Kline Institute, Orangeburg, New York, USA. [85]University of Iowa College of Medicine, Iowa City, Iowa, USA. [86]USF Health Byrd Alzheimer's Institute, University of South Florida, Tampa, Florida, USA. [87]Department of Defense, Arlington, Virginia, USA. [88]Stanford University, Stanford, California, USA.

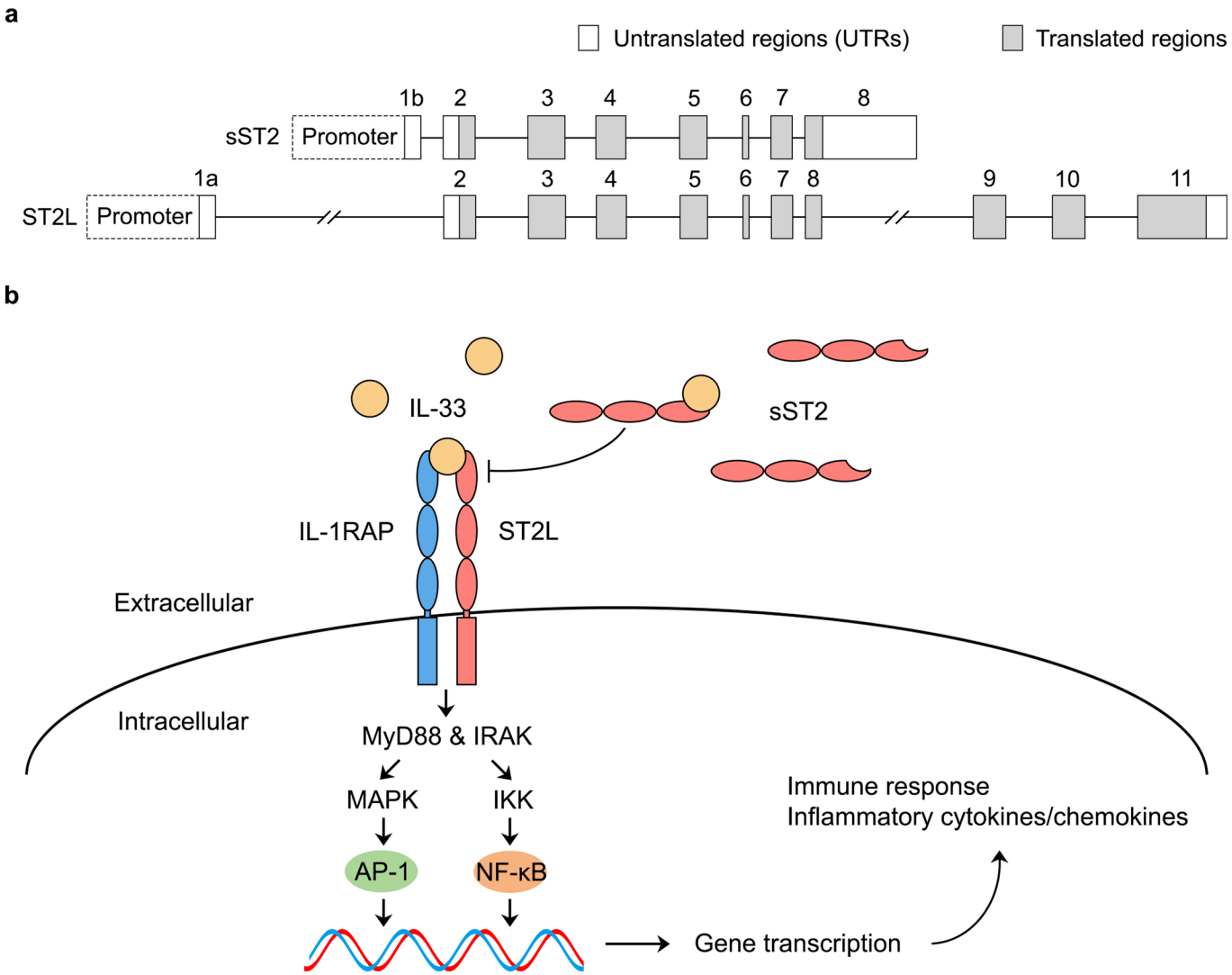

Extended Data Fig. 1 | Diagrams illustrating IL-33–ST2 signaling. (a) Schematic showing the soluble ST2 (sST2) and full-length ST2 (ST2L) transcripts. (b) The IL-33/ST2 signaling pathways. IL-33, interleukin 33.

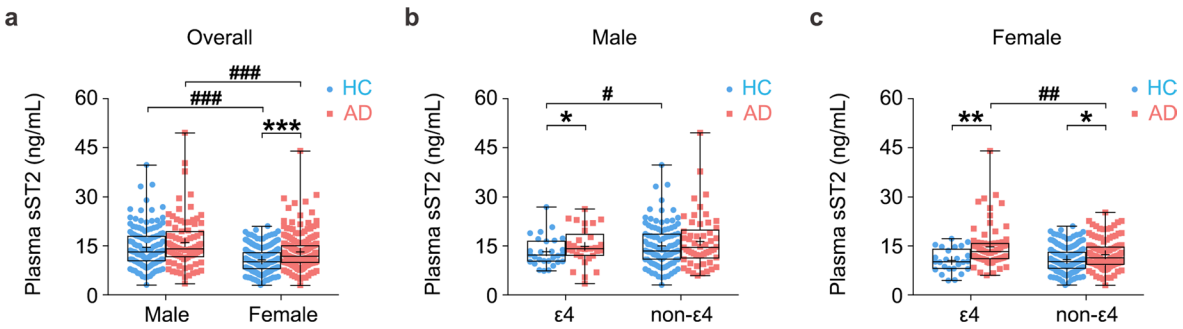

Extended Data Fig. 2 | Associations between plasma soluble ST2 levels and Alzheimer's disease in the Chinese_cohort_1, stratified by sex and *APOE*-ε4 genotypes. (a) Individual plasma soluble ST2 (sST2) levels stratified by sex and disease phenotype (male: $n=132$ healthy controls [HCs], $n=84$ individuals with Alzheimer's disease [AD]; female: $n=204$ HCs, $n=193$ individuals with AD). Test for effects of sex: $\beta=-3.848$ and -3.257 in HCs and individuals with AD, respectively; test for effects of AD: $\beta=1.926$ and 2.235 in males and females, respectively. (b, c) Individual plasma sST2 levels stratified by *APOE*-ε4 genotypes and disease phenotype in (b) males (male ε4: $n=28$ HCs, $n=29$ individuals with AD; male non-ε4: $n=104$ HCs, $n=55$ individuals with AD), and (c) females (female ε4: $n=25$ HCs, $n=71$ individuals with AD; female non-ε4: $n=179$ HCs, $n=122$ individuals with AD). Test for effects of *APOE*-ε4: $\beta=-1.809$, -1.499, -0.248, and 2.425 in male HCs, male individuals with AD, female HCs, and female individuals with AD, respectively; test for effects of AD: $\beta=2.034$, 1.098, 3.833, and 1.811 in male ε4, male non-ε4, female ε4, and female non-ε4, respectively. ε4, *APOE*-ε4 carriers; non-ε4, *APOE*-ε4 noncarriers. Data are presented as box-and-whisker plots including maximum, 75th percentile, median, 25th percentile, and minimum values; plus signs (+) denote corresponding mean values. Linear regression test, adjusted for age, cardiovascular disease status, body mass index (BMI), and education level, with multiple testing correction; $^{\#}FDR<0.05$, $^{\#\#}FDR<0.01$, $^{\#\#\#}FDR<0.001$; $^{*}FDR<0.05$, $^{**}FDR<0.01$, $^{***}FDR<0.001$. *FDR*, false discovery rate.

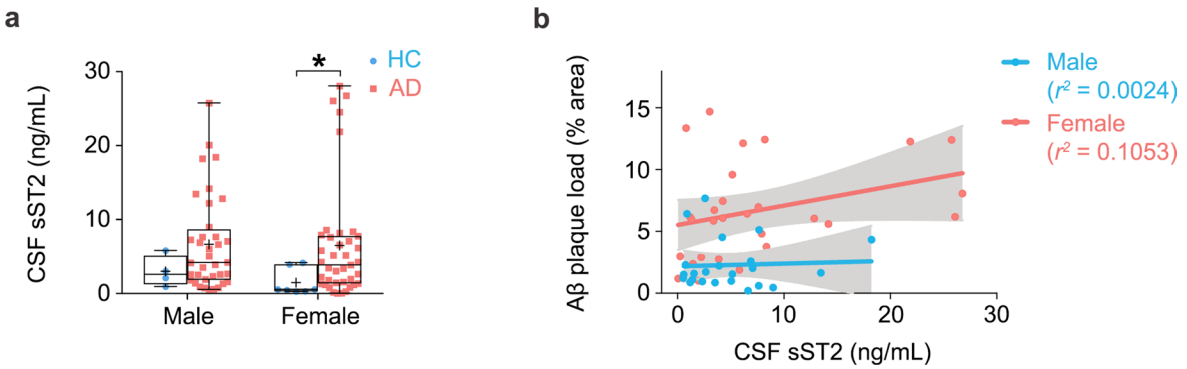

Extended Data Fig. 3 | Associations between cerebrospinal fluid soluble ST2 levels and Alzheimer's disease and amyloid-beta depositions in the UKBBN cohort, stratified by sex. (a) Individual cerebrospinal fluid (CSF) soluble ST2 (sST2) levels stratified by sex and disease phenotype ($n = 4$ male healthy controls [HCs], $n = 36$ male individuals with Alzheimer's disease [AD], $n = 7$ female HCs, $n = 39$ female individuals with AD). Test for effects of sex: $\beta = -1.307$ and -0.675 in HCs and individuals with AD, respectively; test for effects of AD: $\beta = 4.019$ and 7.766 in males and females, respectively. Data are presented as box-and-whisker plots including maximum, 75th percentile, median, 25th percentile, and minimum values; plus signs (+) denote corresponding mean values. Linear regression test, adjusted for age and postmortem duration (PMD), with multiple testing correction; *$FDR < 0.05$. (b) Associations between amyloid-beta (Aβ) staining in the postmortem frontal cortex and CSF sST2 levels in male and female individuals with AD ($n = 23$ males and 28 females in the UKBBN cohort, respectively). The regression lines and 95% confidence intervals are indicated in red/blue and gray, respectively. Linear regression test, adjusted for age and PMD, with multiple testing correction. Test in males: $\beta = 0.0256$, Pearson's $r^2 = 0.0024$, $FDR = 0.7866$; test in females: $\beta = 0.2188$, Pearson's $r^2 = 0.1053$, $FDR = 0.0407$. *FDR*, false discovery rate.

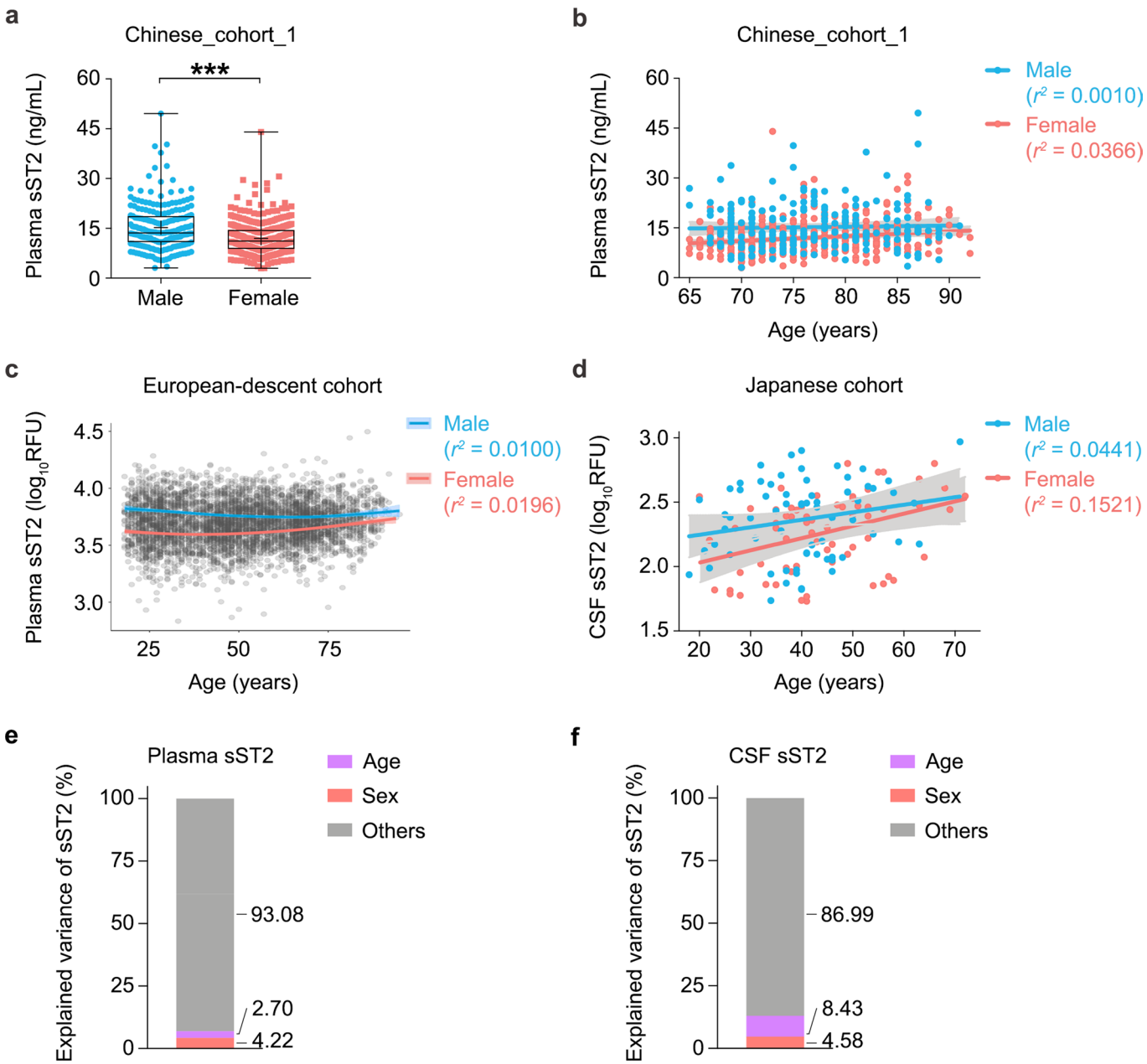

Extended Data Fig. 4 | Effects of sex and age on soluble ST2 levels. (a) Individual plasma sST2 levels stratified by sex ($n = 216$ males, and 397 females from Chinese_cohort_1). $\beta = -3.577$ for females vs. males, $P = 1.58E-12$. (b) Associations between plasma sST2 levels and age in males and females ($n = 216$ males, and 397 females from Chinese_cohort_1). Test in males: $\beta = 0.0134$, Pearson's $r^2 = 0.0010$, $P = 0.8661$; test in females: $\beta = 0.1256$, Pearson's $r^2 = 0.0366$, $P = 0.0016$. (c) Correlations between plasma sST2 level and age in males and females from the INTERVAL and LonGenity cohort ($n = 1{,}685$ males, and 1,616 females from INTERVAL cohort; $n = 432$ males, and 530 females from LonGenity cohort). Test in INTERVAL cohort (ages 18–76), males: Pearson's $r^2 = 0.0169$, $P < 0.0001$; females: Pearson's $r^2 = 0.0001$, $P = 0.7715$. Test in LonGenity cohort (ages 65–94), males: Pearson's $r^2 = 0.0100$, $P = 0.0093$; females: Pearson's $r^2 = 0.0196$, $P = 0.0001$. (d) Correlations between CSF sST2 level and age in males and females from the Japanese cohort ($n = 68$ males, $n = 65$ females). Test in males: Pearson's $r^2 = 0.0441$, $P = 0.0812$; test in females: Pearson's $r^2 = 0.1521$, $P = 0.0014$. (e, f) Contributions of age and sex to the variance of sST2 levels. Numbers denote the proportions of plasma sST2 (e) and CSF sST2 (f) variance explained by age, sex, and other factors in the Chinese_cohort_1 and Japanese cohort, respectively. Data in box-and-whisker plots are presented with maximum, 75th percentile, median, 25th percentile, and minimum values; plus signs (+) denote mean values; data in regression lines are presented as slope (red/blue) and 95% CIs (gray). Statistical tests were performed by linear regression analysis, additionally adjusted for AD diagnosis, CVD status, BMI, education level in the Chinese_cohort_1. $^*P < 0.05$, $^{**}P < 0.01$, $^{***}P < 0.001$.

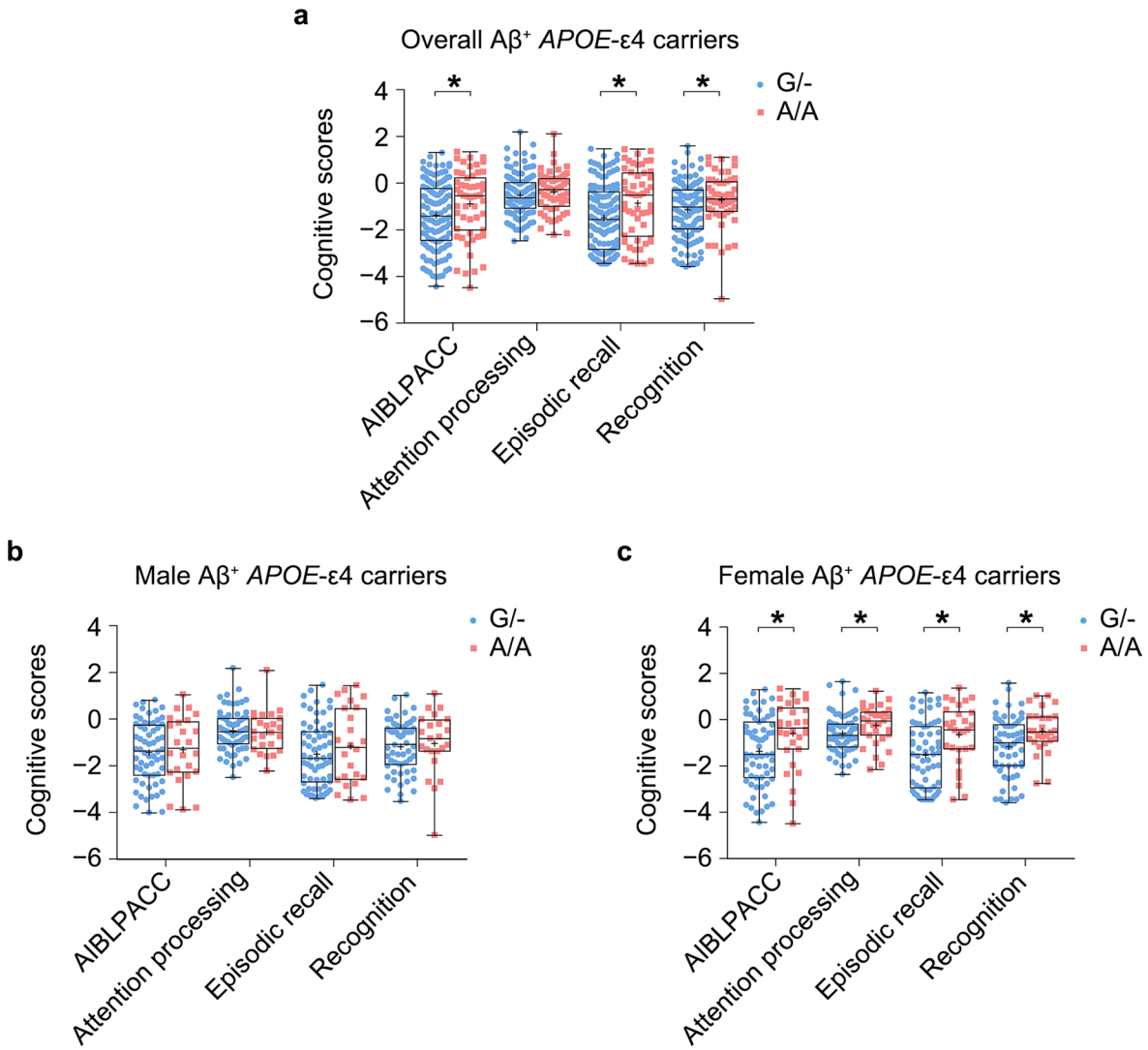

Extended Data Fig. 5 | The rs1921622 A allele is associated with better cognitive performance in female *APOE*-ε4 carriers in the AIBL Aβ+ cohort. Individual cognitive scores in (a) overall Aβ+ *APOE*-ε4 carriers ($n = 122$ G carriers [G/-], $n = 53$ A/A carriers), (b) male Aβ+ *APOE*-ε4 carriers ($n = 63$ G carriers [G/-], $n = 24$ A/A carriers), and (c) female Aβ+ *APOE*-ε4 carriers ($n = 59$ G carriers [G/-], $n = 29$ A/A carriers) stratified according to rs1921622 genotype. Test in the overall Aβ+ *APOE*-ε4 carriers, $W = 3782.0$, 3671.0, 3842.0, and 3319.0 for the effects of rs1921622 genotype on AIBL Preclinical Alzheimer Cognitive Composite (AIBLPACC) score, attention processing score, episodic recall score, and recognition score, respectively; test in the male Aβ+ *APOE*-ε4 carriers, $W = 784.0$, 727.0, 823.5, and 740.0 for the effects of rs1921622 genotype on AIBLPACC score, attention processing score, episodic recall score, and recognition score, respectively; test in the female Aβ+ *APOE*-ε4 carriers, $W = 1087.0$, 1115.5, 1083.0, and 916.5 for the effects of rs1921622 genotype on AIBLPACC score, attention processing score, episodic recall score, and recognition score, respectively. Data in box-and-whisker plots are presented with maximum, 75th percentile, median, 25th percentile, and minimum values; plus signs (+) denote mean values. Statistical tests are performed by Wilcoxon rank-sum test, with multiple testing correction. *$FDR < 0.05$, **$FDR < 0.01$, ***$FDR < 0.001$. *FDR*, false discovery rate.

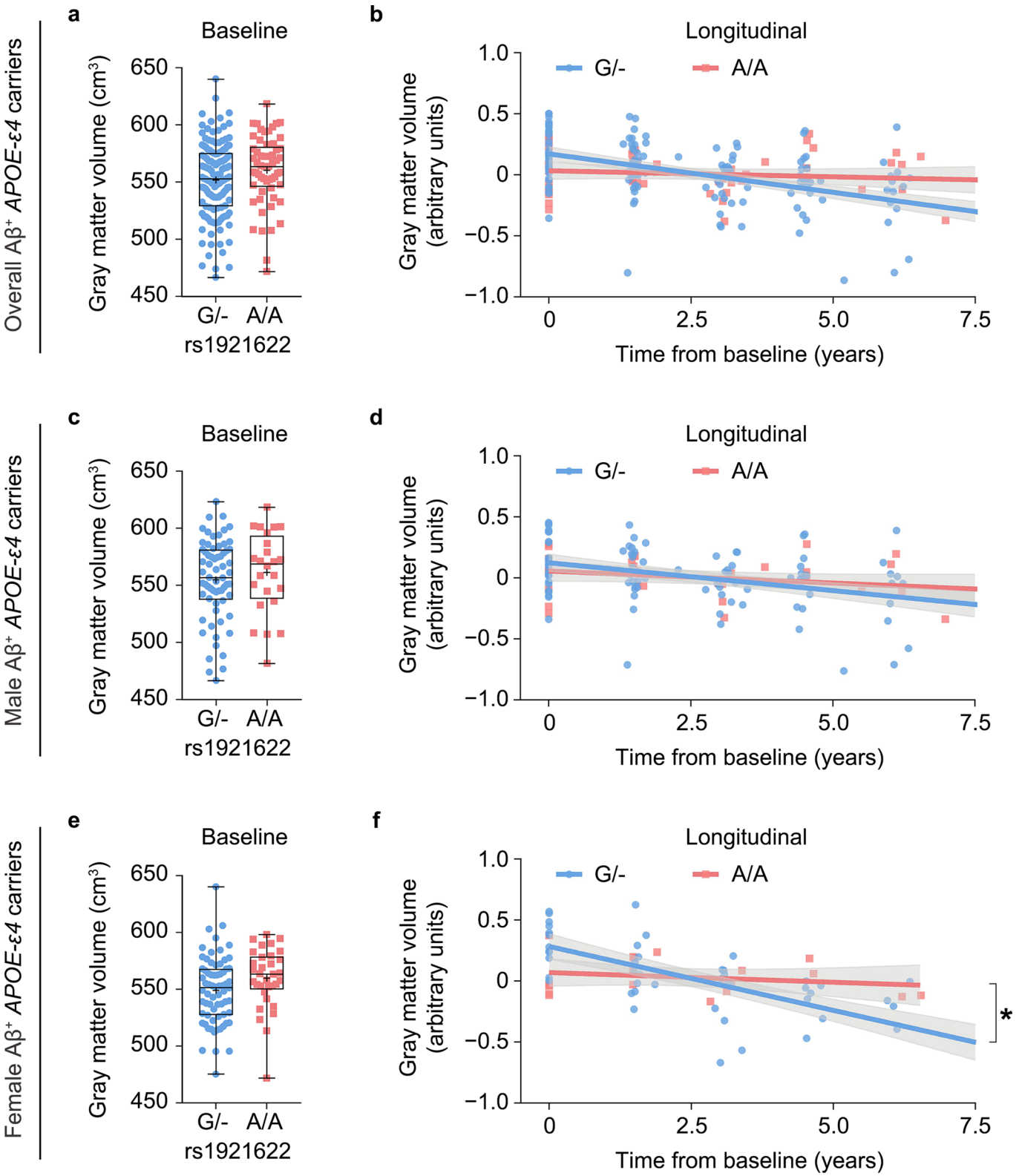

Extended Data Fig. 6 | See next page for caption.

Extended Data Fig. 6 | The rs1921622 A allele is associated with slower gray matter atrophy in female *APOE*-ε4 carriers in the AIBL Aβ⁺ cohort. (a, b) Individual baseline (a: $n = 128$ G carriers [G/-], and 55 A/A carriers) and longitudinal gray matter volume (b: $n = 148$ datapoints from 37 G/- carriers, and 55 datapoints from 14 A/A carriers) in overall Aβ⁺ *APOE*-ε4 carriers stratified by rs1921622 genotype. Test on baseline data: $W = 4109.0$, $FDR = 0.109$. Test on longitudinal data: $\beta = -0.089$ and -0.051 in G/- and A/A carriers, respectively; $F = 3.830$, $FDR = 0.087$. (c, d) Individual baseline (c: $n = 64$ G/- carriers, and 24 A/A carriers) and longitudinal gray matter volume (d: $n = 98$ datapoints from 25 G/- carriers, and 36 datapoints from 9 A/A carriers) in male Aβ⁺ *APOE*-ε4 carriers stratified by rs1921622 genotype. Test on baseline data: $W = 852.0$, $FDR = 0.434$. Test on longitudinal data: $\beta = -0.069$ and -0.053 in G/- and A/A carriers, respectively; $F = 0.272$, $FDR = 0.607$. (e, f) Individual baseline (e: $n = 64$ G/- carriers, and 31 A/A carriers) and longitudinal gray matter volume (f: $n = 50$ datapoints from 12 G/- carriers, and 19 datapoints from 5 A/A carriers) in female Aβ⁺ *APOE*-ε4 carriers stratified by rs1921622 genotype. Test on baseline data: $W = 1240.0$, $FDR = 0.109$. Test on longitudinal data: $\beta = -0.159$ and -0.027 in G/- and A/A carriers, respectively; $F = 8.804$. Data in box-and-whisker plots are presented with maximum, 75th percentile, median, 25th percentile, and minimum values; plus signs (+) denote mean values; data in regression lines are presented as slope (red/blue) and 95% confidence intervals (gray). Statistical tests on baseline data were performed by Wilcoxon rank-sum test, with multiple testing correction; and statistical tests on longitudinal data were performed by linear mixed model test, adjusted for baseline age and MRI scanners, with multiple testing correction. *$FDR < 0.05$, **$FDR < 0.01$, ***$FDR < 0.001$.

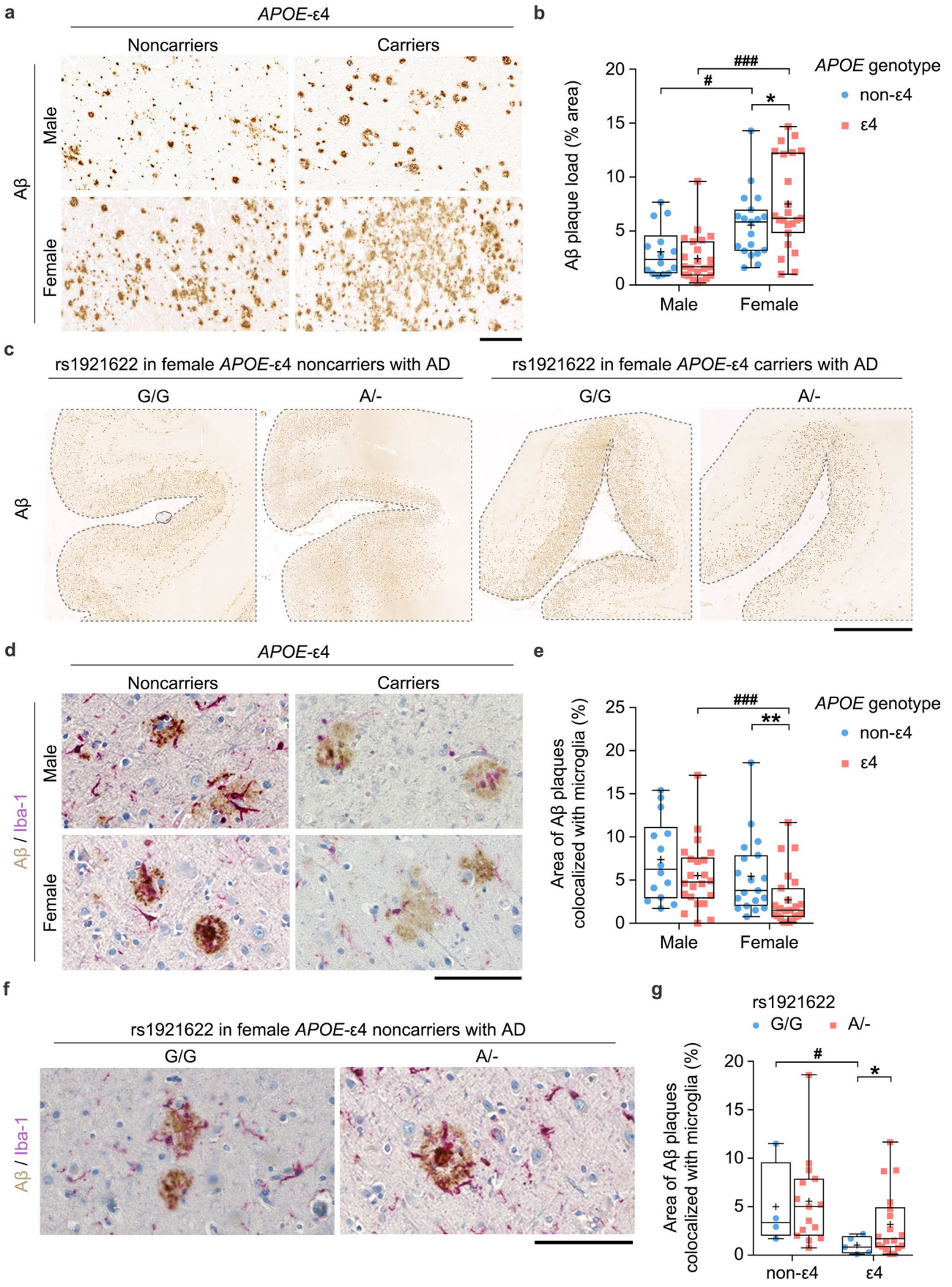

Extended Data Fig. 7 | See next page for caption.

Extended Data Fig. 7 | The rs1921622 A allele restores impaired microglial activities toward amyloid-beta in female *APOE*-ε4 carriers with Alzheimer's disease. (a, b) Representative images (a) and quantification (b) of Aβ plaques in the frontal cortices of individuals with AD stratified by sex and *APOE*-ε4 genotype ($n = 14$ male *APOE*-ε4 noncarriers [non-ε4], 22 male *APOE*-ε4 carriers [ε4], 19 female non-ε4, and 23 female ε4 from UKBBN cohort). Test for sex: $\beta = 2.871$ (non-*APOE*-ε4) and 4.927 (*APOE*-ε4), $P = 2.09E-2$ (non-ε4) and $4.61E-5$ (ε4); for *APOE*-ε4: $\beta = -0.621$ (males) and 1.967 (females), $P = 4.22E-1$ (males) and $4.84E-2$ (females). Scale bar, 200 μm. (c) Representative images of Aβ plaques in the frontal cortices of females with AD stratified by *APOE*-ε4 and rs1921622 genotype. Scale bar, 5 mm. (d, e) Representative image (d) and quantification (e) of Aβ plaques (brown) and Iba-1$^+$ microglia (purple) in the frontal cortices of individuals with AD stratified by sex and *APOE*-ε4 genotype ($n = 14$ male non-ε4, 22 male ε4, 19 female non-ε4, and 23 female ε4). Test for sex: $\beta = -1.214$ (non-ε4) and −4.133 (ε4), $P = 4.61E-1$ (non-ε4) and $3.52E-4$ (ε4); for *APOE*-ε4: $\beta = -0.965$ (males) and −2.818 (females), $P = 3.27E-1$ (males) and $6.00E-3$ (females). Scale bar, 100 μm. (f, g) Representative image (f) and quantification (g) of Aβ plaques and microglia in the frontal cortices of females with AD stratified by *APOE*-ε4 and rs1921622 genotype ($n = 4$ G/G and 15 A/- carriers among non-ε4, 5 G/G carriers and 18 A/- carriers among ε4, respectively). Test for *APOE*-ε4: $\beta = -3.745$ (G/G) and −1.944 (A/-), $P = 3.09E-2$ (G/G) and $9.32E-2$ (A/-); for rs1921622: $\beta = 0.781$ (non-ε4) and 2.017 (ε4), $P = 7.70E-1$ (non-ε4) and $2.53E-2$ (ε4). Scale bar, 100 μm. Data in box-and-whisker plots are presented with maximum, 75th percentile, median, 25th percentile, and minimum values; plus signs (+) denote mean values. Statistical tests were performed by linear regression analysis, adjusted for age, PMD. $^*P < 0.05$, $^{**}P < 0.01$, $^{***}P < 0.001$; $^{\#}P < 0.05$, $^{\#\#}P < 0.01$, $^{\#\#\#}P < 0.001$.

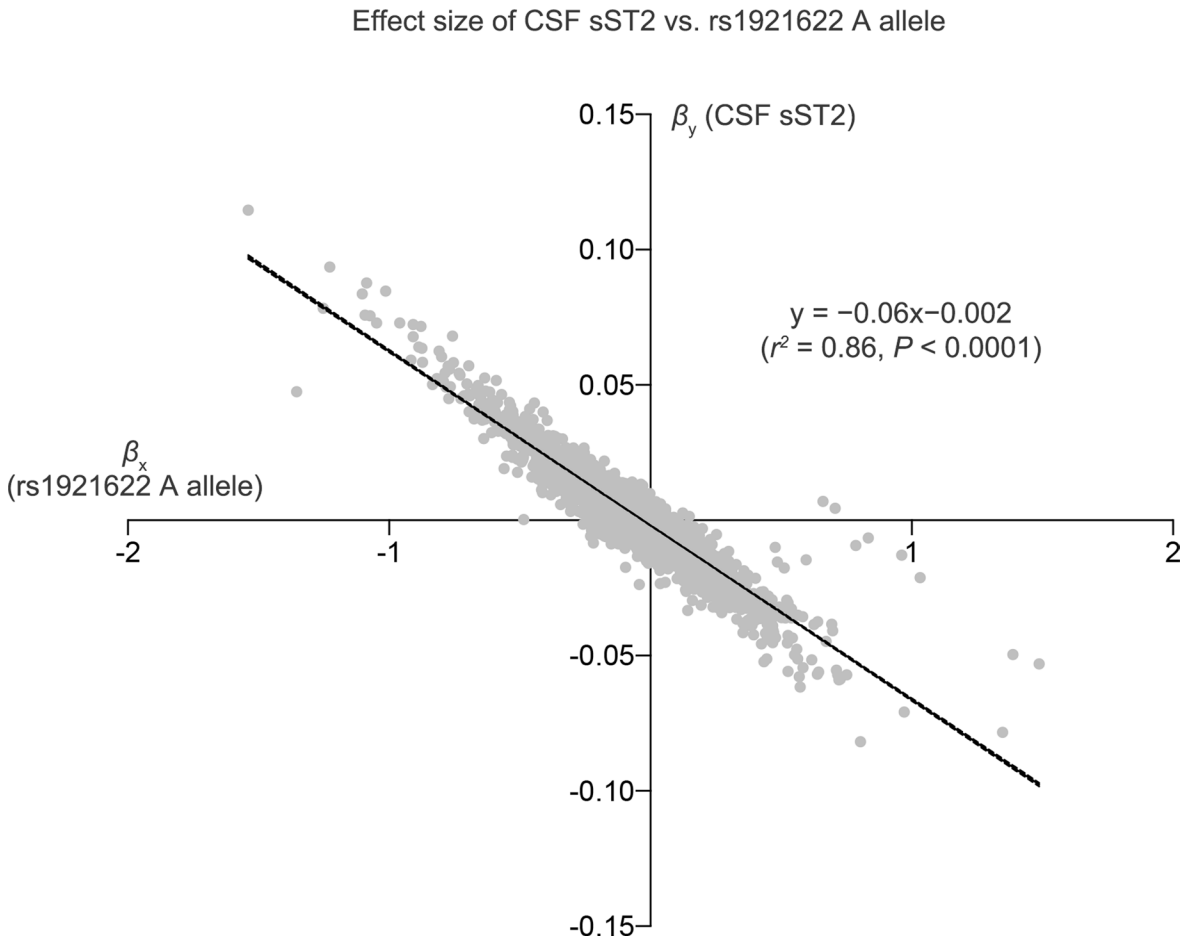

Extended Data Fig. 8 | The rs1921622 A allele and cerebrospinal fluid soluble ST2 level exhibit opposite effects on the microglial transcriptome in female *APOE*-ε4 carriers with Alzheimer's disease. Scatterplot showing the correlation between the normalized effect size (β) of cerebrospinal fluid (CSF) soluble ST2 (sST2) levels and the rs1921622 A allele on microglial gene expression in the frontal cortices of female *APOE*-ε4 carriers with Alzheimer's disease (AD) (n = 2,636 microglia from 8 individuals from the UKBBN cohort).

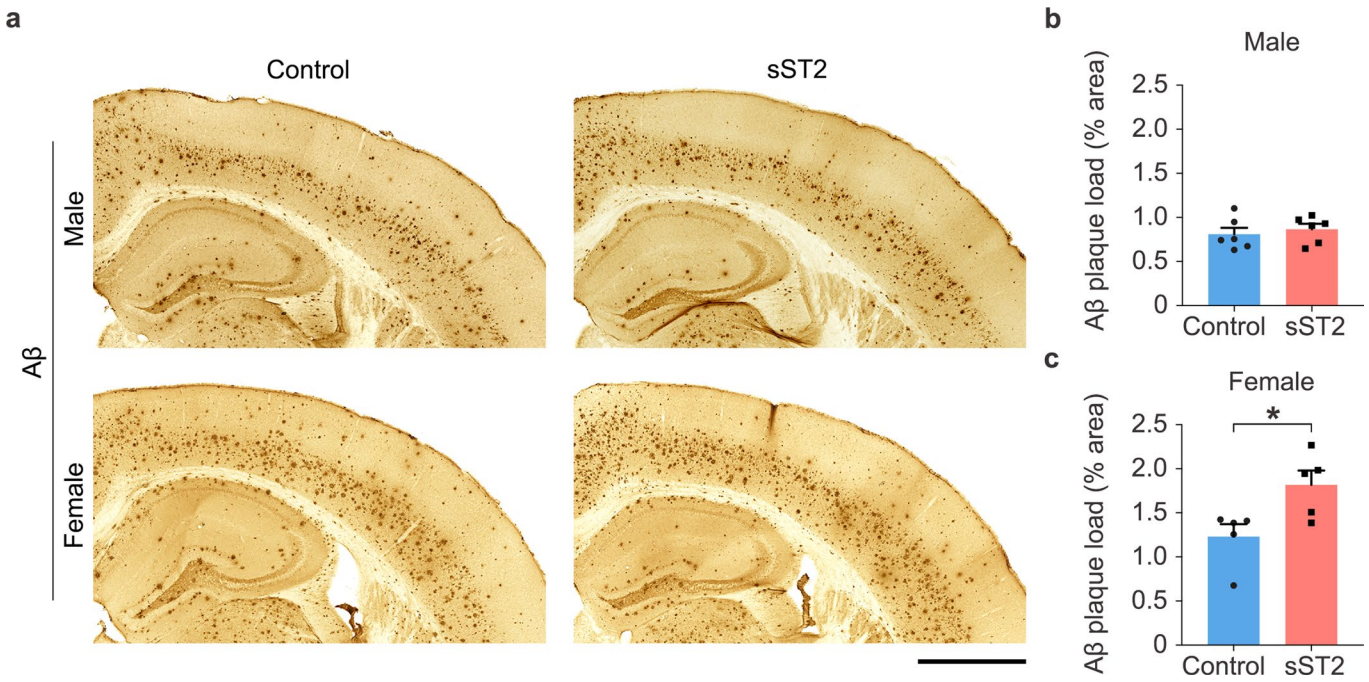

Extended Data Fig. 9 | Elevated brain soluble ST2 level exacerbates amyloid-beta deposition in female but not male 5XFAD mice. (a, b) Amyloid-beta (Aβ) deposition in the cortices of 4-month-old male and female 5XFAD mice after 28-day intracerebroventricular delivery of soluble sST2 (sST2)-Fc or Fc as a control. (a) Representative images of Aβ staining. Scale bar, 1mm. (b) Quantification of Aβ plaques (% of total cortical area) (control: $n=6$ male and 5 female mice, sST2: $n=6$ male and 5 female mice). $T=0.590$ (males) and 2.721 (females); $P=0.568$ (males) and 0.026 (females). Data in bar charts are mean + SEM. Statistical tests were performed as two-sided unpaired Student's *t*-tests. $^{*}P<0.05$, $^{**}P<0.01$, $^{***}P<0.001$.

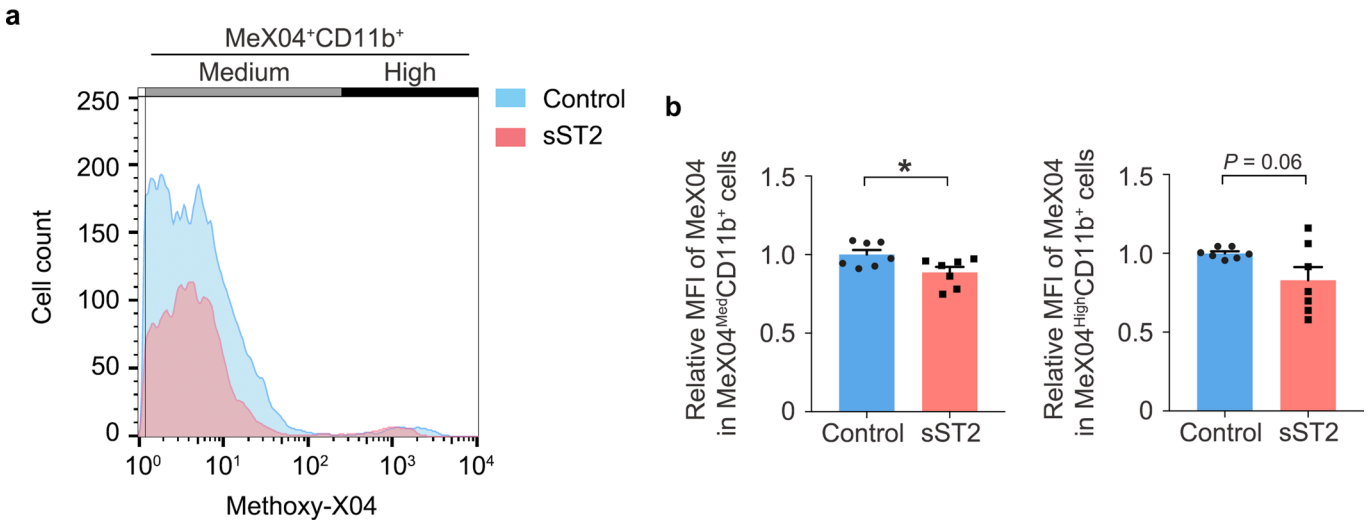

Extended Data Fig. 10 | Elevated brain soluble ST2 level leads to decreased amyloid-beta phagocytosis by microglia in female 5XFAD mice. (a, b) Microglial amyloid-beta (Aβ) uptake activity in the cortices of 4-month-old female 5XFAD mice after 28-day intracerebroventricular delivery of soluble ST2 (sST2)-Fc or Fc as a control. Representative distribution (a) and quantification (b) show the mean fluorescent intensity (MFI) of methoxy-X04-labeled Aβ in the methoxy-X04$^+$ CD11b$^+$ microglia (control: $n = 7$ mice, sST2: $n = 7$ mice). $T = -2.490$ and -2.014 for the tests in microglial with medium Aβ uptake (MeX04^{Med}CD11b$^+$; *left*) and high Aβ uptake (MeX04^{High}CD11b$^+$; *right*), respectively; $P = 0.028$ and 0.067, respectively. Data in bar charts are mean + SEM. Statistical tests were performed as two-sided unpaired Student's *t*-tests. $^*P < 0.05$, $^{**}P < 0.01$, $^{***}P < 0.001$.

nature portfolio

Corresponding author(s): Nancy Y. Ip

Last updated by author(s): Apr 28, 2022

Reporting Summary

Nature Portfolio wishes to improve the reproducibility of the work that we publish. This form provides structure for consistency and transparency in reporting. For further information on Nature Portfolio policies, see our Editorial Policies and the Editorial Policy Checklist.

Statistics

For all statistical analyses, confirm that the following items are present in the figure legend, table legend, main text, or Methods section.

n/a	Confirmed
☐	☒ The exact sample size (*n*) for each experimental group/condition, given as a discrete number and unit of measurement
☐	☒ A statement on whether measurements were taken from distinct samples or whether the same sample was measured repeatedly
☐	☒ The statistical test(s) used AND whether they are one- or two-sided *Only common tests should be described solely by name; describe more complex techniques in the Methods section.*
☐	☒ A description of all covariates tested
☐	☒ A description of any assumptions or corrections, such as tests of normality and adjustment for multiple comparisons
☐	☒ A full description of the statistical parameters including central tendency (e.g. means) or other basic estimates (e.g. regression coefficient) AND variation (e.g. standard deviation) or associated estimates of uncertainty (e.g. confidence intervals)
☐	☒ For null hypothesis testing, the test statistic (e.g. *F*, *t*, *r*) with confidence intervals, effect sizes, degrees of freedom and *P* value noted *Give P values as exact values whenever suitable.*
☒	☐ For Bayesian analysis, information on the choice of priors and Markov chain Monte Carlo settings
☒	☐ For hierarchical and complex designs, identification of the appropriate level for tests and full reporting of outcomes
☐	☒ Estimates of effect sizes (e.g. Cohen's *d*, Pearson's *r*), indicating how they were calculated

Our web collection on statistics for biologists contains articles on many of the points above.

Software and code

Policy information about availability of computer code

Data collection	We worked with the commercial software integrated in Simoa HD-X, VersaMax microplate reader, illumina HiSeq X, QuantStudio 7 Flex Real-Time PCR system, BD Influx cell sorter flow cytometer, MRI imaging, and Amyloid-PET technologies Image Acquisition: ZEN microscope software (v3.2 and v3.3)
Data analysis	SNP array genotyping: TaqMan genotyper software (Applied Biosystems) Imaging analysis: GraphPad Prism (v8.0), Fiji-ImageJ (v1.53c), Imaris (v9.7.2) Flow Cytometry analysis: FlowJo software (v10.5.0) SnRNAseq analysis: Cell Ranger (v3.0.1), Seurat (v3.0) Haplotype and fine-mapping analysis: Haploview (v4.2), CAVIAR software (v2.2) Association analysis: PLINK (v1.9), METASOFT (v2.0.0), R (v3.6.2) with packages installed including plotly (v4.9.1), relaimpo (v2.2-3), GenABEL (v1.8), TwoSampleMR (v0.5.6), ForestPMPlot (v1.0.2), OptimalCutpoints (v1.1-4), survival (v1.3-24), ggplot2 (v3.2.1), qqman (v0.1.4). Additional details on parameters can be found in the Methods section. The custom codes for statistical analyses and data visualization are available on GitHub (https://github.com/yjiangah/sST2-in-AD)

For manuscripts utilizing custom algorithms or software that are central to the research but not yet described in published literature, software must be made available to editors and reviewers. We strongly encourage code deposition in a community repository (e.g. GitHub). See the Nature Portfolio guidelines for submitting code & software for further information.

Data

Policy information about availability of data

All manuscripts must include a data availability statement. This statement should provide the following information, where applicable:

- Accession codes, unique identifiers, or web links for publicly available datasets
- A description of any restrictions on data availability
- For clinical datasets or third party data, please ensure that the statement adheres to our policy

All statistical data associated with this study are contained in the Main Text, Supplementary Information, Supplementary Data Files, or Source Data Files. The consent forms signed by individual participants from the Chinese_cohort_1 state that the research content will be kept private under the supervision of the hospital and research team. Therefore, the phenotypic, genomic, and proteomic data of individual participants will only be available and shared in formal collaborations. A review panel hosted at HKUST will process and review any applications for data sharing and project collaboration and promptly notify applicants with the decision. Researchers may contact [sklneurosci@ust.hk] for details about data sharing and project collaboration related to the present study. The GRCh38/hg38 reference genome is available at https://hgdownload.soe.ucsc.edu/downloads.html. The human frontal cortex snRNA-seq dataset of the UKBBN cohort has been deposited in GEO (accession no. GSE157827). The genomic, demographic, and clinical data of the LOAD cohort are available on the National Institutes of Health (NIH) database of Genotypes and Phenotypes (dbGaP) project (accession number: phs000168.v2.p2). The genomic, demographic, and clinical data of the ADC1–3 cohorts are available on the NIH dbGaP project (accession number: phs000372.v2.p1). The genomic, demographic, clinical and brain imaging data of the ADNI cohort are available at adni.loni.usc.edu upon request. The proteomic and demographic data from the INTERVAL and LonGenity cohorts are available at https://twc-stanford.shinyapps.io/aging_plasma_proteome/. The genomic, demographic, and transcriptomic data from the GTEx cohort are available on the NIH dbGaP project (accession number: phs000424.v6.p1). The genomic, demographic, clinical and brain imaging data of the AIBL cohort are available at www.aibl.csiro.au upon request. All other data are available from the corresponding authors upon reasonable request.

Field-specific reporting

Please select the one below that is the best fit for your research. If you are not sure, read the appropriate sections before making your selection.

☒ Life sciences ☐ Behavioural & social sciences ☐ Ecological, evolutionary & environmental sciences

For a reference copy of the document with all sections, see nature.com/documents/nr-reporting-summary-flat.pdf

Life sciences study design

All studies must disclose on these points even when the disclosure is negative.

Sample size	No statistical methods were used to predetermine sample size. For human subjects, we took all available genomic, proteomic/transcriptomic, brain imaging and phenotypic data from the Chinese_cohort_1, Chinese_cohort_2, LOAD cohort, ADC cohorts, ADNI cohort, UKBBN cohort, AIBL cohort, GTEx cohort, ADRC cohort and Japanese cohort. Sample sizes are either listed in Supplementary Table 1, Supplementary Table 5, Supplementary Data, or in corresponding main text and figure legends. For mouse model studies, sample size was determined based on the number of animals used in prior experiments conducted (Fu et al., PNAS 2016; Lau et al., Cell Reports 2020.)
Data exclusions	No data was excluded.
Replication	All data presented were obtained from two to three independent experiments with consistent outcomes.
Randomization	All human samples in different disease conditions (e.g., healthy controls, patients with AD etc.) were collected and randomly assigned with a code, with a corresponding decoding file. All non-human samples (e.g,. mice, cultured cells) were randomly assigned into experimental groups and conditions before the experiments and sample collection. The operator was blinded towards the code and decoding file.
Blinding	All samples had a random code and the operator was blinded towards the code.

Reporting for specific materials, systems and methods

We require information from authors about some types of materials, experimental systems and methods used in many studies. Here, indicate whether each material, system or method listed is relevant to your study. If you are not sure if a list item applies to your research, read the appropriate section before selecting a response.

Materials & experimental systems

n/a	Involved in the study
☐	☒ Antibodies
☐	☒ Eukaryotic cell lines
☒	☐ Palaeontology and archaeology
☐	☒ Animals and other organisms
☐	☒ Human research participants
☒	☐ Clinical data
☒	☐ Dual use research of concern

Methods

n/a	Involved in the study
☒	☐ ChIP-seq
☐	☒ Flow cytometry
☐	☒ MRI-based neuroimaging

Antibodies

Antibodies used

Primary Antibodies:
Mouse anti-Aβ monoclonal antibody (clone NAB228; SC-32277; Santa Cruz Biotechnology)
Mouse anti-Aβ monoclonal antibody (clone 4G8; 800703; BioLegend)
Rabbit anti-Aβ monoclonal antibody (clone D54D2; 8243S; Cell Signaling Technology)
Rabbit anti-Iba-1 polyclonal antibody (019-19741; FUJIFILM Wako Pure Chemical Corporation)
Rat anti-Ki67 monoclonal antibody (clone SolA15; 14-5698-80; eBioscience)
Alexa Fluor 488-conjugated mouse CD11b antibody (53-0112-82; eBioscience)
Rabbit Histone H3K4me3 polyclonal antibody (39159; Active Motif)
Rabbit Histone H3K27ac polyclonal antibody (39133; Active Motif)
Human IgG, Fc fragment (009-000-008; Jackson ImmunoResearch)
Normal Rabbit IgG Control (AB-105-C; R&D Systems)

Secondary Antibodies:
HRP-labelled anti-mouse IgG (QD440-XAKE; BioGenex)
HRP-labelled anti-mouse Ig and AP-labelled anti-rabbit Ig detection cocktail (HK597-50K; BioGenex)
Biotin-conjugated anti-mouse secondary antibody (BA2000; Vector Laboratories)
Goat anti-mouse IgG (H+L) Alexa Fluor488-conjugate (A-11001; Invitrogen Life Technologies)
Goat anti-rabbit IgG (H+L) Alexa Fluor568-conjugate (A-11011; Invitrogen Life Technologies)
Goat anti-rat IgG (H+L) Alexa Fluor647-conjugate (A-21247; Invitrogen Life Technologies)

Validation

All antibodies used were validated by manufacturers. Data sheet is available from the web links as described below.
Mouse anti-Aβ monoclonal antibody (clone NAB228; SC-32277; Santa Cruz Biotechnology): https://datasheets.scbt.com/sc-32277.pdf
Mouse anti-Aβ monoclonal antibody (clone 4G8; 800703; BioLegend): https://www.biolegend.com/en-us/global-elements/pdf-popup/purified-anti-beta-amyloid-17-24-antibody-11233?filename=Purified%20anti-beta-Amyloid%2017-24%20%20Antibody.pdf&pdfgen=true
Rabbit anti-Aβ monoclonal antibody (clone D54D2; 8243S; Cell Signaling Technology): https://www.cellsignal.com/products/primary-antibodies/b-amyloid-d54d2-xp-rabbit-mab/8243
Rabbit anti-Iba-1 polyclonal antibody (019-19741; FUJIFILM Wako Pure Chemical Corporation): https://labchem-wako.fujifilm.com/us/product/detail/W01W0101-1974.html
Rat anti-Ki67 monoclonal antibody (clone SolA15; 14-5698-80; eBioscience): https://www.thermofisher.com/order/genome-database/generatePdf?productName=Ki-67&assayType=PRANT&detailed=true&productId=14-5698-82
Alexa Fluor 488-conjugated mouse CD11b antibody (53-0112-82; eBioscience): https://www.thermofisher.com/order/genome-database/generatePdf?productName=CD11b&assayType=PRANT&detailed=true&productId=53-0112-82
Rabbit Histone H3K4me3 polyclonal antibody (39159; Active Motif): https://www.activemotif.com/documents/tds/39159.pdf
Rabbit Histone H3K27ac polyclonal antibody (39133; Active Motif): https://www.activemotif.com/documents/tds/39133.pdf
Human IgG, Fc fragment (009-000-008; Jackson ImmunoResearch): https://www.jacksonimmuno.com/lots/000000142895
Normal Rabbit IgG Control (AB-105-C; R&D Systems): https://resources.rndsystems.com/pdfs/datasheets/ab105c.pdf?v=20220413&_ga=2.85229085.521716042.1649913381-812846025.1649913381

Eukaryotic cell lines

Policy information about cell lines

Cell line source(s)	The human cerebral microvascular endothelial cell line (hCMEC/D3) (Cedarlane)
Authentication	Immunofluorescence staining of hCMEC/D3 for endothelial cell specific markers, specifically Tight junction protein ZO-1 and VECadherin was used to validate the cell line.
Mycoplasma contamination	The hCMEC/D3 cells were tested negative for mycoplasma contamination.
Commonly misidentified lines (See ICLAC register)	No commonly misidentified cell lines were used.

Animals and other organisms

Policy information about studies involving animals; ARRIVE guidelines recommended for reporting animal research

Laboratory animals	C57BL6J male and female mice (3 months of age) were purchased from the Jackson Laboratory. 5XFAD male and female mice (B6.Cg-Tg(APPSwFlLon,PSEN1*M146L*L286V)6799Vas/Mmjax) (3 months of age) were provided by Sookja Kim Chung (The University of Hong Kong). All mice were housed in the HKUST Animal and Plant Care Facility. We housed 4 mice of the same sex per cage at 22 degrees Celsius and at a relative humidity of 60%, with a 12-h light/dark cycle as well as food and water ad libitum
Wild animals	The study did not involve wild animals.
Field-collected samples	The study did not involve samples collected from the field.
Ethics oversight	All animal experiments were approved by the HKUST Animal Ethics Committee and conducted in accordance with the Guidelines of the Animal Care Facility of HKUST.

Note that full information on the approval of the study protocol must also be provided in the manuscript.

Human research participants

Policy information about studies involving human research participants

Population characteristics	The Chinese_cohort_1 consisted of 345 patients with AD and 345 healthy controls (all ≥60 years old). All participants underwent a medical history assessment, clinical assessment, cognitive and functional assessments using the Montreal Cognitive Assessment (MoCA) test, and neuroimaging assessment by magnetic resonance imaging (MRI), and only those with cognitive dysfunctions (i.e., those having Alzheimer's dementia with MoCA score < 21) were included in the AD group in this study. Participants with any significant neurological disease besides AD or psychiatric disorder were excluded. We recorded age, sex, years of education, medical history, and history of CVDs (i.e., heart disease, hypertension, diabetes mellitus, and hyperlipidemia).The detailed characteristics of the cohort including age, gender, genotypic information and phenotypic information are listed in Supplementary Table 1. The characteristics of other datasets are listed in Supplementary Table 5, Supplementary Data, or in corresponding main text and figure legends.
Recruitment	The Chinese_cohort_1 consisted of 690 Hong Kong Chinese participants who visited the Specialist Outpatient Department of the Prince of Wales Hospital of the Chinese University of Hong Kong from April 2013 to February 2018 . All participants underwent medical history assessment, clinical assessment, cognitive and functional assessment using the Montreal Cognitive Assessment (MoCA) test and neuroimaging assessment by MRI. The clinical diagnosis of AD was established on the basis of the American Psychiatric Association's Diagnostic and Statistical Manual of Mental Disorders, Fifth Edition (DSM-5). Participants with any significant neurologic disease besides AD or psychiatric disorder were excluded. All participants provided written informed consent for both study enrollment and sample collection. The recruitment of other cohorts are described in Supplementary Notes section. No selection biases were identified.
Ethics oversight	The study of Chinese_cohort_1 was approved by the Joint Chinese University of Hong Kong-New Territories East Cluster Clinical Research Ethics Committee at the Prince of Wales Hospital, the Chinese University of Hong Kong, and the Hong Kong University of Science and Technology. All participants provided written informed consent for both study enrollment and sample collection. The samples of UKBBN cohort are provided by South West Dementia Brain Bank (SWDBB), which gets approval from North Somerset and South Bristol Research Ethics Committee to operate as a research tissue bank. The SWDBB is part of the Brains for Dementia Research program, jointly funded by Alzheimer's Research UK and Alzheimer's Society and supported by BRACE (Bristol Research into Alzheimer's and Care of the Elderly) and the Medical Research Council.

Note that full information on the approval of the study protocol must also be provided in the manuscript.

Flow Cytometry

Plots

Confirm that:

☒ The axis labels state the marker and fluorochrome used (e.g. CD4-FITC).

☒ The axis scales are clearly visible. Include numbers along axes only for bottom left plot of group (a 'group' is an analysis of identical markers).

☒ All plots are contour plots with outliers or pseudocolor plots.

☒ A numerical value for number of cells or percentage (with statistics) is provided.

Methodology

Sample preparation	5XFAD or C57BL6J (4 months of age) mice were intraperitoneally injected with methoxy-X04 (10 mg/kg) to label Aβ. The mice were anesthetized with isoflurane 3 h after methoxy-X04 injection, and the left ventricle was perfused with ice-cold PBS. Their forebrains were isolated, minced, and incubated at 37 °C for 30 min in 5 U/mL papain (LS003126) and 35 U/mL DNase I (LS002140; Worthington Biochemical) for enzymatic digestion. After incubation, myelin debris was depleted by 30% isotonic Percoll (P1644; Sigma-Aldrich) gradient centrifugation, and mononuclear cell suspensions were obtained in DMEM/F12

	medium with ice-cold 10% heat-inactivated FBS. Unstained controls were prepared from mixtures of different sample cell suspensions for cell population identification. To label microglia, an Alexa Fluor 488-conjugated mouse CD11b antibody (1:200; 53-0112-82; eBioscience) was used to stain the cell suspensions for 45 min at 4 °C.
Instrument	BD Influx cell sorter
Software	FlowJo software (v10.5.0)
Cell population abundance	Post-sort fractions for methoxy-X04+ CD11b+ cells were >95%
Gating strategy	Cells were gated on forward (FSC = size) and sideward scatter (SSC = internal structure). FSC and trigger pulse width were used to discriminate single cells from cell doublets/aggregates. Unstained controls were used to identify CD11b+ cell populations. Samples from C57BL6J mice were used to identify methoxy-X04+ cell populations.

☒ Tick this box to confirm that a figure exemplifying the gating strategy is provided in the Supplementary Information.

Magnetic resonance imaging

Experimental design

Design type	Cross-sectional morphometry analysis (structural MRI only)
Design specifications	One T1-weighted structural MRI was conducted per participant for relationships with sST2 protein levels and genotypes
Behavioral performance measures	None

Acquisition

Imaging type(s)	Structural MRI
Field strength	3T
Sequence & imaging parameters	In Chinese_cohort_1, 3D FFE (gradient echo) pulse sequence was used. The images were acquired from coronal view, with slice thickness 5mm, TE/TR/flip angle = 3ms /7ms /8. The acquired image matrix size was 240 × 25 × 240. In ADNI, structural MRI was recorded using a 3D T1 weighted MPRAGE sequence with 1mm isotropic voxel-size and a TR=2300ms
Area of acquisition	Whole brain

Diffusion MRI ☐ Used ☒ Not used

Preprocessing

Preprocessing software	In Chinese_cohort_1, the MRI data were preprocessed by AccuBrain® IV1.2 (BrainNow Medical Technology Ltd), a brain quantification tool that performs brain structure and tissue segmentation and quantification in a fully automatic mode. Given the T1-weighted MRI data, several brain structures (e.g., hippocampus, lateral ventricle, amygdala, etc) and three major brain tissues (i.e., white matter, gray matter and CSF) are segmented automatically based on prior anatomical knowledge specified by experienced radiologists. The anatomical information is automatically transformed into the individual brain. In ADNI, FSL, ANTs, AFNI were used
Normalization	In Chinese_cohort_1, for details please refer to Abrigo et al., Acta Radiologica 2018. In ADNI, non-linear spatial normalization parameters were estimated based on structural T1-weighted images using Advanced Normalization Tools (ANTs), to normalize all images to Montreal Neurological Institute (MNI) standard space.
Normalization template	In Chinese_cohort_1, for details please refer to Abrigo et al., Acta Radiologica 2018. In ADNI, MNI was used.
Noise and artifact removal	For details please refer to Abrigo et al., Acta Radiologica 2018
Volume censoring	Not applicable to structural MRI

Statistical modeling & inference

Model type and settings	Only structural MRI was used in analyses with ROI-based approach. Additional details on statistical methods, including all model parameters can be found in the Methods section.
Effect(s) tested	We tested for associations between imaging measures (gray matter volume) and sST2 levels or genotypes

Specify type of analysis: ☐ Whole brain ☒ ROI-based ☐ Both

Anatomical location(s) Automated labelling by Accubrain

Statistic type for inference (See Eklund et al. 2016)	Neither voxel-wise or cluster-wise was used
Correction	FDR

Models & analysis

n/a	Involved in the study
☒	☐ Functional and/or effective connectivity
☒	☐ Graph analysis
☒	☐ Multivariate modeling or predictive analysis